Bond Graph Model and Computer Simulation of a Hydrostatic Drive Test Stand

by

Richard B. League

Thesis submitted to the Faculty of the
Virginia Polytechnic Institute and State University
in partial fulfillment of the requirements for the degree of
MASTER OF SCIENCE
in
Agricultural Engineering

APPROVED:

Dr. J. S. Cundiff

Dr. J. V. Perumpral

Dr. H. H. Robertshaw

Dr. R. K. Byler

May, 1985
Blacksburg, Virginia

BOND GRAPH MODEL AND COMPUTER SIMULATION OF A HYDROSTATIC DRIVE TEST STAND

by

Richard B. League

Committee Chairman: Dr. John S. Cundiff
Agricultural Engineering

(ABSTRACT)

A hydrostatic drive test stand was constructed to aid in the instruction of the characteristics of hydrostatic transmissions and to develop a time-varying load in a shaft to compare torque transducers. A mathematical model of the device was derived using the bond graph approach and was implemented using the Advanced Continuous Simulation Language (ACSL). The test stand was used to obtain experimental data to try to refine the model parameters. To facilitate the measurement of system flows, a microprocessor-based digital flow indicator was developed. Steady-state tests were performed at various constant pump swashplate angles; for the dynamic tests, the pump swashplate angle was cycled from zero degrees to 6.5 degrees.

ACKNOWLEDGEMENTS

The author wishes to express appreciation to the members of his graduate committee, Dr. J. V. Perumpral, Dr. H. H. Robertshaw, and Dr. R. K. Byler. The considerable time and effort spent by Dr. Robertshaw on behalf of the author are deeply appreciated. Special thanks and appreciation go to Dr. John S. Cundiff, the chairman of the author's committee, whose continual support and encouragement formed the basis of a good relationship and a rewarding experience.

Thanks go to , , and who built the test stand.

Special thanks is due for her invaluable advice on both micro-processor system design and computer simulation.

Finally, I wish to acknowledge the loving support of my wife, without whom this effort would have been impossible.

TABLE OF CONTENTS

LIST OF FIGURES

LIST OF TABLES

INTRODUCTION

The use of fluid power for agricultural and industrial machinery applications has been increasing. Fluid power is dependable, facilitates power transmission on a machine, provides convenient load and speed control, and has high power density.

As the use of fluid power increases, instruction in fluid power design must increase. Demonstration of the principles of hydraulic mechanisms generally requires the use of actual hydraulic circuits. In use, these circuits are often noisy, cumbersome and messy, all of which reduce the effectiveness of a presentation. A micro-computer based simulator which accurately emulates its hydraulic counterpart, in both function and appearance, could alleviate these problems.

The first step in developing such a simulator is to derive an analytical model of the hydraulic components, connect them in a circuit, and simulate the circuit operation on a digital computer. The second step is to refine the parameters within the analytical model with experimentally obtained data, measure the circuit performance, and verify the simulation predictions.

The research presented here is the initial stage of the development of such a simulator for a hydrostatic transmis-

sion. A hydrostatic transmission test stand was built, the components tested, and a computer simulation performed.

OBJECTIVES

1. Develop a test stand with a variable-displacement pump and fixed-displacement motor that will demonstrate the characteristics of a hydrostatic transmission.

2. Incorporate in the test stand a means for developing a dynamic load in a shaft.

3. Develop an analytical model for the test stand and simulate it on a digital computer.

4. Obtain experimental data, including the development of a flow measurement device, to refine the model parameters.

LITERATURE REVIEW

Steady-State Hydrostatic Transmission Models

Several different research efforts to predict the steady-state performance of hydrostatic transmissions have been reported in recent years. Wilson and Lemme (1970) developed a set of coefficient models to describe the actual performance of hydraulic pumps and motors as functions of both system variables and coefficients. These models were developed to facilitate the design of hydrostatic vehicle transmissions, and the authors presented no test data to verify them. To simplify the discussion these equations will hereafter be referred to as Wilson's equations.

Reid and Woods (1972) based their transmission model on Wilson's pump and motor models. Their research was on the control of a hydrostatic transmission by means of fluidic devices, and not on the characterization of the transmission itself. They used step inputs of swashplate angle, and were able to limit the steady-state error of the speed or torque output of their transmission to ±2 percent.

Wilson's models were modified by Elder and Otis (1973) to account for the fact that viscous drag and dry friction torque losses are not constants but functions of displacement. They reported errors of less than ±3 percent.

Pacey (1979) based his models on Wilson's equations, and also incorporated Elder and Otis's modification. He further rearranged the equations so that the speeds replaced the flows as the dependent variables in the model. In doing so, he was able to describe pump speed and pump torque as functions of motor speed and motor torque, and vice versa, thereby eliminating the need to measure flow-rates. Errors of less than ±2 percent were reported.

Dynamic Hydrostatic Transmission Models

Merritt (1967) described a set of differential equations for modeling a pump-controlled motor, which is tantamount to a hydrostatic transmission. His equations were essentially the Wilson models with terms added to account for the compliance of the fluid. Merritt also included a load term in the motor torque equation.

A set of equations very similar to those of Merritt was proposed by Blackburn, Reethoff and Shearer (1960). One difference is that they allow the return line pressure from the motor to the pump to vary, where Merritt assumes it always has the charge pump pressure.

Karnopp and Rosenberg (1975) described one means by which the differential equations might be developed, i.e. bond graphs. However, their hydraulic pump-motor model

served only to illustrate the technique and not to adequately describe a hydrostatic transmission.

Simulation Programs and Languages

The Steady State Flow Analysis (SSFAN) program (Levek and Young, 1977) was developed to analyze hydraulic systems for aircraft. It uses an iterative solution process to predict flow in complicated networks with several subsystems operating simultaneously. However, the public software version obtained through the National Technical Information Service had a number of errors and limitations that made it unusable. The program had several instances of unlabled executable statements following unconditional branches, and was unable to compute the flow in legs with very small resistances, i.e. legs containing only check valves.

Interactive Simulation Language (ISL) developed at Queen Mary College of London University (1982) is a program that enables the user to solve problems on a digital computer that would normally be delegated to an analog computer. The input to the program required a block diagram approach, which with a large model, became cumbersome and tedious to input and edit.

Mitchell and Gauthier (1981) wrote the Advanced Continuous Simulation Language (ACSL) to solve systems of differential equations on digital computers. An ACSL program is

written with FORTRAN-like statements that need not be sequenced by the order of variable definition. It also gives the user the ability to set the error limits he desires and to choose the type of integration scheme that best suits his needs.

DEVICE DESCRIPTION

The system constructed was a device for the instruction of the principles of hydrostatic transmissions. The premise was to have a variable displacement pump drive a fixed displacement hydraulic motor, and provide a means for loading the motor. The secondary purpose of the device was to dynamically test different torque transducers by developing a time-varying torque in a shaft in which a commercial and an experimental torque cell were mounted in series.

It was decided to drive the pump through a long shaft, and to develop torque in the shaft by creating a pressure drop across the pump. Placing the torque transducers in this shaft accomplished the secondary purpose of the system. Furthermore, any scheme to load the pump that did so only by creating heat was considered to be too inefficient. This eliminated such ideas as using a variable relief valve or orifice, driving a Prony brake with a hydraulic motor, or driving a generator with a hydraulic motor and dissipating the electrical energy with a resistor bank.

A schematic of the physical arrangement of the system and a schematic of the hydraulic circuity are shown in Figures 1 and 2, respectively. A 7.54 kW (10 hp) electric motor powers the pump, via the pump jackshaft and pump drive shaft. The pump jackshaft speed is nominally reduced to

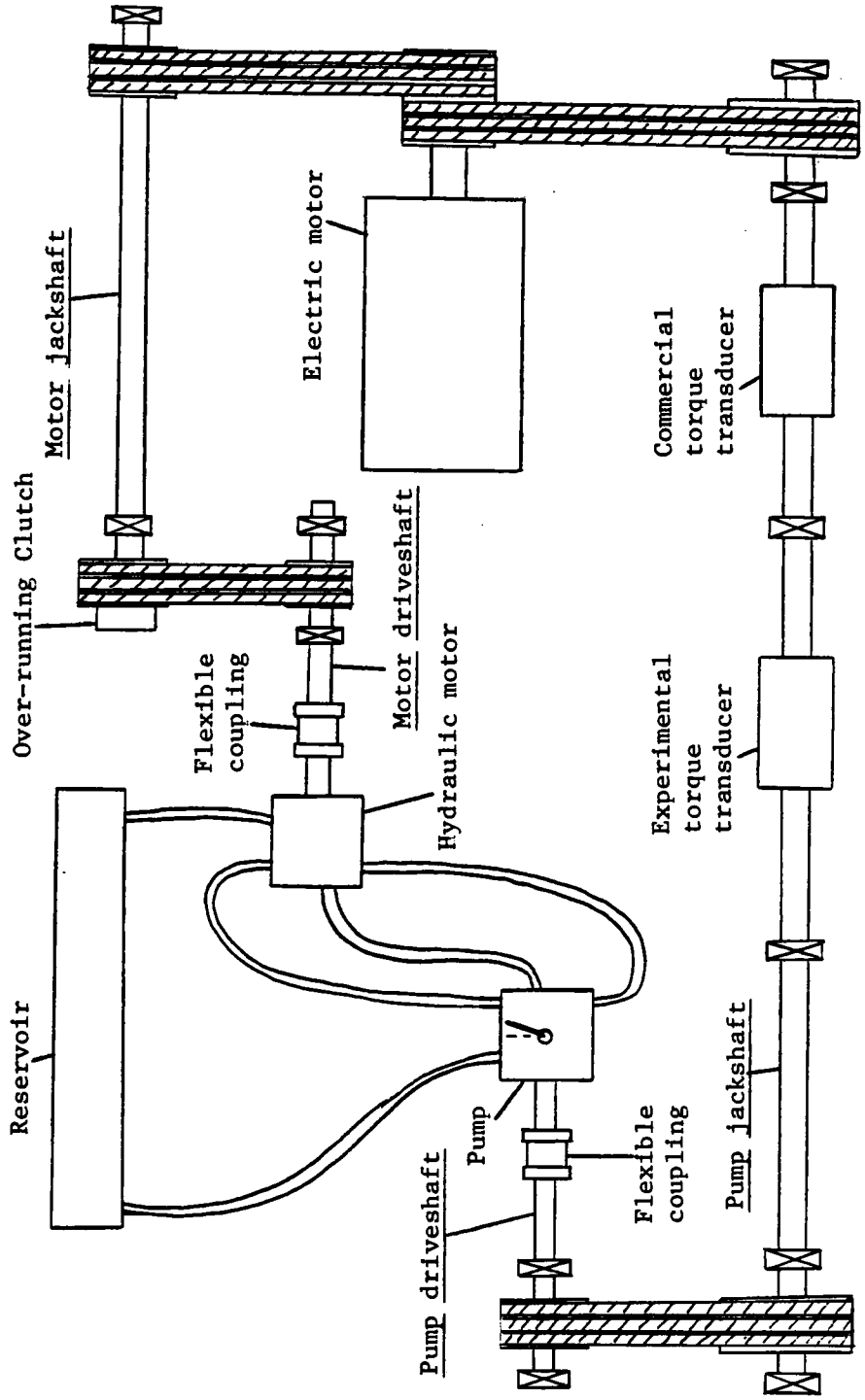

Figure 1: Schematic of hydrostatic drive test stand showing proposed positions for experimental and commercial torque transducers

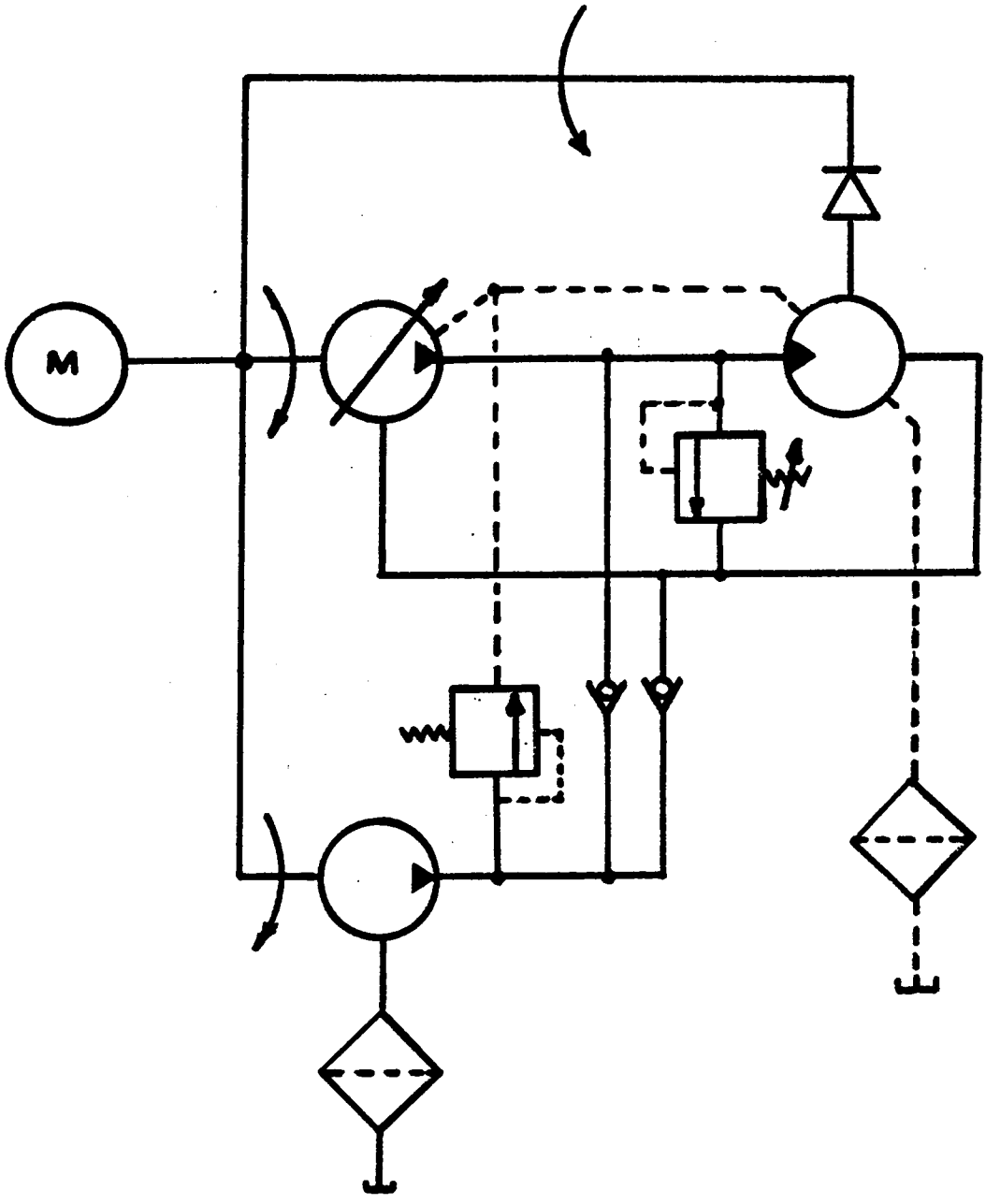

Figure 2: Hydraulic system schematic for the hydrostatic drive test stand

0.309 times that of the electric motor speed by a v-belt drive whose sheaves are sized at 10.67 cm and 34.54 cm. With an electric motor speed of 1790 rpm, the pump jackshaft speed was 573 rpm. The pump driveshaft is powered by the pump jackshaft at 2404 rpm achieved with a 46.74 cm diamter sheave on the pump jackshaft and a 12.7 cm sheave on the driveshaft. The pump, in turn, is driven by the pump driveshaft through a flexible coupling. Fluid is drawn into the charge pump inlet from the reservoir, through a filter. The excess charge pump flow is dumped into the case of the pump, whose drain flow is routed to the drain inlet port on the hydraulic motor. Fluid flow from the motor drain outlet is returned to the reservoir through another filter. This circuit provides continuous cooling flow through the pump and motor cases

Hydraulic power is transmitted from the pump to the hydraulic motor which is connected by means of another flexible coupling to the motor driveshaft, which drives the motor jackshaft through a v-belt drive. This drive has two sheaves of 21.84 cm nominal diameter, one mounted on the motor driveshaft, the other on the outer race of the overrunning clutch. In theory, the outer race of the clutch is free to turn until its speed equals or exceeds that of the inner race at which point the clutch engages and transmits

torque from the motor driveshaft to the motor jackshaft. The motor jackshaft then drives the electric motor through a speed increasing sheave pair whose diameters are 21.84 cm on the jackshaft and 10.67 on the electric motor shaft.

The motor jackshaft turns at a nominal rate 0.488 times that of the electric motor at all times. The over-running clutch prevents the hydraulic motor from being driven by the electric motor via the motor jackshaft. Were this to happen, the hydraulic motor would act as a pump and oppose the hydraulic pump, with disastrous results.

The system generates a torque in the pump jack-shaft once the over-running clutch engages. Prior to that point, the torque in the shaft is due only to friction losses. With the clutch engaged, the system becomes analogous to a pair of shafts upon which are mounted two sets of gears with different teeth ratios. The hydraulic system on the device acts as one pair of gears and the mechanical drives as the other. Theoretically, the gear pairs are locked, as is the hydraulic system. However, the actual system has leakages, a relief valve, and other phenomena that allow the system to operate without damage.

The power required from the electric motor is that needed to overcome friction and hydraulic losses. As the clutch engages, the power through the hydrostatic transmis-

sion increases, but the increased load on the electric motor is due only to the increased hydraulic line flows and bearing friction. The power from the hydraulic motor is fed back into the pump, forming a loop. The only power lost from the loop is heat from the hydraulic and friction losses. This power loss is what is supplied by the electric motor.

Once the clutch is engaged, any additional flow due to an increase in swashplate angle must be accounted for in leakage. The only way leakage can increase is for the system pressure to increase. The system pressure, then, is very sensitive to swashplate angle. The relief valve will open when the pressure exceeds 3000 psi. It can be seen that without a relief valve, there would be no limiting factor other than the yield stress a hose or fitting, probability.

The system cannot be used to test some of the characteristics of hydraulic pumps and motors because the system pressure is not independent of swashplate angle and because the pump speed is relatively constant. The operating points of the system can be altered by changing the sheaves on the pump or motor driveshafts to cause the hydraulic motor to load up at different swashplate angles.

ANALYTICAL METHODS

Bond Graphs

Bond graphs are a convenient, yet mathematically formal, method of denoting the power flows in systems that involve the interaction of power transmission. Complex systems that involve the interaction of mechanical, hydraulic, and electrical components, for example, may be described on the same graph using the same symbols. This is possible because bond graphs denote the direction of power flow regardless of the means by which it is transmitted. This is accomplished by the use of energy and power variables, and generalized elements to describe their functional relationships. Elements are not restricted to being linear, though linearity simplifies the mathematics.

Tetrahedron of State

Four generalized variables, assumed to be functions of time, are used to describe the nature of any system. They are:

Power:	e	effort	force, torque, voltage, pressure
	f	flow	velocity, angular velocity, current, flow-rate
Energy:	q	displacement	displacement, angle, charge, volume
	p	momentum	momentum, angular momentum, flux linkage, pressure momentum

The relationship between these variables is shown by the tetrahedron of state (Figure 3). Each line in the tetrahedron represents a functional relationship between the variable at its end. Momentum is related to effort by the integral function, and conversely, effort to momentum by the time derivative. Similarly, displacement is the integral of flow, or flow is the time derivation of displacement. In algebraic form:

$$q = \int f\, dt \quad \text{or} \quad f = d(q)/dt$$
$$p = \int e\, dt \quad \text{or} \quad e = d(p)/dt$$

For convention, the variable to the left of the equal sign is assumed to be the dependent variable.

One-Port Elements

The lettered legs of the tetrahedron are three of the one-port elements used in bond graphs. They are thus designated because they relate one independent variable to one dependent variable. Each bond in a bond graph specifies an independent or forward effect variable and a dependent or back effect variable. One-port elements, then, require only one bond to be fully defined. The five types of one-port elements are resistance, inertance, conductance, effort source, and flow source.

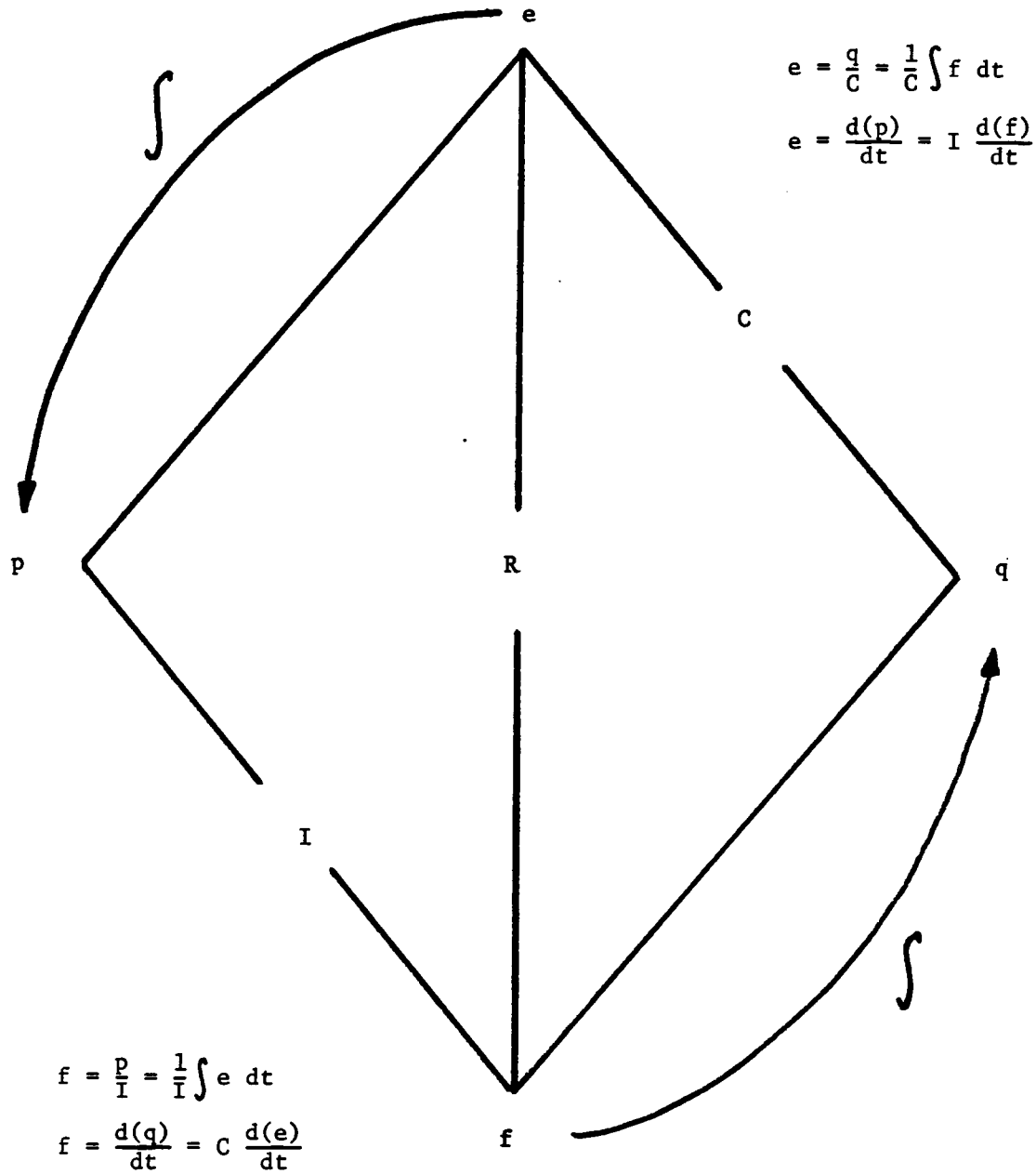

Figure 3: Tetrahedron of state for bond graphs
(from Figure 3.6 in Karnopp and Rosenberg, 1975)

Resistance

The "R" element is the generalized resistance element. For example, it can represent a dashpot, an electrical resistance, or a hydraulic line loss. The "R" element is used to directly relate flow with effort by:

$$e = \Phi_R(f) \quad \text{or} \quad f = \Phi_R^{-1}(e)$$

In the linearized form,

$$e = R\ f \quad \text{or} \quad f = e\ /\ R$$

Inertance

The "I" element is the generalized inertia element. It commonly represents mass, rotational inertial, or inductance. The "I" element is used to relate flow to momentum by:

$$p = \Phi_I(f) \quad \text{or} \quad f = \Phi_I^{-1}(p)$$

By relating momentum to effort, the relationship of flow and effort for an inertia may be derived. Maintaining the general notation,

$$f = \Phi_I^{-1}\left(\int e\ dt\right) \quad \text{or} \quad e = d(\Phi_I(f))/dt$$

Linearized,

$$f = (1/I)\int e\ dt \quad \text{or} \quad e = I\ \ d(f)/dt$$

Capacitance

The generalized capacitance element is denoted with a "C". It can represent linear or torsional springs, electrical capacitances, or fluid capacitances. The "C" element is used to relate displacement to effort by:

$$q = \Phi_C(e) \quad \text{or} \quad e = \Phi_C^{-1}(q)$$

By relating displacement to flow, the relationship of flow and effort for a capacitance may be derived. Maintaining the general notation,

$$e = \Phi_C^{-1}\left(\int f\, dt\right) \quad \text{or} \quad f = d(\Phi_C(e))/dt$$

Linearized,

$$e = (1/C)\int f\, dt \quad \text{or} \quad f = C\ d(e)/dt$$

Effort Source

The effort source (S_e) is an element which supplies the system to which it is bonded with a constant effort. The flow of an effort source is determined by the system. An example of an effort source is a voltage source.

Flow Source

The flow source (S_f) is an element which supplies a constant flow to the system. The effort of a flow source is determined by the system. A flow source is an idealized

vibration shaker or constant flow system (Karnopp and Rosenberg, 1975).

Two-Port Elements

Two ideally conservative two-port elements used in bond graphs are transformers and gyrators. For both of these elements, the power input equals the power output. The gyrator was not used in the model and will not be discussed here. The symbol for a transformer is:

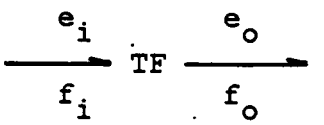

Examples of transformer elements are a rigid lever, a gear pair, an electrical transformer, and a hydraulic ram. The constitutive equations are:

$$e_i = m\, e_o$$
$$f_o = m\, f_i$$

The variable "m" is the transformer modulus, which is not necessarily a constant over time, f or e but is the same for the two equations at all times.

Multi-Port Elements

The two categories of elements which may be bonded to more than two other elements are fields and junctions. The

former was not used and will not be discussed here. Junctions are conservative elements that are used to link other elements together to form system models.

Flow Junction

A flow junction, also called a zero junction or a common-effort junction, designates a node in a graph where all bonds radiating from it have the same effort. An example of a flow junction is a tee joint in a hydraulic circuit. There is one pressure associated with the tee and a different flows in each of the branches.

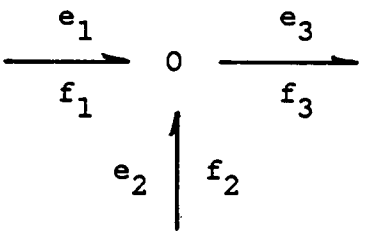

Therefore, to be a power-conserving element, the sum of the flows at this junction must be zero. The equations resulting from this example are:

$$e_1 = e_2 = e_3$$

and

$$f_1 + f_2 + f_3 = 0$$

where $f_3 < 0$

Effort Junction

The other type of junction is the effort junction, also called a one junction or a common-flow junction. This element is similar to the zero junction; the efforts in the bonds sum to zero and all the bonds have the same flow.

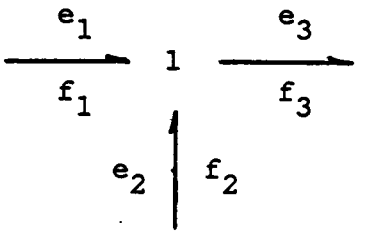

The equations from this example are:

$$e_1 + e_2 + e_3 = 0$$

where $e_3 < 0$

and

$$f_1 = f_2 = f_3$$

Causality

The storage elements, capacitance and inertance, involve either integral or derivation functions, as determined by the choice of the independent variables. For example, if the flow is selected as the independent variable in an "I" element, the effort is a function of the derivative of the flow. This selection of independent variables, called assignment of "causality", is designated on a bond

graph with a perpendicular bar at one end of the bond. The bar, called the causal stroke, is adjacent to the element and indicates that the effort is the forward effect and the flow is the back effect. The causal stroke away from an element denotes flow as the forward effect and effort as the back effect. The bonds for storage elements are shown along with their constitutive equations.

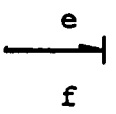

$$f = \Phi_I^{-1}\left(\int e \, dt \right)$$

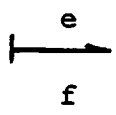

$$e = \Phi_I\left(d(e)/dt \right)$$

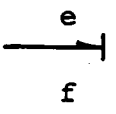

$$f = \Phi_C^{-1}\left(d(e)/dt \right)$$

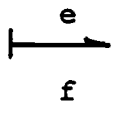

$$e = \Phi_C\left(\int f \, dt \right)$$

For effort and flow sources, the causality is automatically defined because, for each, one variable is held constant and the other is determined by the system. Sources are always written:

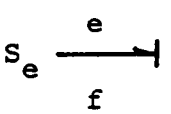

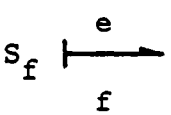

The causal strokes for transformers are either:

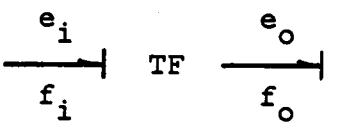

or

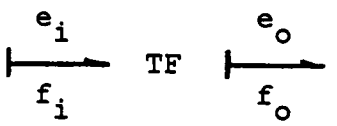

This implies that the causality remains the same through a transformer. The forward effect on one side is the same as that on the other side.

At a junction, one variable is the same in all adjacent bonds. For zero-junctions, it is flow, for one-junctions, effort. Only one of the bonds at a junction determines this common value. Therefore, at a zero-junction, there must be only one causal stroke. Two causal strokes at a zero-junction would imply that two independent forward effects are necessarily equal. Similarly, at a one-junction, there must only be one bond without a causal stroke. The flow associated with this bond determines the flow in all connected bonds. The junctions appear in the following form.

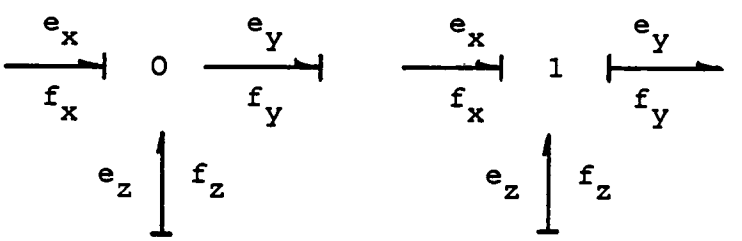

With the use of bond graphs, complex systems may be mathematically described and analyzed with a concise, graphical approach. Philosophical questions as to causes and effects in a system may also be addressed.

Bond Graph Development for Hydrostatic Test Stand

The model for the previously described hydro-mechanical system was developed by using the procedure outlined by Karnopp and Rosenberg (1975) and Wilson's equations (Table 1). The methods for both hydraulic and mechanical systems were utilized, and to facilitate the development of the bond graph, the system was segmented into five subsystems: mechanical power transmission, main pump, charge pump, hydraulic power transmission, and hydraulic motor.

Mechanical Power Transmission

The mechanical power transmission subsystem was defined to be the system of shafts and belt drives from the output of the hydraulic motor to the input of the pump, including the electric motor. The first step in the construction of the bond graph was to represent the known rotational velocities with common-flow junctions. These speeds were the electric motor speed, pump jackshaft speed, hydraulic motor speed, and the motor jackshaft speed. These 1-junctions

Table 1: Wilson's equations for steady-state hydrostatic transmission performance

$$Q_p = D_p N_p - \frac{C_{sp} D_{pmax} \Delta P}{2 \pi \mu} - \frac{L_{cp}}{\mu}$$

$$T_p = \frac{\Delta P D_p}{2 \pi} + \frac{C_{fp} \Delta P D_{pmax}}{2\pi(1-\tan \alpha_p)} + \frac{C_{Dp} \mu N_p D_{pmax}}{2\pi(1-\tan \alpha_p)} + T_{cp}$$

$$Q_m = D_m N_m + \frac{C_{sm} D_{mmax} \Delta P}{2 \pi \mu} - \frac{L_{cm}}{\mu}$$

$$T_m = \frac{\Delta P D_m}{2 \pi} - \frac{C_{fm} \Delta P D_{mmax}}{2\pi(1-\tan \alpha_m)} + \frac{C_{Dm} \mu N_p D_{mmax}}{2\pi(1-\tan \alpha_m)} + T_{cm}$$

where

- C_{sp} - coefficient of slip, pump (dimensionless)
- L_{cp} - constant leakage coefficient, pump (L/min/m^2/s)
- C_{fp} - coefficient of dry friction, pump (dimensionless)
- C_{Dp} - coefficient of viscous drag, pump (dimensionless)
- T_{cp} - constant friction torque, pump (N-m)
- C_{sm} - coefficient of slip, motor (dimensionless)
- L_{cm} - constant leakage coefficient, motor (L/min/m^2/s)
- C_{fm} - coefficient of dry friction, motor (dimensionless)
- C_{Dm} - coefficient of viscous drag, motor (dimensionless)
- T_{cm} - constant friction torque, motor (N-m)
- α_p - swashplate angle of pump (degrees)
- α_m - swashplate angle of motor (degrees)

were laid out to resemble the orientation of the physical system (Figure 4).

Next, the sheaves were added to the graph in the form of transformers, with the corresponding sheave diameter ratios as the transformer moduli. Four transformers were needed to model the following sheave pairs: hydraulic motor to motor jackshaft, motor jackshaft to electric motor, electric motor to pump jackshaft, and pump jackshaft to the pump. The assumed direction of power flow was out of the hydraulic motor, through the electric motor, and into the pump.

This configuration neglected the over-running clutch between the motor jackshaft and the hydraulic motor. Since the hydraulic motor speed was not necessarily the same as that of the motor jackshaft, a common-effort junction had to be placed between the transformer and the hydraulic motor speed junction. With the clutch engaged, the 0-junction appeared to vanish, and with the clutch disengaged, the forward effort through the clutch vanished. To resolve this problem, the clutch was modeled as a non-linear resistance bonded to the common-effort junction and the resistance was modulated by the difference in the speeds. While the motor jackshaft speed was greater than the hydraulic motor speed, the resistance was zero and no torque was transmitted. When

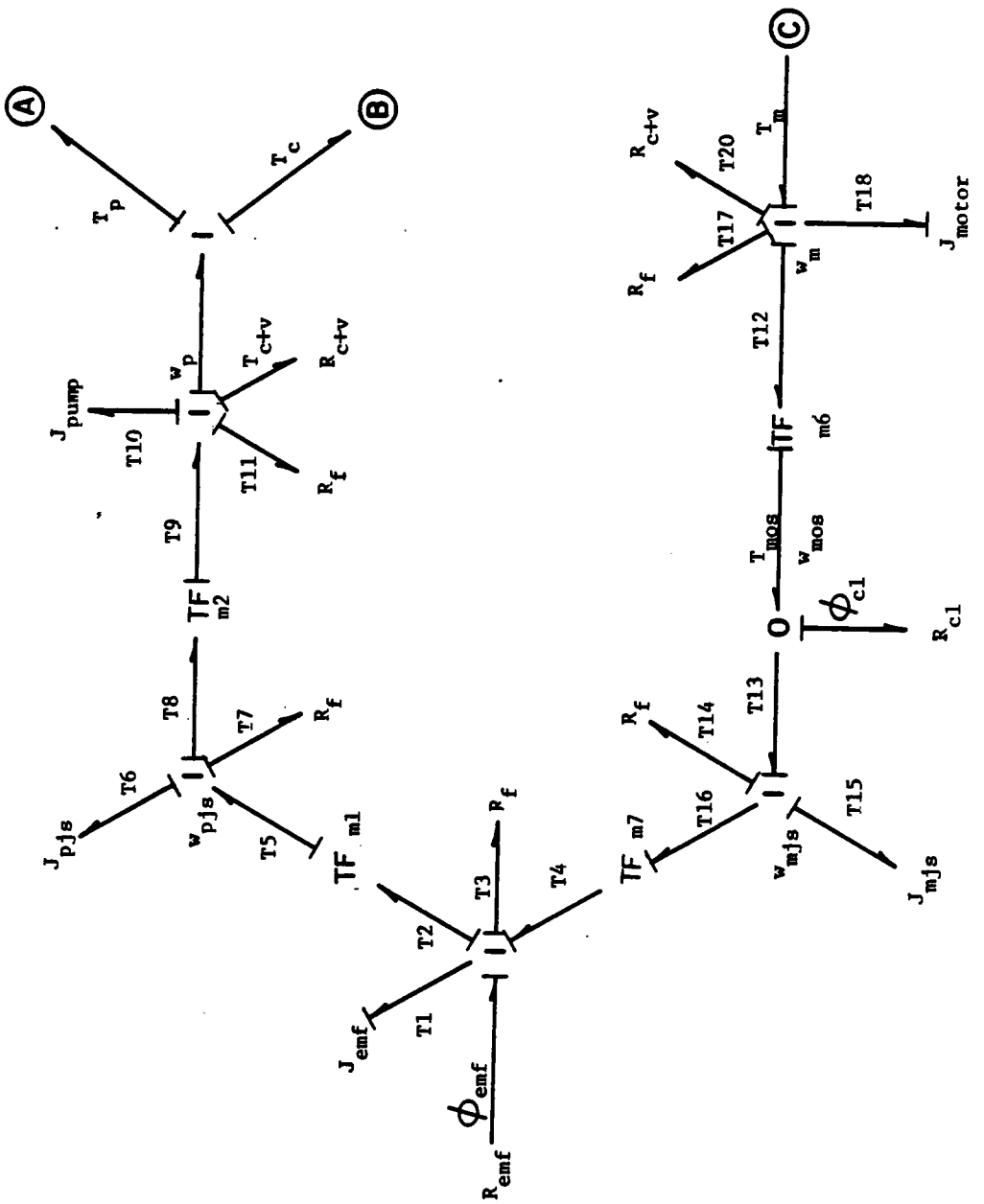

Figure 4: Mechanical transmission bond graph

the hydraulic motor speed equalled or surpassed the motor jackshaft speed, the resistance became a large finite value.

Five inertia elements were used to model the following components: pump jackshaft with sheaves on each end, motor jackshaft with sheaves on each and, armature electric motor sheave-sheave, pump rotating mass-shaft-sheave, and hydraulic motor rotating mass-shaft-sheave. Each of these was bonded to its respective common-flow junction, and a bearing resistance was also bonded to each common-flow junction.

For the electric motor, the output torque was assumed to be a function of speed. As such, the electric motor could be modeled as a non-linear resistance with the power direction away from the element, opposite the usual sense.

The other power input to the mechanical power transmission subsystem, besides the electric motor, came from the hydraulic motor. With the clutch engaged, as noted above, the hydraulic motor helped to drive the system. A bond was added to the hydraulic motor speed junction from the hydraulic motor to represent the motor output torque and speed.

The power output from this subsystem graph, other than friction losses, was the power required to drive the pump. The pump was divided into two parts, one to describe the main pump, the other for the charge pump.

Main Pump

Three pressures were of interest in the main pump. These were the supply pressure at the output side of the pump, the return pressure at the input side of the pump, and the drain pressure. These pressures were assigned to common-flow junctions, as shown in Figure 5.

The mechanical input power to the pump came through the pump shaft. A transformer, whose modulus included the product of the percent of swashplate angle and the maximum pump displacement, and the dry friction torque term, was used to convert the input torque to a pressure difference, and the input speed to a flow-rate.

The flow from the transformer was bonded to a common-flow junction. This flow represented the theoretical flow out of the supply side and also into the return side of the pump, therefore, the common-flow junction had bonds to the supply and return junctions. The effort from the transformer then represented the amount of pressure difference between supply and return. The power direction associated with these bonds was from the transformer, towards supply, and away from return.

Fluid compressibility was accounted for by bonding a storage element to each of the pressure junctions. Volumetric inefficiencies in the pump and motor were due to leak-

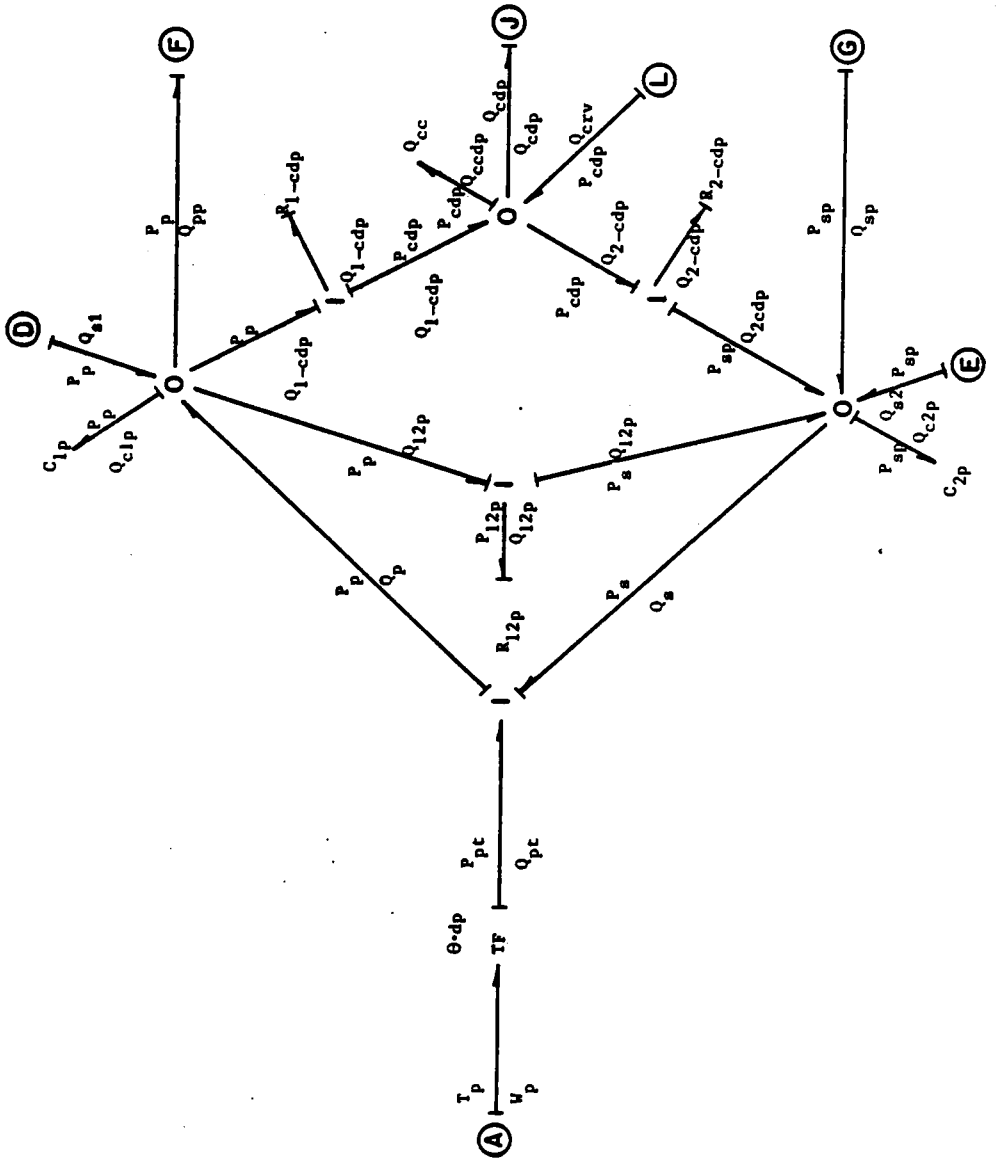

Figure 5 : Main pump bond graph

age. This leakage might be modeled by simply bonding a resistance to a pressure junction, however this would indicate a leakage path between the pressure at the bond and the reference pressure (atmospheric). In other words, it would indicate a leak outside the case. Rather, the resistance had to be bonded to a common-flow junction bonded between the two pressures. The pressure difference then caused, or was caused by, the leakage flow. All leakages were assumed to have laminar flow.

Three such leakage paths were added to the main pump. One represented the cross-port leakage directly between the supply and return pressures, the other two represented the leakage to the drain from the supply and return pressures, respectively. The direction of flow was assumed to be from the case to the return side because it was presumed that the case would have the greater pressure.

There were two hydraulic inputs to and two outputs from the main pump. One input was the return flow from the hydraulic motor, the other was the flow into the drain through the charge pump relief valve. The supply flow to the hydraulic motor, was output as well as the drain flow.

Charge Pump

The charge pump bond graph (Figure 6) was, in essence, very similar to that of the main pump. The mechanical input

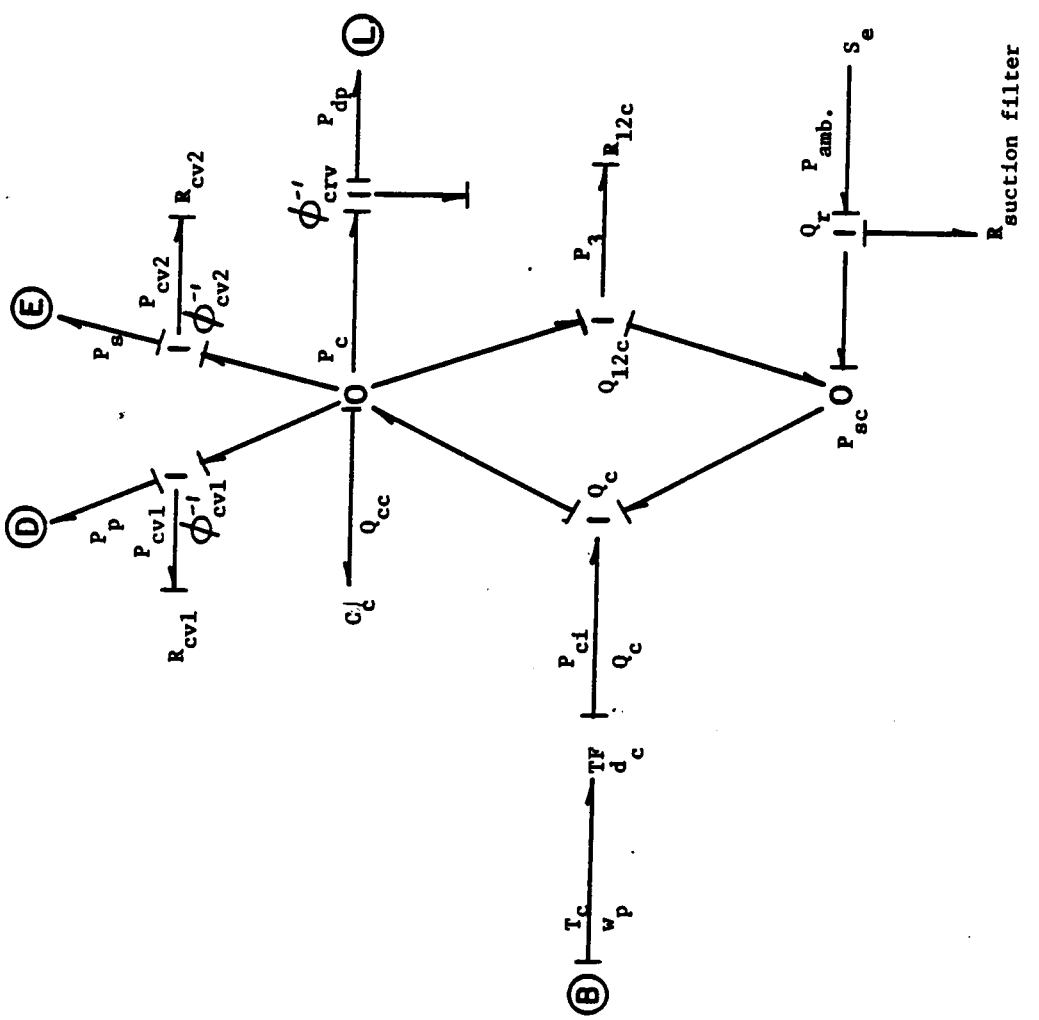

Figure 6: Charge pump bond graph

torque and speed were converted to a pressure difference and a flow-rate by means of a transformer element. Because the charge pump had a fixed displacement, the modulus of the transformer was a constant.

Two pressure junctions were established, denoting charge and suction pressure. They were bonded together to a common-flow junction at the terminus of the transformer and also by a leakage path bond. The power direction was assumed to be similar to that in the main pump.

A suction filter was used between the reservoir and the suction side of the charge pump. The effects of the pressure drop across the filter were included because there was the possibility of cavitating the charge pump. The reservoir pressure was denoted by an effort source, which had zero gage pressure. The reservoir was bonded to the suction side of the charge pump through a common-flow junction to which the resistance of the suction filter was also bonded.

The charge pressure side of the pump had a storage capacitance bonded to it to account for fluid compressibility, and to create a state variable to simplify the mathematics of the model. The flow from the charge pump had three possible flow paths; two were through check valves to the supply and return sides of the main pump to replenish leakage losses, and the other was through the charge pump

relief valve to the case. This flow served to cool the pump and motor.

The two check valves were modeled as non-linear resistances bonded to common-flow junctions between their appropriate pressures, much like one-way leakage paths. With the flow from the charge pump to either supply or return, the check valve resistance was small; when the flow reversed, the resistance was large.

The charge pump relief valve was also modeled as a non-linear resistance. This "R" element was bonded to a common-flow junction between the charge pressure and the drain pressure, and was assumed to have a two-slope curve. Below the cracking pressure the flow through the valve was very small, and above cracking pressure, the flow increased until full flow for the charge pump was attained at the full open pressure.

Hydraulic Power Transmission

This subsystem included the hydraulic hoses used to plumb the pump, motor, and relief valve. Figure 7 illustrates the three primary flow paths in this subsystem, i.e. from the supply port of the pump to the inlet side of the motor, from the outlet side of the motor to the inlet side of the pump, and from the drain port on the pump to the drain inlet port of the hydraulic motor.

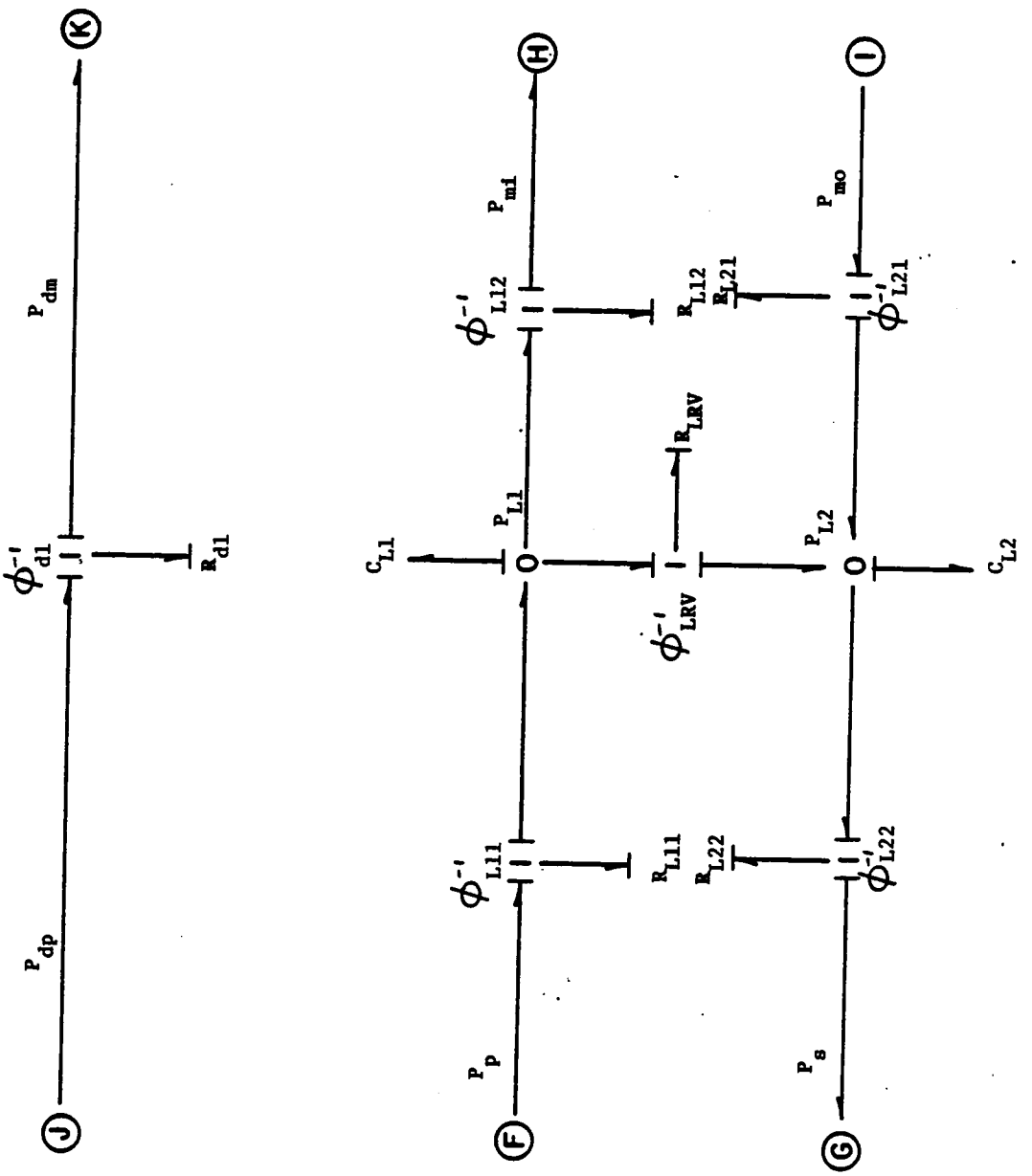

Figure 7: Hydraulic transmission bond graph

Since the pressures at the ends of the hoses were modeled in other subsystems, they were not included as O-junctions in this subsystem. The two pressures that affected the relief valve are the mid-point line pressures of the supply and return lines.

The supply line pressure was bonded to the supply pressure of the main pump and the inlet pressure of the motor. To account for line losses, these two bonds were broken, common-flow junctions inserted, and line resistances bonded to the flow junctions. This procedure lumped the pressure drops in each line into two distinct pressure drops.

Capacitance elements were bonded to both the supply line pressure and the return line pressure O-junctions. These storage elements represented the lumped capacitance due to fluid compressibility and hose compliance.

The line relief valve was modeled as a two-slope nonlinear resistance using the same procedure as the charge pump relief valve. The relief valve resistance was bonded to a common-flow junction between the supply line and return line pressure junction.

The power flow directions were assumed to be toward the motor in the supply and drain lines, and toward the pump in the return line. All resistances represented losses. The drain line itself was not deemed to have much influence on

the dynamics of the model, and was modeled much the same as the other line loss resistances.

Hydraulic Motor

The hydraulic motor was functionally the mirror image of the main pump. The motor converted fluid power back to mechanical power. Correspondingly, the motor bond graph, Figure 8, bears a great likeness to the pump bond graph.

Inlet, outlet, and drain pressures were of significance in the motor, each being denoted with a common-effort junction. Leakage paths similar to those in the main pump were added with the exception that the direction of the flow from the low pressure side to the drain was reversed in the motor. Storage elements were bonded to each of the pressure junctions to account for fluid compressibility. Each junction was also bonded to the respective end of the bonds in the hydraulic power transmission subsystem.

The inlet and outlet pressures were also bonded together through a common-flow junction. The variables on these bonds represented the effective flow and pressure difference exhibited at the output of the motor. These effective values were converted into output torque and speed by a transformer element whose modulus was the fixed displacement of the motor.

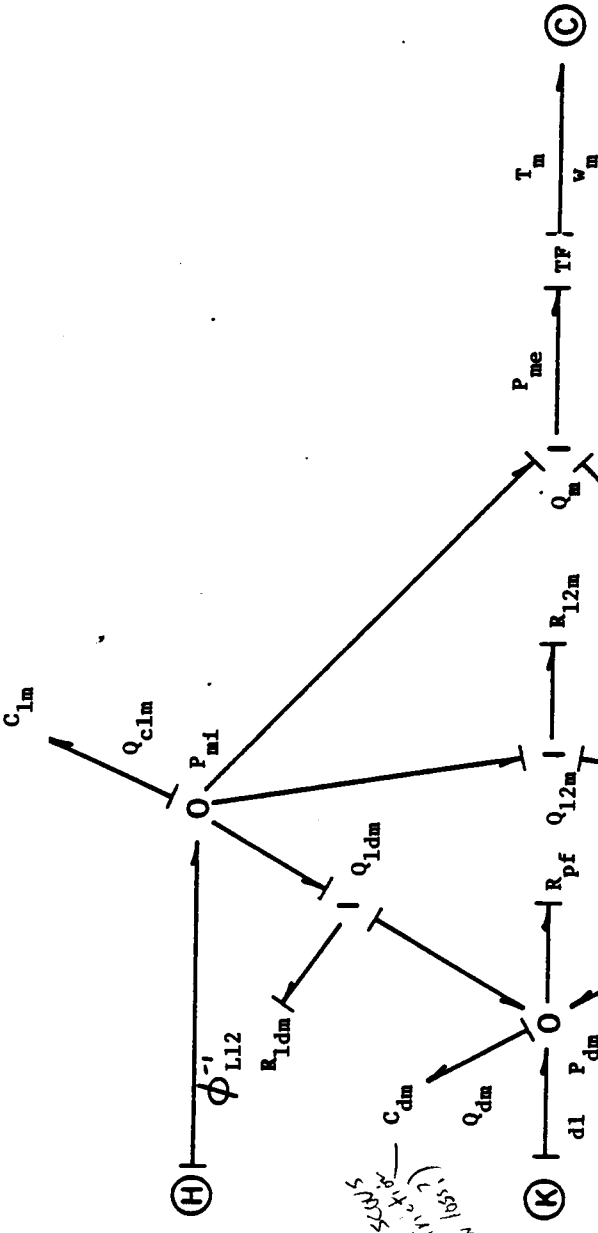

Figure 8: Hydraulic motor bond graph

The outlet drain port of the motor was fed back to the reservoir through another filter. The outlet line and the filter loss were lumped into a single resistance that was bonded to the motor drain flow junction.

Assigning Causality

Once the bond graph was laid out, it was necessary to assign causality to the bonds. Doing so defined the order of the simulation model and the relationships between the flow and effort variables for each bond in the graph.

The first step in the procedure outlined by Karnopp and Rosenberg (1975) is to assign the appropriate causality to the source elements and to propagate it as far as possible using the elemental causality rules listed above. The system modeled here had only one source, the effort source representing the ambient pressure in the reservoir. The causal strokes were placed at the end of the source bonds away from the source element to indicate the pressure was the forward effect from the reservoir. This causality could not be propagated any farther because there was no preference on the resistance at the adjacent 1-junction.

The second step was to start assigning causality to storage elements one at a time, and propagating it. Integral causality was preferred because the digital computer can integrate numerically with better results than it can differentiate.

Arbitrarily, the electric motor inertia was chosen to have integral causality. This placed the causal stroke toward the "I" element, away from the common-flow junction to which it was bonded. This implied that the flow (rotational speed) at this junction was defined by the inertia of the electric motor. This also required that all other bonds at that junction have causal strokes toward the junction. The electric motor was required to be modeled as having torque as a function of speed, even though the power direction was away from the resistance element.

The causality resulting from this initial assumption was propagated as far as the over-running clutch 0-junction in one direction, and into the 1-junctions beyond the pump displacement transformers in the other. Upon doing this, it was found that all inertias except those of the motors had derivative causality. This indicated, as can be seen by inspection, that these inertias were not independent. The torques on each of these inertias were dependent on the electric motor speed, modulated by the various sheave ratio transformers.

The forward effect into both pumps was discovered to be flow, i.e. speed, which was consistent with Wilson's models. The second storage element assumed to have integral causality was the hydraulic motor inertia. The resulting

causality was propagated first to the remaining bonds attached to the common-flow junction, then back through the hydraulic motor displacement transformer. This established that the forward effect out of the hydraulic motor was torque, again consistent with Wilson's models.

Propagating causality through the sheave ratio transformer in the other direction terminated in designating that the over-running clutch would have its torque defined as a function of the two motor speeds. This seems reasonable because torque could ideally be transmitted by the clutch only when the input speed equalled or slightly exceeded the output speed. After assigning the clutch causality, the possible definitions based on the second assumption were exhausted.

The nine remaining storage elements were all capacitances bonded to common-effort junctions. Every capacitance 0-junction was separated from each of its 0-junction neighbors by a resistance bonded to a 1-junction. It can be easily shown that all nine capacitances with integral causality were linearly independent. Assigning integral causality to a capacitance implies that the capacitance effort defines the effort in each of the adjacent bonds. Two such bonds entering a common-flow junction to which only a resistance is bonded will require the resistance to have an effort for-

ward effect, thus avoiding a causal conflict and maintaining the independence of the capacitance efforts.

By assigning integral causality to all the capacitances and propagating, all line and leakage resistances were forced to have effort as a forward effect, except the cross-port leakage in the charge pump and the suction filter resistance, which were still unassigned. In other words, the leakage and line flows were to be driven by the pressure differentials they experienced, rather than vice versa.

The third step, described by Karnopp and Rosenberg (1975), involved the arbitrary assignment of the causality of one of the remaining resistances. It had to be employed because the first two steps had failed to complete the process. The cross-port leakage resistance in the charge pump was assumed to have effort as its forward effect to be consistent with all the other leakage resistances. Propagating this causality ended in assigning the suction filter with flow as its forward effect, opposite that of the pressure filter causality. This difference arose from the exclusion of a capacitance on the charge pump suction pressure junction. Had this capacitance not been omitted, no arbitrary assignments would have had to have been made.

The assignment of causality was thus accomplished, and the augmented bond graph is shown in Figure 9. The resulting system was found to have eleven independent integrals.

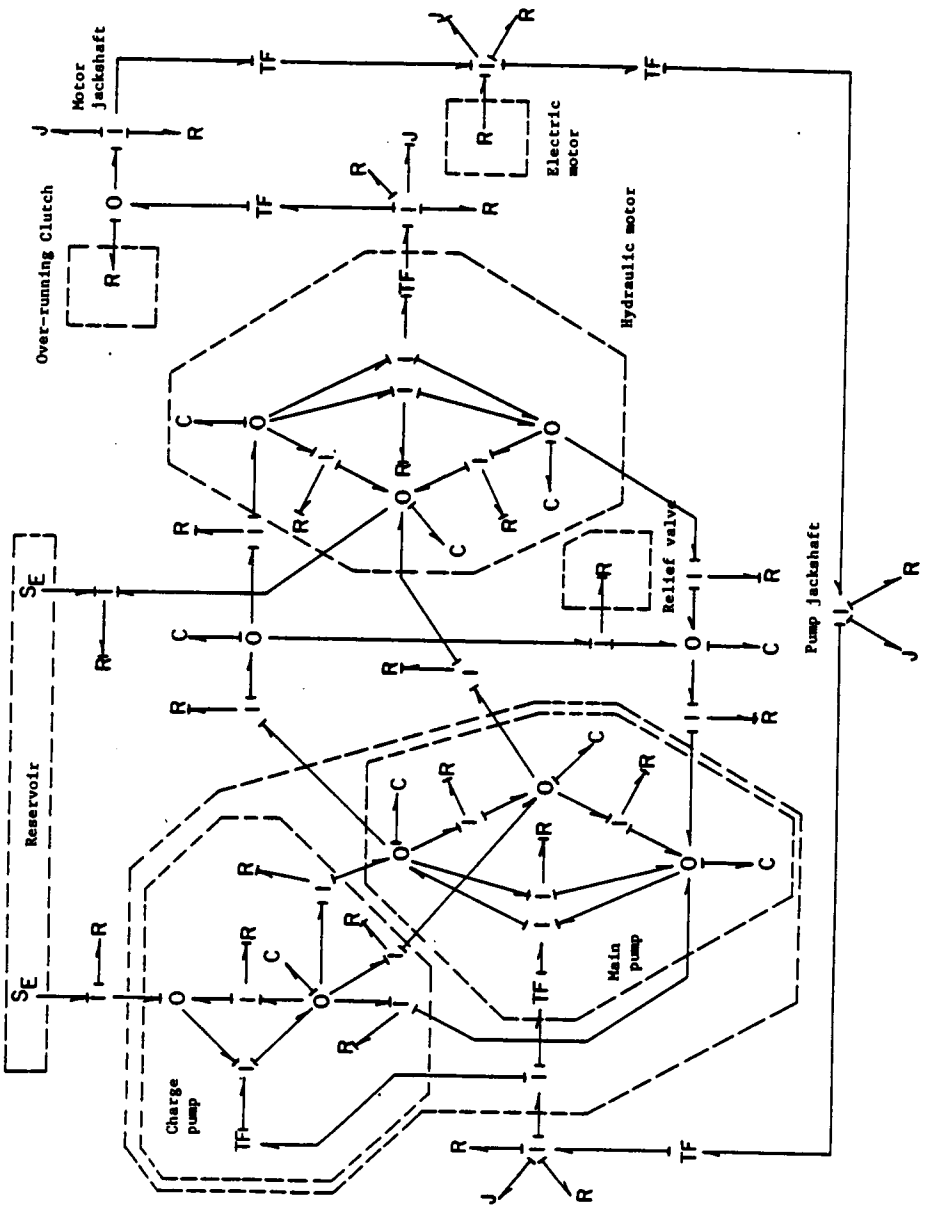

Figure 9: Completed bond graph

Model Development

Once the bond graph had been completed, the next step was to distill from it the equations it represented. Not all of the equations described by the bonds were significant, only those that were necessary to define the states of the system. The "state" variables are those by which all other variables in the system are defined. The number of "states" in this causal system is determined by the number of linearly independent integrals in the system.

The system modeled had eleven storage elements with integral causality, therefore it could have been written as one eleventh order equation, eleven first order equations, or any combination of equations whose orders summed to eleven. The approach taken was to use eleven first order equations to maintain simplicity.

The method used to develop the state equations was similar to that described in Karnopp and Rosenberg (1975). They suggest the use of energy variables, displacement and momentum, on the storage elements with integral causality as state variables, i.e. the "p" variable on "I" elements and the "q" variable on "C" elements. The "e" variable on integral "I" elements would then be replaced by a "$\dot{p}$" for the "C" elements, "$\dot{q}$" would replace "f".

Each state variable would be solved for in terms of energy variables. This would be accomplished by using the constitutive relations to develop the equations for each forward effect in the integral causality elements as functions of the state variables. The result would be a set of equations of the form:

$$d(p \text{ or } q)/dt = \Phi \text{ (state variables, inputs)}$$

Integrating each equation yields the states as energy variables. The system power variables could then be found by dividing by the appropriate inertance or capacitance.

$$e = q / C \quad \text{and} \quad f = p / I$$

The energy variables were not informative in the system modeled. The displacement of the electric motor, for example, was not as desirable as its speed, nor the volume of the supply line as enlightening as its pressure. Therefore, the states were defined in terms of power variables, effort and flow. For inertances, the "f" variables were the state, and for capacitances, the "e" variables. The derivation for a capacitance element is similar to the following one for an inertance element. From above,

$$F = p / I$$

$$e = \dot{p}$$

$$p = \Phi \text{ (state variables, inputs)}$$

Then $$f = \int (\dot{p} / I) \, dt$$

and $$f = \int (\Phi \text{ (state variables, inputs)} / C) \, dt$$

For a capacitance,

$$e = \int (\Phi \text{ (state variables, inputs)} / C) \, dt$$

With this procedure, the state variables were defined as power variables.

Electric Motor Speed

The state equation for the electric motor inertia was the most complicated equation to be derived because of the inertias coupled to it. Figure 4 shows the mechanical power transmission subsystem bond graph with the labelled bonds that were used in the following derivation.

Using the constitutive relationship for an inertia, the electric motor speed is defined by:

$$\omega_1 = \int (T1 / J_{emf}) \, dt \qquad (1)$$

or $$\dot{\omega}_1 = T1 / J_{emf} \qquad (2)$$

(See Appendix A for a complete listing of variables).

At the 1-junction, T1 is determined by summing the efforts (torques).

$$T1 = \Phi_{emf} - T2 - T3 + T4 \tag{3}$$

where Φ_{emf} - torque output from electric motor (N-m)

T2 - torque output to pump jackshaft (N-m)

T3 - friction torque in electric motor (N-m)

T4 - torque input from motor jackshaft (N-m)

The torque delivered to the pump jackshaft is given by:

$$T2 = m1\ T5 \tag{4}$$

where T5 is the transferred torque from electric motor and is given by:

$$T5 = T6 + T7 + T8 \tag{5}$$

where T6 - torque input to motor jackshaft inertia (N-m)

T7 - friction torque in pump jackshaft (N-m)

T8 - torque output to pump shaft (N-m)

These terms are:

$$T6 = J_{pjs}\ \dot{\omega}_{pjs} = J_{pjs}\ m1\ \dot{\omega}_1 \tag{6}$$

$$T7 = 5\ R_f\ \omega_{pjs} = 5\ R_f\ m1\ \omega_1 \tag{7}$$

$$T8 = m2\ T9 \tag{8}$$

The transmitted torque from pump jackshaft to the pump driveshaft is given by:

$$T9 = T10 + T1 + T_c + T_v + T_p + T_{CP} \tag{9}$$

where T10 - torque input to pump inertia (N-m)

T11 - friction torque in pump shaft (N-m)

T_c - constant friction torque (N-m)

T_v - viscous drag torque (N-m)

T_p - torque required by main pump (N-m)

T_{CP} - torque required by charge pump (N-m)

These terms are defined by:

$$T10 = J_{pump}\ \dot{\omega}_p = J_{pump}\ m2\ m1\ \dot{\omega}_1 \tag{10}$$

$$T11 = 3\ R_f\ \omega_p = 3\ R_f\ m2\ m1\ \omega_1 \tag{11}$$

$$T_c = R_c \tag{12}$$

$$T_v = R_v\ \nu \tag{13}$$

$$T_{CP} = d_c\ (P_c - P_{sc}) \tag{14}$$

Based on Wilson's equations, the torque of the pump is the sum of the torques that 1) go directly into developing the pressure rise, 2) are lost to friction, primarily between the slippers and the swashplate, 3) are lost to viscous drag, and 4) are lost to a constant resistance. The latter two were accounted for by the T_c and T_v torque terms in equation (12).

The first two terms in Wilson's pump torque equation were factored for pressure drop and maximum displacement, and $\alpha\ D_{pmax}$ substituted for D_p.

$$T_p = \Delta P \, D_{pmax} \, [\alpha + C_{fp}/(1 - \tan \theta \,] \tag{15}$$

In the bond graph sense, the last term of the equation is the modulus of the pump transformer.

An expression for T9 is obtained by substituting eqs. (10), (11), (12), (13), (14) and (15) into eq. (9). This result replaces T9 in eq. (8) to yield:

$$\begin{aligned} T8 = m2 \; \{ & J_{pump} \; m2 \; m1 \; \dot{\omega}_1 + 4 \; R_f \; m2 \; m1 \; \omega_1 \\ & + R_c + R_v \; \nu + [\alpha + C_{fp}/(1-\tan\theta)] \; d_p \; (P_p - P_s) \\ & + d_c \; (P_c - P_{sc}) \} \end{aligned} \tag{16}$$

All the terms to solve for T2 have now been determined. Substituting eqs. (6), (7) and (16) into eq. (5) yields T5, which when substituted into eq. (4) gives:

$$\begin{aligned} T2 = m1 \Big(& J_{pjs} \; m1 \; \omega_1 + 5 \; R_f \; m1 \; \omega_1 \\ & + m2 \; \{ J_{pump} \; m2 \; m1 \; \omega_1 + 3 \; R_f \; m2 \; m1 \; \omega_1 + R_c \\ & + R_v \; \nu + [\alpha + C_{fp} \; /(1-\tan\theta)] \; d_p \; (P_p - P_s) \\ & + d_c \; (P_c - P_{sc}) \} \Big) \end{aligned} \tag{17}$$

The friction torque in the electric motor, and the input torque from the motor jackshaft are, respectively:

$$T3 = 2 \; R_f \; \omega_1 \tag{18}$$

$$T4 = m7 \; T16 \tag{19}$$

The torque transferred to the electric motor is given by:

$$T16 = T13 - T14 - T15 \tag{20}$$

where T13 - torque transferred through clutch (N-m)

T14 - friction torque in motor jackshaft (N-m)

T15 - torque input to motor jackshaft inertia (N-m)

These terms are defined by:

$$T13 = \Phi_{cl} \tag{21}$$

$$T14 = 2\ R_f\ \omega_{mjs} = 2\ R_f\ m7\ \omega_1 \tag{22}$$

$$T15 = J_{mjs}\ \dot{\omega}_{mjs} = J_{mjs}\ m7\ \dot{\omega}_1 \tag{23}$$

Now substituting eqs. (21), (22) and (23) into eq. (20), then into eq. (19), we obtain:

$$T4 = m7\ (\Phi_{cl} - 2\ R_f\ m7\ \omega_1 - Jmjs\ m7\ \dot{\omega}_1) \tag{24}$$

The equation for ω_1 is determined by substituting eqs. (17), (18) and (24) into eq. (3) to give T1; then, by replacing T1 in eq. (2),

$$\begin{aligned}\dot{\omega}_1 = (1/J_{emf}) \Big(&\Phi_{emf} - J_{pjs}\ m1^2\ \omega_1 + 5\ R_f\ m1^2\ \omega_1 \\ &+ m1\ m2\ \{J_{pump}\ m2\ m1\ \omega_1 + 3\ R_f\ m2\ m1\ \omega_1 + R_c \\ &+ R_v\ \nu + [\alpha + C_{fp}/(1-\tan\theta)]\ d_{pmax}\ (Pp-Ps) \\ &+ d_c\ (P_c - P_{sc})\} + m7(\Phi_{cl} - 2\ R_f\ m7\ \omega_1 \\ &- J_{mjs}\ m7\ \omega_1)\Big)\end{aligned} \tag{25}$$

Solving for $\dot{\omega}_1$, and putting the electric motor speed equation into integral form gives:

$$\omega_1 = \int \{ \Phi_{emf} + m7\ \Phi_{c1} - R_f\ \omega_1\ [(3\ m2^2 + 5)m1^2 + 1 + 3\ m7^2] - m1\ m2\ (R_c + R_v \nu) - m1\ m2\ d_c\ (P_c - P_{sc}) - m1\ m2\ [\alpha + C_{fp}/(1-\tan\theta)]\ d_{pmax}\ (P_p - P_s) \} / J_{lump}\ dt \qquad (26)$$

where the inertia terms have been combined into a single inertia given by:

$$J_{lump} = J_{emf} + J_p m1^2\ m2^2 + J_{mjs} m7^2 + J_{pjs} m1^2 \qquad (27)$$

Hydraulic Motor Speed

The hydraulic motor inertia had no other inertias dependent upon its speed, so no implicit relations developed. The derivation for this state equation was, therefore, more straight forward. The hydraulic motor speed is defined by:

$$\omega_m = \int (T18 / J_{motor})\ dt \qquad (28)$$

or

$$\dot{\omega}_m = T18 / J_{motor} \qquad (29)$$

T18 is determined by summing the efforts (torques) at the 1-junction.

$$T18 = T_m - T12 - T17 - T_c - T_v \qquad (30)$$

where T_m - torque output from hydraulic motor (N-m)

T12 - torque output to over-running clutch (N-m)

T17 - friction torque in hydraulic motor (N-m)

T_c - constant friction torque (N-m)

T_v - viscous drag torque (N-m)

The torque output from the hydraulic motor is:

$$T_m = d_m \left[1 - C_{fm}/(1 - \tan 15°)\right] P_{me} \tag{31}$$

where P_{me} is the effective pressure difference in hydraulic motor and is given by:

$$P_{me} = P_{mi} - P_{mo} \tag{32}$$

where P_{mi} - hydraulic motor inlet pressure (MPa)

P_{mo} - hydraulic motor outlet pressure (MPa)

Substituting eq. (32) into eq. (31) gives motor torque, Tm, as a function of state variables.

$$T_m = (P_{mi} - P_{mo})\, d_m \left[1 - C_{fm}/(1 - \tan 15°)\right] \tag{33}$$

Note that the expression for T_m is similar to T_p, [eq. (15)], with the exception that the motor swashplate angle equals 15° and is a constant. The other terms are defined below.

$$T12 = m6\, \Phi_{cl} \tag{34}$$

where Φ_{cl} - torque transmitted through over-running clutch (N-m)

$$T17 = 3\ R_f\ \omega_m \tag{35}$$

$$T_c = R_c \tag{36}$$

where R_c - constant torque in pump or hydraulic motor (N-m)

$$T_v = R_v\ \nu \tag{37}$$

where R_v - viscous drag torque in pump or hydraulic motor (N-m)

Substituting eqs. (33), (34), (35), (36) and (37) into eq. (30) and the result into eq. (28), gives the state equation for the hydraulic motor speed.

$$\omega_m = \int \{d_m\ [1-C_{fm}/(1-\tan 15°)]\ (P_{mi}-P_{mo}) - m6\ \Phi_{cl} - 3\ R_f\ \omega_m - R_c + R_v\ \nu\} / J_{motor}\ dt \tag{38}$$

Main Pump Supply Pressure

As in the case of assigning causality, there is a great similarity among the derivations of the state equations for the nine capacitances. The development is also analogous to that previously described for the inertias. Therefore, the procedure will be demonstrated for the main pump outlet

pressure and only the state equations shown for the other capacitances.

The main pump outlet pressure was defined by the integral capacitance relationship.

$$P_p = \int q_{clp} / C_{lp} \; dt \tag{39}$$

or $$\dot{P}_p = q_{clp} / C_{lp} \tag{40}$$

The equation for q_{clp}, the flow into the pump supply pressure capacitance, is determined by summing the flows at the 0-junction.

$$q_{clp} = q_p + q_{sl} - q_{ldp} - q_{l2p} - q_{pp} \tag{41}$$

where
- q_p - theoretical flow from the main pump (L/min)
- q_{sl} - flow through check valve 1 (L/min)
- q_{ldp} - leakage flow to the pump drain (L/min)
- q_{l2p} - cross-port leakage flow (L/min)
- q_{pp} - actual flow from the main pump (L/min)

Again, defining each of these flows defines q_{clp}. The theoretical flow from the main pump is given by:

$$q_p = d_{pmax} \; \alpha \; \omega_p = d_p \; \alpha \; m2 \; m1 \; \omega_1 \tag{42}$$

where
- d_{pmax} - maximum displacement of main pump (2.38×10^{-6} m^3/rad)
- α - displacement of pump swashplate (decimal)

The various flows are defined by:

$$q_{sl} = \Phi_{cvl}^{-1}(P_c - P_p) \tag{43}$$

$$q_{ldp} = (P_p - P_{dp})/R_{ldp} \tag{44}$$

$$q_{l2p} = (P_p - P_s)/R_{l2p} \tag{45}$$

$$q_{pp} = \Phi_{Ll1}^{-1}(P_p - P_{Ll}) \tag{46}$$

where
- P_p - main pump outlet pressure (MPa)
- P_c - charge pump outlet pressure (MPa)
- P_{dp} - pump drain pressure (MPa)
- P_s - main pump return pressure (MPa)
- P_{Ll} - supply line hose pressure (MPa)
- Φ_{cvl}^{-1} - nonlinear flow in check valve 1 (L/min)
- Φ_{Ll1}^{-1} - nonlinear flow in supply line (L/min)

Substitution of eqs. (42), (43), (44), (45) and (46) into eq. (41) gives the equation for q_{clp}, which when substituted into eq. (39) gives the state equation for the main pump outlet pressure.

$$P_p = \int [d_{pmax}\ \alpha\ m2\ m1\ \omega_1 + \Phi_{cvl}^{-1}(P_c - P_p) - (P_p - P_{dp})/R_{ldp} - (P_p - P_s)/R_{l2p} \Phi_{Ll1}^{-1}(P_p - P_{Ll})] / C_{lp}\ dt \tag{47}$$

The other eight state equations were similarly derived and are listed below.

Main Pump Return Pressure

$$P_s = \int \{ -d_{pmax} \alpha \, m2 \, m1 \, \omega_1 + \Phi_{cv2}^{-1}(P_c - P_s) + (P_p - P_{dp})/R_{1dp} + (P_p - P_s)/R_{12p} + \Phi_{L22}^{-1}(P_p - P_{L1}) \} / C_{2p} \, dt \quad (48)$$

Main Pump Drain Pressure

$$P_{dp} = \int [\Phi_{crv}^{-1}(P_c - P_{dp}) + (P_p - P_{dp})/R_{1dp} + (P_s - P_{dp})/R_{2dp} - \Phi_{d1}^{-1}(P_{dp} - P_{dm})] / C_{dp} \, dt \quad (49)$$

Charge Pump Outlet Pressure

$$P_c = \int [d_c \, m2 \, m1 \, \omega_1 - \Phi_{cv1}^{-1}(P_c - P_p) - \Phi_{cv2}^{-1}(P_c - P_s) - \Phi_{crv}^{-1}(P_c - P_{dp}) - q_{12c}] / C_c \, dt \quad (50)$$

Supply Line Hose Pressure

$$P_{L1} = \int [\Phi_{L11}^{-1}(P_p - P_{L1}) - \Phi_{L12}^{-1}(P_{L1} - P_{mi}) - \Phi_{1rv}^{-1}(P_{L1} - P_{L2})] / C_{L1} \, dt \quad (51)$$

Return Line Hose Pressure

$$P_{L2} = \int [\Phi_{L21}^{-1}(P_{mi} - P_{L2}) - \Phi_{L22}^{-1}(P_{L2} - P_s) + \Phi_{1rv}^{-1}(P_{L1} - P_{L2})] / C_{L2} \; dt \quad (52)$$

Hydraulic Motor Inlet Pressure

$$P_{mi} = \int [-d_m \omega_m + \Phi_{L12}^{-1}(P_{L1} - P_{mi}) - (P_{mi} - P_{dm})/R_{1dm} - (P_{mi} - P_{mo})/R_{12m}] / C_{1m} \; dt \quad (53)$$

Hydraulic Motor Outlet Pressure

$$P_{mo} = \int [d_m \omega_m - \Phi_{L21}^{-1}(P_{mo} - P_{L2}) - (P_{mo} - P_{dm})/R_{2dm} + (P_{mi} - P_{mo})/R_{12m}] / C_{2m} \; dt \quad (54)$$

Hydraulic Motor Drain Pressure

$$P_{dm} = \int [(P_{mi} - P_{dm})/R_{1dm} + (P_{mo} - P_{dm})/R_{2dp} - P_{dm}/R_{pf} + \Phi_{dl}^{-1}(P_{dp} - P_{dm})] / C_{dm} \; dt \quad (55)$$

Charge Pump Suction Pressure

The charge pump suction pressure resulted in an implicit function because one of the resistances had arbitrary causality. The suction pressure is defined by the pressure drop across the filter.

$$P_{sc} = P_{amb} - q_r R_{sf} \tag{56}$$

where q_r - flow through the suction filter

This flow is given by:

$$q_r = q_c - q_{12c} \tag{57}$$

where q_c - theoretical flow from the charge pump (L/min)

q_{12c} - cross-port leakage in charge pump (L/min)

Now, $$q_c = d_c \omega_p \tag{58}$$

and $$q_{12c} = (P_c - P_{sc})/R_{12c} \tag{59}$$

Substituting eqs. (58) and (59) into eq. (57), then into eq. (56), gave:

$$P_{sc} = P_{amb} - R_{sf} [d_c \omega_1 \, m1 \, m2 - (P_c - P_{sc})/R_{12c}] \tag{60}$$

Solving eq. (58) for P_{sc} we obtain:

$$P_{sc} = P_{amb} - R_{sf} (d_c \omega_1 \, m1 \, m2 - P_c - R_{12c}) / (1 + R_{sf}/R_{12c}) \tag{61}$$

Equation Development Summary

The state equations developed above include Wilson's equations for the steady-state response and Merritt's for the dynamic response. Wilson's describe the torque equations more fully, and Merritt's the leakage flows. The combination of the two is offered as a complete model of the hydrostatic drive.

SIMULATION MODEL

The digital simulation of the state equations developed above was implemented on an IBM 370 mainframe computer using ACSL. ACSL removed some of the programming overhead that would have been required by strictly FORTRAN subroutines, such as those provided in the International Mathematical and Statistical Libraries (IMSL). The ACSL source program is written in a more understandable format because it was sorted before it is compiled. The documented listing of the program is included as Appendix C.

A variable step-size Gear's Stiff integration scheme, selected by the statement ALGORITHM in the program, was utilized because it allows systems with greatly differing time constants to be integrated more efficiently. It was felt that the difference in time constants, between the large mass attributed to the electric motor and the small capacitance of the charge pump, warranted such an approach. Furthermore, the variable step size reduced the computation time needed to predict the steady-state conditions by allowing the integration step size to increase as the transients in the system damped out. The maximum step size, set by MAXTERVAL, was increased from the default value of 1.0×10^{-4} to 1.0×10^{-2} seconds to take advantage of this capability.

The INITIAL section of the program assigns values to constants and evaluates variables that will not change during program execution. The DYNAMIC section contains the DERIVATIVE section, in which the integrals are computed, and the output statements that need to occur at each communications interval. The statements in the DERIVATIVE section are evaluated at each integration time step. The expressions for the state variable time derivatives were used in the integration statements to reduce the number of variables evaluated. The integration equations are designated by "INTEG" statements in the program listing.

FORTRAN statements and subroutines are allowed in ACSL, but are not included in ACSL error diagnostics. WRITE statements were used in the INITIAL and DYNAMIC section to output the desired variables more conveniently than with the available ACSL statements. A FORTRAN subroutine was used to compute the the non-linear flow-rate as a function of pressure, rather than defining an ACSL PROCEDURAL block that would have required a much longer argument list.

Steady-State Swashplate Simulation

To obtain steady-state values with the dynamic model, the simulation was run with a ramping step-type function for the swashplate angle. This angle as a function of time was called "STHET" in the program. The angle was held at zero

for the first five seconds of simulation to allow the start-up transients to damp out, then every ten seconds the swashplate angle was ramped up 0.5 degrees in 0.5 seconds. The angle was then held at that level for the duration of ten seconds and the predictions recorded at the end of the interval.

Dynamic Swashplate Simulation

The simulation of the system with a continuously varying swashplate angle was accomplished by replacing the ramping-step function with a sinusoidal function. An attempt was also made to model the actual four-bar linkage using the equations developed by Shigley (1969), however, the large increase in computation time did not justify the small increase in accuracy. The displacement of the sinusoidal swashplate angle function was offset from zero by one-half of the desired magnitude to limit the angle to non-negative values. It was also displaced in time by one-half a period so that the angle would increase smoothly from zero and not create an initial step.

MODEL PARAMETER TESTS

Tests were conducted to estimate the model parameters for the purpose of simulation. The hydrostatic test stand was instrumented to measure pump and motor output flows, pump jackshaft speed and torque, hydraulic motor and motor jackshaft speeds, and fluid temperature. The model parameter tests are described and the results included in this section rather than in the Results section to simplify the organization of the thesis.

Unverified Component Models

Even the available instrumentation, some components were internal to the pump case, making the measurement of their performace characteristics impossible. For the electric motor, the facilities for testing were not available. In all, the characteristics of five system components were not experimentally determined. These included the electric motor, the line relief valve, the charge pump relief valve, and the check valves.

Electric Motor Model

The characteristics for the 7.5 kW (10 hp) single phase electric motor, whose rated speed was 1750 rpm, were estimated from a typical electric motor speed-torque curve given in Smith (1976), and are shown in Figure 10. The rated tor-

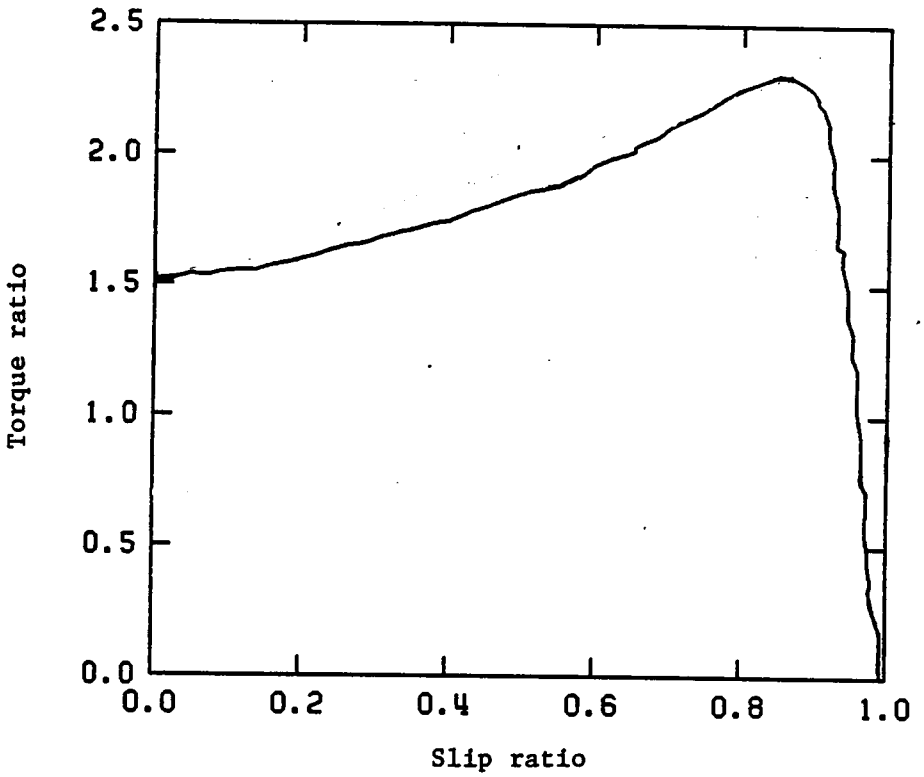

Figure 10: Typical torque vs slip curve for an AC induction motor (from Figure 25.21 in Smith, 1976)

que for the motor was 40 N-m, giving a stall torque of 60 N-m, and a peak torque of 90 N-m. From these values, and a no-load speed of 188.5 rad/s, the speed-torque curve was linearized to two straight line segments intersecting at the peak torque, break-over speed point. The equations for these segments are:

$$\Phi_{emf} = 60.0 + 0.1697\ \omega_1 \quad \text{for } \omega_1 < 176.8 \tag{61}$$

$$\Phi_{emf} = 1450.0 - 7.6923\ \omega_1 \quad \text{for } \omega_1 \geq 176.8 \tag{62}$$

where the units for Φ_{emf} are N-m and rad/s for ω_1.

Line Relief Valve

A line relief valve was installed between the midpoints of the supply and return lines. It was included in the bond graph and the model equations; however, it was installed in the system only for saftey purposes. It was not meant to be a continuously operating component of the system, and as such, its chacteristics were omitted from the model.

Charge Pump Relief Valve

The charge pump maintained a minimum pressure in the return line to prevent cavitation in the main pump. This was accomplished by porting the charge pump outlet through a check valve to the return line to restore the volume lost to leakage, and dumping the excess flow into the case. The

only evidence of the existence and operation of this valve was the return line pressure.

Literature from Sundstrand Corporation, the manufacturer of the hydraulic pump and motor, gave the relief valve setting in the range of 0.827 MPa to 1.240 MPa. The fully open pressure was asssumed to be 1.034 MPa, the middle of the range. The cracking pressure was arbitrarily assumed to be 0.689 MPa.

At the maximum speed of 4000 rpm, the charge pump flow would theoretically be 21.6 L/min. It was assumed that the fully open pressure would be developed at the maximum flow.

The partially open characteristics of the relief valve were linearized between the maximum pressure-flow point and the cracking pressure-zero flow point. The resulting relationships of flow as functions of pressure are:

$$\Phi_{crv}^{-1} = \Delta P/1.0 \times 10^{20} \qquad \text{for } \Delta P < 0.689 \qquad (64)$$

$$\Phi_{crv}^{-1} = 34.77\ \Delta P - 24.0 \qquad \text{for } \Delta P \geq 0.689 \qquad (65)$$

where the units for q are L/min and MPa for ΔP.

Charge Pump Check Valves

The actual operating parameters of the charge pump check valves were not deemed important to the system and were modeled as closely to the ideal as was practical. With a forward pressure, resistance was small; a reverse pressure caused the resistance to greatly increase.

The relationships assumed were:

$$\Phi_{cv}^{-1} = \Delta P/1.0 \times 10^{20} \qquad \text{for } \Delta P < 0.0 \qquad (66)$$

$$\Phi_{cv}^{-1} = \Delta P/0.01 \qquad \text{for } \Delta P \geq 0.0 \qquad (67)$$

where the units for q are L/min and MPa for ΔP.

Shaft Inertias

Estimates of the inertias of the sheaves were made from approximations of their cross-sections and the density for steel, 78.3 Mg/m^3 (Popov, 1976). The cross-section for each sheave was segmented, the polar moment of inertia calculated, and the parallel axis theorem used to translate the inertia about the central axis. The 47.2 cm. sheave had an inertia of 0.80 $kg\text{-}m^2$, the 34.0 cm. sheave 0.36 $kg\text{-}m^2$, the 10.7 in. sheaves 0.005 $kg\text{-}m^2$ each, the 12.7 cm. sheave 0.007 $kg\text{-}m^2$, and the 21.8 cm. sheaves 0.11 $kg\text{-}m^2$ each.

Fluid Properties

The characteristic properties of the transmission fluid (Texaco fluid 9226, code number 1841), dynamic viscosity and density, were determined from experimental data and empirical relationships. Both are functions of temperature, and were calculated from the measured temperature.

Temperature Measurement

The temperature of the fluid was determined with a thermistor probe. The device was placed at different times in the reservoir, the motor drain outlet, and the pump return port. The probe electrical resistance decreased as its temperature increased in a manner that was well described by a conic curve. The equation describing temperature as a function of resistance was assumed to have the following form, which, when solved for the coefficients, gave:

$$T = d\,R + e - (a + b\,R + c\,R^2)^{1/2} \qquad (68)$$

where T - temperature (°C)

R - electrical resistance (kohms)

a - -2077.423

b - 4681.344

c - 498.4451

d - 21.7356

e - 100.1315

Kinematic Viscosity

Three temperature-kinematic viscosity data points were received from Texaco for the fluid used in the system. These were plotted, a smooth curve drawn through them, and two additional points obtained by arbitrarily selecting two

temperatures between the data points and estimating their corresponding viscosities. A curve closely agreeing with the drawn curve was fit through the five points. The resulting relationship for kinematic viscosity dependent on temperature was:

$$\nu = d\ T + e - (a + b\ T + c\ T^2)^{1/2} \qquad (69)$$

where ν - dynamic viscosity (cSt)

T - temperature (C)

a - 0.39780×10^6

b - 0.26496×10^5

c - 0.19692×10^4

d - -0.44183×10^2

e - -0.34290×10^3

Density

The specific gravity given by Texaco was 31.4 API degrees. The following equation (Binder, 1972) was used to convert API degrees to specific gravity.

$$\text{Sp. gr.}|_{15.6°C} = 141.5 \ / \ (\text{API}° + 131.5) \qquad (70)$$

This gave a specific gravity of 0.869. The assumed density was then 869 kg/m^3 at 15.6 °C. The equation relating density to temperature was taken from Shortley and Williams (1971).

$$\rho = \rho_{ref} [1 - \beta_{den} (T - T_{ref})] \quad (71)$$

where ρ - density (kg/m^3)

T - temperature (C)

T_{ref} - reference temperature = 15.6 °C

ρ_{ref} - reference density = 869 kg/m^3

β_{den} - expansion coefficient = 1.0 x 10^3 1/°C

Capacitances

Merritt (1967) gives the equation for computing the capacitance of a fluid due to its compressibility as:

$$C = V / \beta_e \quad (72)$$

where C - capacitance (m^3/MPa)

V - volume (m^3)

β_e - effective bulk modulus = 690 MPa

He also recommended using a β_e of 690 MPa if no better estimate was available.

The largest capacitances in the system were the supply and return lines. They were computed as:

$$C_L = [(0.127 \text{ m})^2 (2.04 \text{ m}) \pi/4] / 690 \quad (73)$$
$$= 3.75 \times 10^{-7} \text{ m}^3/\text{MPa}$$

The capacitances of the pump and hydraulic motor chambers were taken to be constant even though the pump capaci-

tances were functions of swashplate angle. Half of the displacement per revolution was attributed to each side on both the pump and the motor.

$$C_{1P} = (0.913 \text{ in}^3/\text{rev}) (0.0254 \text{ m/in})^3 / 690 \quad (74)$$
$$= 1.085 \times 10^{-8} \text{ m}^3/\text{MPa}$$

and $$C_{1P} = C_{2P} = C_{1M} = C_{2M}$$

The full charge pump displacement was used to compute the charge pump capacitance.

$$C_C = (0.330 \text{ in}^3/\text{rev}) (0.0254 \text{ m/in})^3 / 690 \quad (75)$$
$$= 7.480 \times 10^{-9} \text{ m}^3/\text{MPa}$$

Mechanical Power Transmission Parameters

Bearing Friction

The coefficient of torque loss in the bearings was determined as a function of speed by disconnecting the coupling at the pump, and measuring the torque required to rotate the pump jackshaft in the bearings that supported it, and the pump drive shaft in its bearings (Figure 11). The torque in the pump jackshaft was measured with a strain gage torque transducer (Lebow model 1104). The output was conditioned by a strain gage amplifier (Validyne model SG71) and recorded with a strip-chart recorder (Gould model 220). As

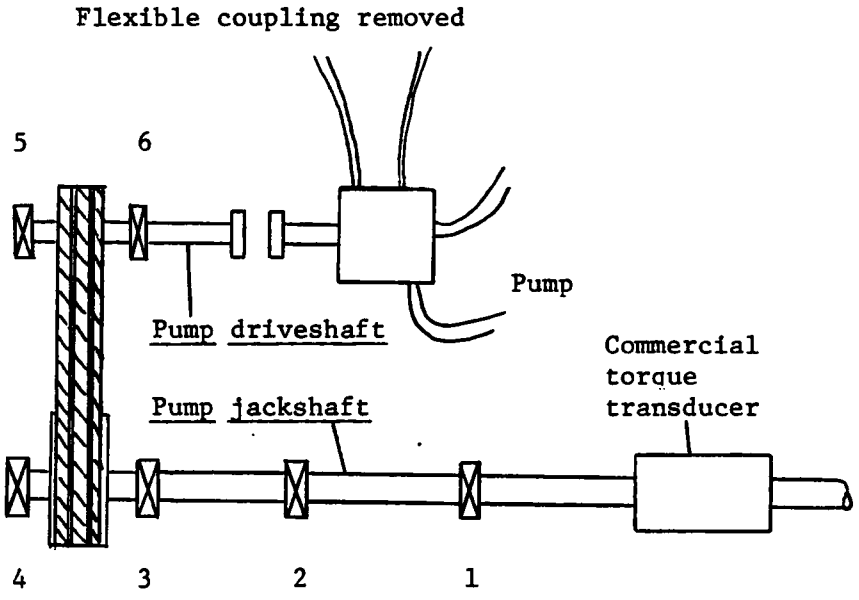

Bearings 3, 4, 5, and 6 are radially loaded by the v-belt drive.

Figure 11: Experimental set-up for measuring bearing friction in the pump jackshaft and pump driveshaft assemblies

specified by the transducer manufacturer, calibration was accomplished by switching a precision resistor into the bridge and adjusting the gain until a 0.683 volt output was obtained.

The measured torque for the two unloaded bearings supporting the experimental torque transducer section, the two loaded bearings on the pump jackshaft, and two loaded bearings on the pump drive shaft was 7.35 N-m. The jackshaft speed was 60.36 rad/s and the pump drive shaft speed 253.7 rad/s when this measurement was made.

It was found from the data that if the measured torque loss was averaged over the six bearings, taking into account the speed differences, the constant friction torque in the pump would have to be negative to maintain the 17.50 N-m zero viscosity torque. (See Viscous Drag and Constant Torque section). Bearings with no radial load, other than the weight of the shaft, were estimated to require only half as much torque as a radially loaded bearing.

The equation developed for torque as a function of speed and bearing friction is:

$$T = R_f \, (n_{pjs} \, \omega_{pjs} + n_p \, \omega_p \, m2) \qquad (76)$$

where T - measured torque (N-m)

R_f - coefficient of bearing friction (N-m-s/bearing)

n_{pjs} - equivalent no. of bearings on pump jackshaft

ω_{pjs} - pump jackshaft speed (rad/s)

n_p - equivalent no. of bearings on pump driveshaft

ω_p - pump driveshaft speed (rad/s)

m2 - sheave ratio from pump jackshaft to pump driveshaft

Solving for R_f gives:

$$R_f = T / (n_{pjs}\ \omega_{pjs} + n_p\ \omega_p\ m2) \qquad (77)$$

Substituting values gave R_f = 0.00318 N-m-s/bearing.

Over-running Clutch

An ideal over-running clutch transmits no torque when the driver speed is less than the driven speed, and infinite torque when the speeds are equal. In other words, it has no drag when disengaged and no slip when engaged.

The clutch in the system demonstrated both appreciable drag and measurable slip, so could not be modeled as an ideal clutch. It was, however, considered a resistance whose value was modulated by the sign of the speed difference it experienced. This allowed the transmitted torque (T_{slip}) and drag torque (T_{drag}) to be modeled as functions of speed difference ($\Delta\omega$).

The function of clutch torque dependent on speed was:

$$\Phi_{cl} = T_{drag} \qquad \text{for } \Delta\omega < 0.0 \tag{78}$$

$$\Phi_{cl} = T_{slip} \qquad \text{for } \Delta\omega \geq 0.0 \tag{79}$$

Drag Torque

While the pump was disconnected to measure bearing friction, it was noticed that the hydraulic motor was turning intermittently. This phenomenon could only be caused by the drag in the clutch. The pressure transducer was placed across the hydraulic motor to measure the cyclic pressure produced (Figure 12). The pressure spike in each period occurred immediately before the motor started to turn. Pressure then dropped as the motor continued to rotate, decreasing abruptly as the motor stopped.

An average pressure of 0.639 MPa was determined by using a planimeter to average the pressure over six cycles. Assuming no bearing friction, because the hydraulic motor speed was never over 100 rpm, the measured average pressure was converted to torque as follows:

$$T_{avg} = \Delta P_{avg}\, d_m \tag{80}$$

where T_{avg} - torque (N-m)

ΔP_{avg} - average pressure (MPa)

d_m - motor dispacement (m^3/rad)

Substituting values gave an average torque of 1.52 N-m.

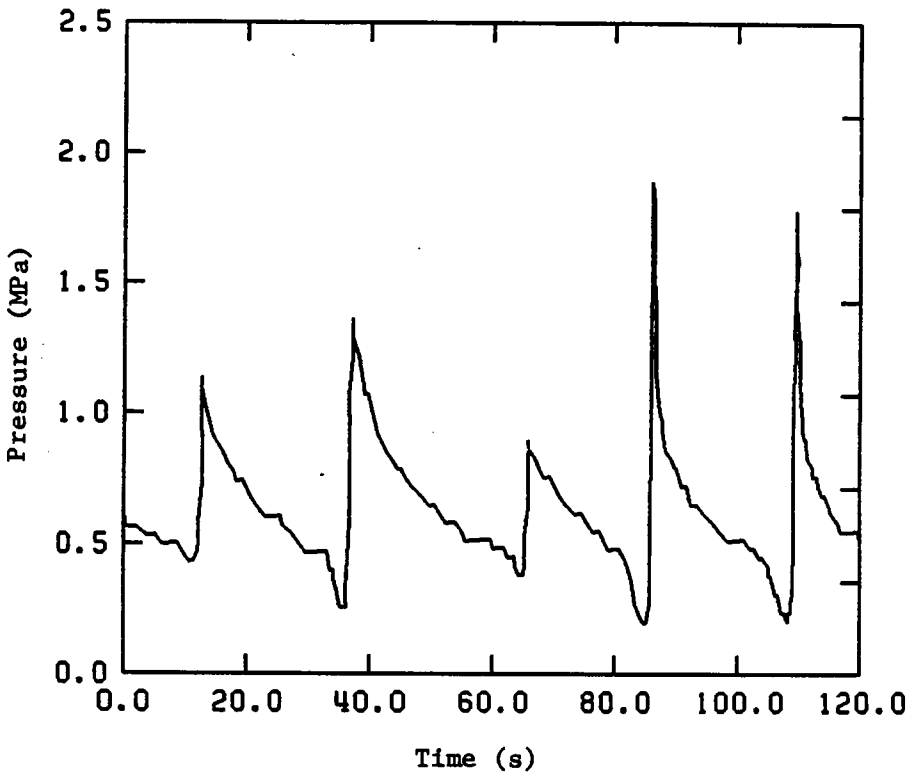

Figure 12: Measured pressure drop across the hydraulic motor when it was driven by the drag torque transmitted through the over-running clutch

It was also assumed, but could not be verified, that drag was also a function of the speed difference. The drag torque was assumed to be proportional to the ratio of the slip to the maximum slip possible, where slip was defined as the speed difference seen by the clutch. The drag torque would be greatest when the hydraulic motor speed was zero, and its least when the hydraulic motor speed exceeded the motor jackshaft speed. The constant of proportionality used was the average drag torque. The equations quantifying these assumptions is:

$$T_{drag} = 1.52\ \omega_{slip} / \omega_{maxslip} \qquad (81)$$

where T_{drag} - torque (N-m)

ω_{slip} - modulated speed difference between hydraulic motor driveshaft and jackshaft (rad/s)

$\omega_{maxslip}$ - speed difference when hydraulic motor was stopped (rad/s)

Slip Torque

The engaged torque transfer characteristics of the clutch were determined by increasing the swashplate angle on the pump until the clutch engaged and a large pressure was developed. The various pressure drops were established by decreasing the line relief valve setting to the desired pressure. The hydraulic motor and motor jackshaft speeds were recorded for each pressure drop. Unfortunately, it was

impossible to measure the transmitted torque directly. The torque was calculated from the pressure difference and the motor displacement, subtracting off the calculated bearing friction. Figure 13 is a plot of torque versus slip. The least squares regression for the plot gave the equation for torque as a function of slip.

$$T_{slip} = 162.9\ \omega_{slip} - 5.10 \tag{82}$$

where T_{slip} - transmitted torque (N-m)

ω_{slip} - speed difference across clutch (rad/s)

Since the slip torque equation had a positive x-intercept of 0.0375 rad/s, the test value on ω_1 in eqs. (78) and (79) raised to 0.0375 rad/s. This implies that the clutch must experience a small positive speed difference before it engages.

Actual Sheave Ratios

Knowing that the manufacture of sheaves for agricultural applications does not require close tolerances of the pitch diameters, the nominal sheave ratios were not trusted to predict the actual sheave speeds. Furthermore, the belt slip on small sheaves is greater than that of the large sheave to which they are coupled, worsening the problem.

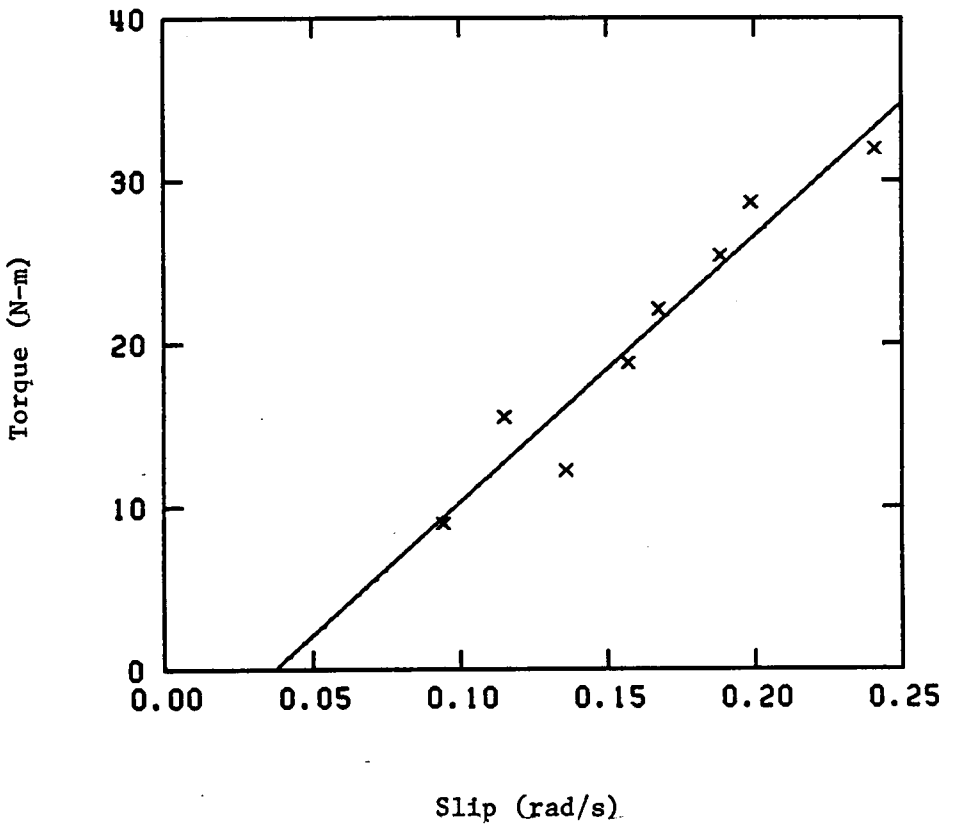

Figure 13: Torque transmitted through the over-running clutch versus clutch slip

The hydraulic motor, motor jackshaft, and pump jackshaft speeds were each sensed with magnetic pick-ups mounted over 60 tooth sprockets. When the output pulses were counted for one second, the speed in revolutions per minute was read directly. The pump shaft and electric motor speeds were measured with a hand-held tachometer.

The measured speeds in rad/s were:

$$\omega_{emf} = 187.4$$
$$\omega_{psj} = 59.9$$
$$\omega_{p} = 251.5$$
$$\omega_{mjs} = 93.3$$

Corresponding actual sheave ratios, compared with the nominal ratios, were: 0.3197 to a nominal of 0.3088 for the electric motor to pump jackshaft sheaves (m1), 4.203 to 3.700 for the pump jackshaft to pump driveshaft pair (m2), and 0.4978 actual to 4.884 nominal for the electric motor to to motor jackshaft sheaves. The related errors were 3.5%, 13.6%, and 1.9%, respectively. The actual sheave ratio from the hydraulic motor to the motor jackshaft was not measurable, and the nominal was assumed. Deviation from this was accounted for by lumping it with clutch slip.

Shaft Dynamics

The implicit assumption that the pump jackshaft was a stiff member and did not experience significant torsional deflection was quickly abandoned after recording the start-up torque in the pump jackshaft. Figure 14 shows the strip chart trace of shaft torque immediately after the electric motor was switched on.

The mechanical power transmission bond graph was altered to include a capacitance representing the spring nature of the shaft. The pump jackshaft inertias were separated, and each was associated with a common-flow junction. Between them was bonded a common effort junction to which the spring capacitance was attached. The resulting bond graph is shown in Figure 15. The motor end of the graph was affected in two ways, the magnitude of the inertia was reduced and so was the equivalent number of bearings. The causality was not affected.

The pump end of the graph, however, was incomplete. The sheave inertia was assumed to have integral causality, which, when propagated, required that the capacitance also have integral causality. This added two additional states to the model.

The equation for the pump jackshaft capacitance is:

$$T_s = \int k \, (\omega_{in} - \omega_{js}) \, dt \qquad (83)$$

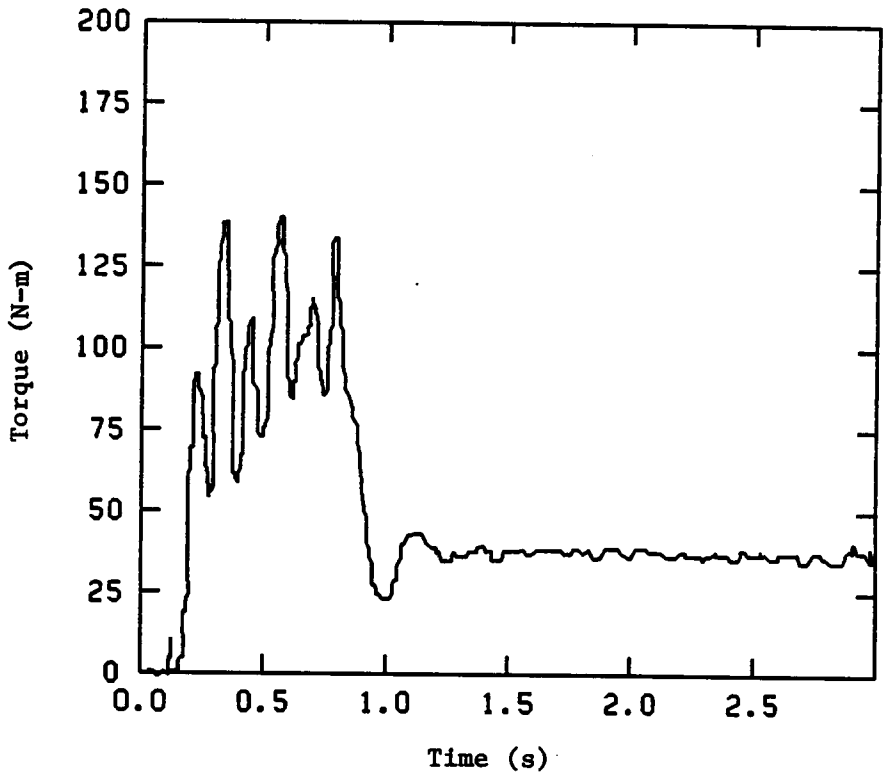

Figure 14: Start-up torque in pump jackshaft with zero swashplate angle

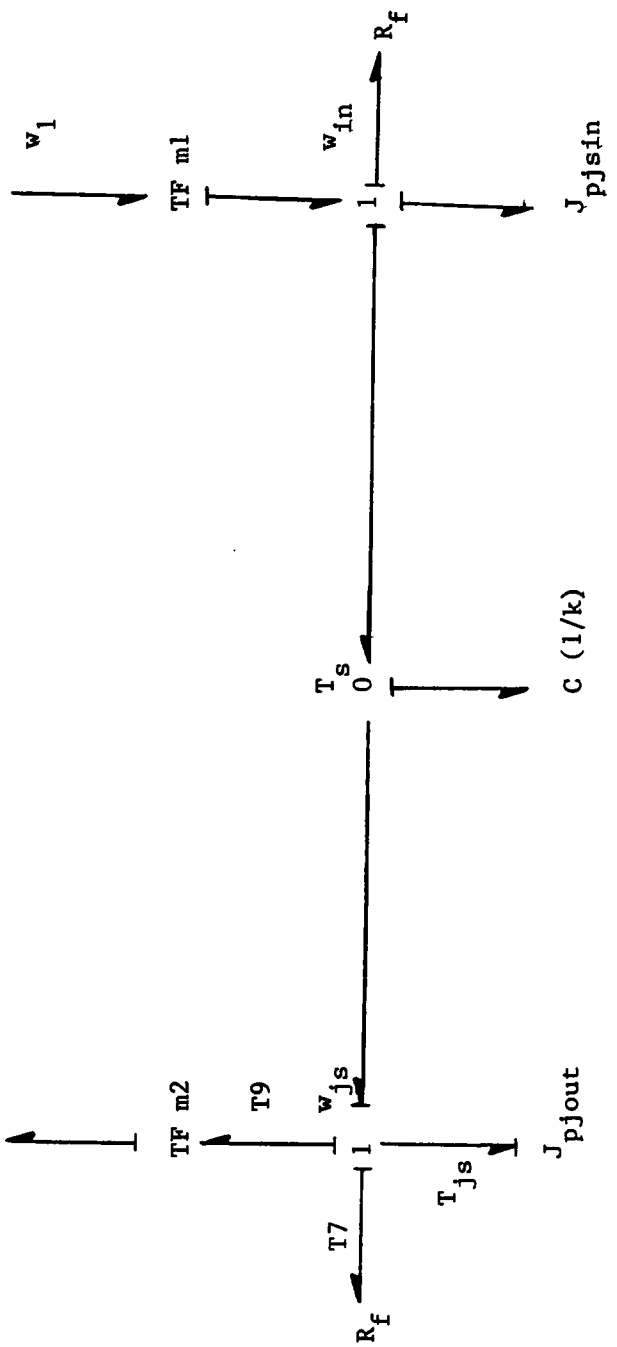

Figure 15 : Bond graph for pump jackshaft with spring dynamics

where T_s - torque in the spring (N-m)

ω_{in} - speed of the motor-end sheave (rad/s)

ω_{js} - speed of the pump-end sheave (rad/s)

k - spring constant (N-m/rad)

but $$\omega_{in} = m1\ \omega_1 \tag{84}$$

Substituting eq. (84) into eq. (83) gives the state equation for pump jackshaft torque.

$$T_s = \int k\ (m1\ \omega_1 - \omega_{js})\ dt \tag{85}$$

The spring constant, k, was calculated from the torsional stiffness formula.

$$\phi = T\ L\ /\ J\ G = T\ /\ k \tag{86}$$

where ϕ - total shaft deflection (rad)

T - torque (N-m)

L - length (1.22 m)

J - polar moment of inertia (1.29×10^{-8} m^4)

G - shearing modulus = 80×10^9 N/m^2 (Popov, 1976)

Then, $$k = J\ G\ /\ L = (1.29 \times 10^{-8})(80 \times 10^9)/(1.22) \tag{87}$$

$$= 845.9 \text{ N-m/rad}$$

The torque transmitted by the pump jackshaft [eq. (5)] is found by the following equation.

$$T5 = T6 + T7 + T8 \tag{88}$$

where T6 - torque input to pump jackshaft inertia (N-m)

T7 - friction torque in pump jackshaft (N-m)

T8 - torque output to pump driveshaft (N-m)

For the large sheave at the pump end of the shaft, the speed is the integral of torque.

$$\omega_{js} = \int T_{js} / J_{pjout} \, dt \tag{89}$$

where T_{js} - torque on large sheave (N-m)

J_{pjout} - inertia of large sheave (kg-m^2)

Now, $$T_{js} = T_s - T7 - T9 \tag{90}$$

where T7 - bearing friction torque in jackshaft (N-m)

T9 - torque output to pump (N-m)

and $$T7 = 3 R_f \omega_{js} \tag{91}$$

$$T9 = m2 \, T_p = m2 \, (T11 + T_c + T_v + T10 + T_{Pt}) \tag{92}$$

where T11 - bearing friction in pump driveshaft (N-m)

T_c - constant torque in pump (N-m)

T_v - viscous drag in pump (N-m)

T10 - torque input to pump inertia (N-m)

T_{Pt} - pressure caused torque in pump (N-m)

m2 - sheave ratio from pump jackshaft to driveshaft

These torques are given by:

$$T11 = 3\ R_f\ \omega_p = 3\ R_f\ m2\ \omega_{js} \tag{93}$$

$$T_c = R_c \tag{94}$$

$$T_v = R_v\ \nu \tag{95}$$

$$T10 = J_{pump}\ \dot{\omega}_p = J_{pump}\ m2\ \dot{\omega}_{js} \tag{96}$$

Substituting eqs. (93), (94), (95), and (96) into eq. (92) gives:

$$T9 = 3\ m2^2\ R_f\ \omega_{js} + m2\ (R_c + R_v\ \nu + T_{pt}) + m2^2\ J_{pump}\ \dot{\omega}_{js} \tag{97}$$

Substituting eqs. (91) and (97) into eq. (90) and the result into eq. (89) gives:

$$\dot{\omega}_{js} = [(T_s - 3\ R_f\ \omega_{js} - 3\ m2^2\ R_f\ \omega_{js} - m2\ (R_c + R_v\ \nu + T_{Pt}) - m2^2\ J_{pump}\ \dot{\omega}_{js}] / J_{pjout} \tag{98}$$

Solving for ω_{js} yields:

$$\omega_{js} = \int [T_s - 3\ R_f\ \omega_1\ (1+m2^2) - m2(R_c + R_v\ \nu + T_{Pt})] / (J_{pjout} + m2^2\ J_{pump})\ dt \tag{99}$$

This equation was added to the model to predict the speed of the output end of the pump jackshaft. The pump and pump driveshaft equations were unaltered.

Hydraulic Pump Parameters

Pressure Measurement

System pressures were measured using a diaphragm type differential pressure transducer (Validyne model DP15TL). The output was conditioned by a signal conditioner (Validyne model CD23) and recorded with a strip chart recorder (Gould model 220).

Calibration of the high pressure diaphragm was done against a large Bourdon-tube type pressure gage manufactured by Heiss, which was calibrated by the Mechanical Engineering Instrument Shop for a range of 0 to 24.8 MPa. Low pressure diaphragms, below 2 MPa, were calibrated against a dead-weight tester. Calibration of the transducer signal conditioner was an iterative procedure that required setting the pressure, adjusting the gain to reflect that pressure, setting a zero pressure, adjusting the zero level, then resetting to the higher pressure and repeating until both were correct.

Swashplate Angle Measurement

A protractor with half-degreee increments was mounted to the pump case concentric with the swashplate axis, and a pointer attached to an extension of the swashplate shaft. The pointer was set by moving the swashplate to its maximum displacement and positioning the pointer to 15 degrees.

Viscous Drag and Constant Torques

The torque in the pump jackshaft required to turn the pump at 252 rad/s with zero swashplate angle was measured at different dynamic viscosities. The system was operated until the fluid reached an appropriate temperature, at which time the torque was recorded manually from a voltmeter display. Figure 16 shows a plot of combined torque versus dynamic viscosity. The slope of this line is the viscous drag coefficient. A least squares regression of the data gave the following equation:

$$T_{measured} = 17.50 + 0.271\ \nu \tag{100}$$

Thus, the torque in the pump at 252 rad/s due to viscous drag is:

$$T_v = 0.271\ \nu\ /\ m2 \tag{101}$$

Therefore,

$$T_v = 0.001075\ \nu\ \omega\ /\ m2 \tag{102}$$

The intercept term in the above regression includes the constant friction torque as well as bearing friction and charge pump torques. Bearing torque is calculated by:

$$T_r = R_f\ (3\ \omega_{pjs} + 3\ \omega_p\ m2) \tag{103}$$

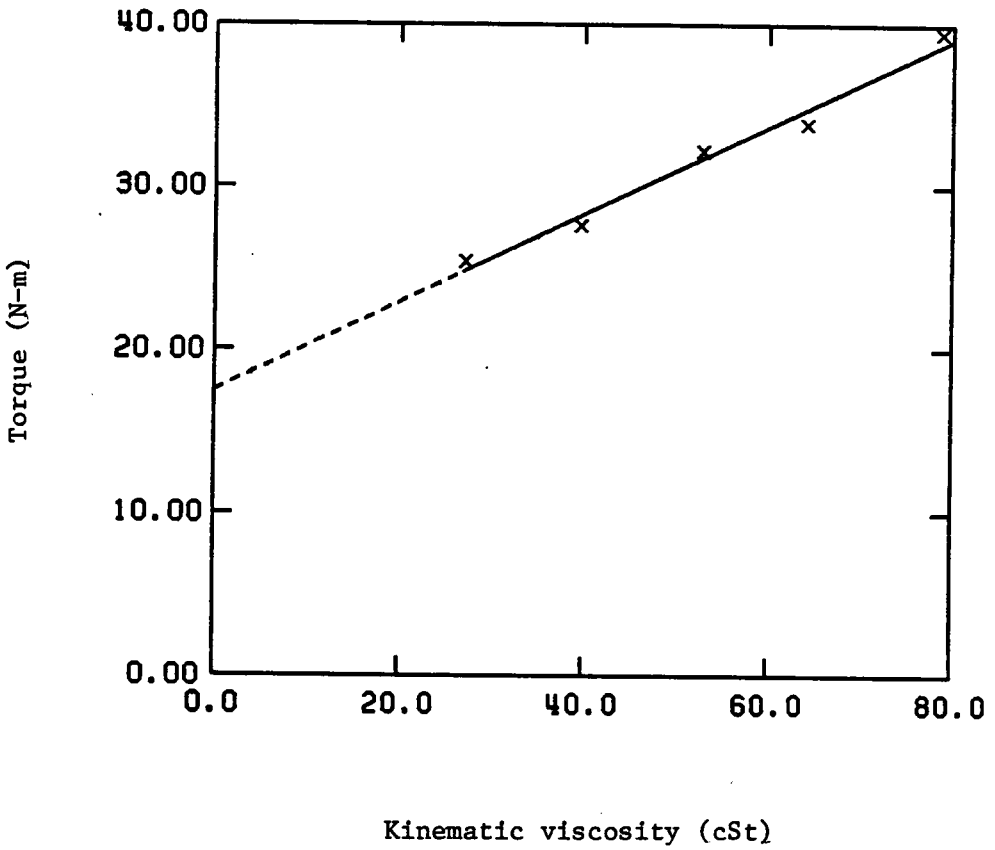

Figure 16: Torque in pump jackshaft with zero swashplate angle versus kinematic viscosity

Substituting values gives:

$$T_r = 0.00318\ [3(59.9) + 3(251.7)(4.203)] = 10.66\ \text{N-m}$$

Charge pump torque is given by:

$$T_{CP} = d_c\ \Delta P\ m2 \qquad (104)$$

and substitution gives:

$$T_{CP} = (804.3 \times 10^{-9})(1.10)(4.203) = 3.72\ \text{N-m}$$

Summing the bearing, charge pump, and constant friction torques and equating them to the measured zero dynamic viscosity value gives:

$$10.66 + 3.72 + T_c = 17.50$$

Then $T_c = 3.12$ N-m

This is the constant friction torque measured in the pump jackshaft, therefore the constant resistance torque is:

$$R_c = 3.12 / m2 = 0.742\ \text{N-m}$$

Pacey (1979) reported a constant friction torque of 8.74 N-m for his hydraulic pump, whose maximum displacement was 6.98×10^{-5} m^3/rev. Comparatively, the constant friction torque of 0.742 N-m for this pump is disproportionately small as its displacement is 1.50×10^{-5} m^3/rev.

Suction Filter Loss

The pressure at the inlet to the charge pump was assumed equal to the pressure drop across the suction filter, and was recorded at different flow rates. Since the speed of the pump was fixed, the flow rate was varied by allowing the fluid to warm up, thus changing its viscosity. The fluid temperature was sensed at the exit of the reservoir and used to calculate the fluid viscosity. The viscosity was input to the flow indicator which then displayed the computed flow-rate.

The flow through the filter was assumed to be laminar, being described by:

$$q = G \Delta P / \mu \tag{105}$$

Solving for the conductance, G:

$$G = q \mu / \Delta P \tag{106}$$

The product of q and μ was defined as a "flow factor" and was plotted against pressure drop (Figure 17). The resistance, R, was then the slope of the flow factor versus pressure curve. The y-intercept was deemed significant, so the linear regression equation was used as the function for pressure dependent upon viscosity and flow.

$$P_{sc} = 0.01752 + 0.07292\ q\ \mu \tag{107}$$

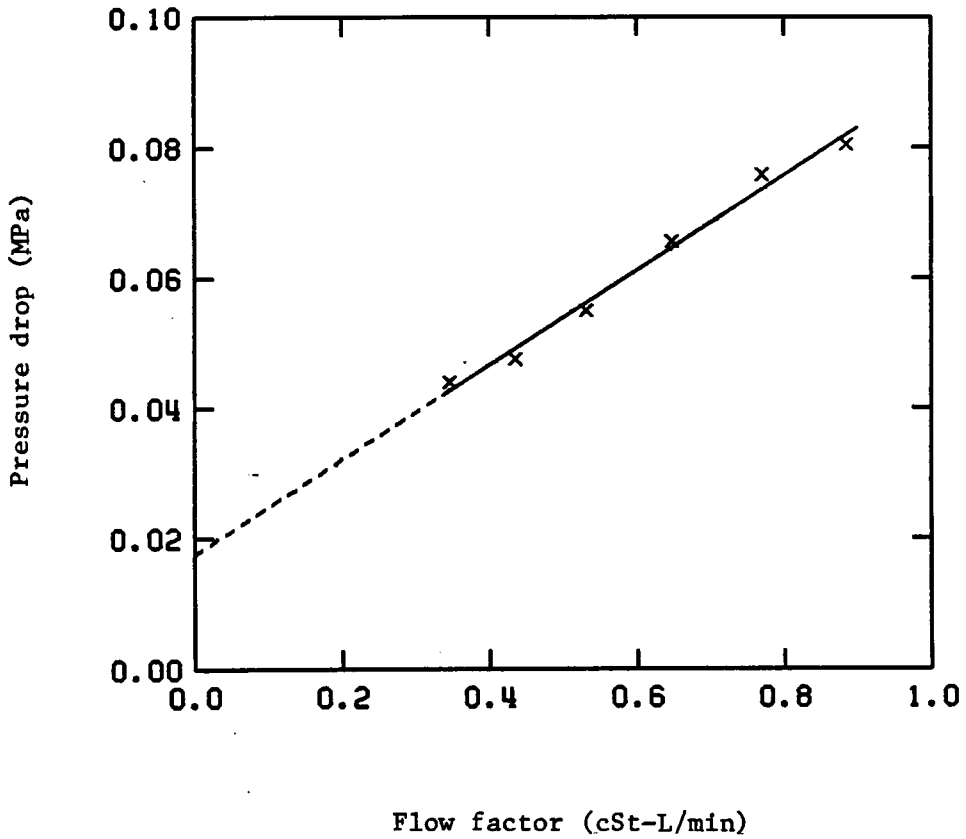

Figure 17: Suction filter pressure drop versus flow factor

Coefficient of Dry Friction

An attempt was made to quantify the coefficient of dry friction, defined as the friction of the pump pistons on the swashplate. The pump jack-shaft torque, fluid temperature, jackshaft speed, and the pump pressure rise were measured at one-half degree increments of the swashplate above the point where the hydraulic motor speed stabilized. Six angles were used, starting at 4.5 degrees and going up to 7.0 degrees.

From the state equation for the pump jackshaft speed, eq. (96), it was found that the steady-state torque in the shaft is given by:

$$T_{js} = T7 + m2\ (T_p + T_{CP} + T_c + T_v + T11) \qquad (108)$$

where
- $T7$ - bearing friction in jackshaft (N-m)
- T_p - main pump torque (N-m)
- T_{CP} - charge pump pressure cause torque (N-m)
- T_c - constant friction torque (N-m)
- T_v - viscous drag torque (N-m)
- $T11$ - bearing friction in pump driveshaft (N-m)

Of these torques, only the pump torque could not be calculated from the known data. Solving for T_p:

$$T_p = (T_{js} - T7)/m2 - T_{CP} - T_c - T_v - T11 \qquad (109)$$

But T_p is comprised of the pressure rise torque and the dry friction torque.

$$T_p = 1.0 \times 10^6 \, \Delta P \, d_p + T_{dry} \tag{110}$$

where ΔP - pressure rise across the pump (MPa)

d_p - displacement of the pump (m^3/rad)

T_{dry} - dry friction torque (N-m)

Then, the dry friction torque is given by:

$$T_{dry} = (T_{js}-T7)/m2 - T_{CP} - T_c - T_v - T11 - \Delta P \, d_p \tag{111}$$

where these torques are evaluated by the following equations.

T_{js} = measured torque (N-m)

$$T7 = (3.0)(0.00318) \, \omega_{js} \quad (N\text{-}m) \tag{112}$$

$$T_{CP} = d_c \, \Delta P = (840.3 \times 10^{-9})(1.10) \tag{113}$$

$$T_c = 0.742 \quad (N\text{-}m) \tag{114}$$

$$T_v = 0.271 \, \mu_{avg} / m2 \quad (N\text{-}m) \tag{115}$$

$$T11 = (3.0)(0.00318) \, \omega_p \quad (N\text{-}m) \tag{116}$$

A computer program was written to evaluate T_{dry} at each swashplate angle, θ. The equation for dry friction torque was solved for the coefficient.

$$C_{fp} = T_{dry} \, (1 - \tan \theta) \, / \, \Delta P_p \, d_{pmax} \tag{117}$$

The resulting plot showed a rather scattered pattern, and, for lack of a better estimate, the zero-intercept slope was assumed, giving:

$$C_{fp} = 0.004177 \text{ (dimensionless)}$$

Hydraulic Motor Parameters

Pressure Filter Loss

The pressure drop across the filter between the motor case drain outlet and the reservoir was measured in like manner to that of the suction filter. This measured pressure drop was found to be insensitive to changes in fluid temperature.

Since the flow-rate through the filter could not be altered due to the fixed pump speed, the data taken represented a single operating point. The filter conductance was calculated from the means of 13 pressure- flow factor data points.

$$q \cdot \mu_{mean} = 0.528 \text{ (L/min m}^2\text{/s)}$$
$$p_{mean} = 0.0213 \text{ (MPa)}$$

The form of the equation for the flow in the pressure filter was assumed to be the same as that for the flow in the suction filter, eq. (106).

Substituting the mean values for flow factor and pressure gave:

$$Gpf = 0.528/0.0213 = 24.83 \text{ (L/min m}^2\text{/s)/MPa}$$

The equation for flow through the filter was then:

$$Q_{dt} = P_{dm} G_{pf} / \mu = 24.83 P_{dm} / \mu \qquad (118)$$

Leakage Coefficients

The internal leakages in the pump and hydraulic motor were phenomena that affected how sensitive the system would be to swasplate angle. It was important to try to quantify these flows. The underlying assumptions were that the leakages were the same in both the pump and the motor, and that they were laminar.

In order to measure these flows, the hydraulic motor drive shaft was restrained from turning, the pump was used to generate flows, and the relief valve to set pressures. The case drain hose was rerouted to bypass the motor; the return line hose was disconnected at the motor and plugged.

The data was taken by setting the pressure using the relief valve and allowing about one minute for the flow to develop. The electrical resistance of the thermistor probe was recorded, the leakage flows collected in separate containers for a full minute, timed by a stop watch, and the

thermistor resistance recorded again. The volumes of fluid were then weighed and the running weight recorded. The measured average temperature was used to calculate viscosity, μ, which was then used to calculate the $q\,\mu$ flow-factor.

Drain Leakage

Figure 18 shows a plot of flow factor versus pressure for the drain leakage. A linear relationship appeared to be justified, as did forcing the line through zero. The resulting leakage coefficient from the linear regression was:

$$G_{xdp} = 6.688 \times 10^{-5} \text{ (m}^2\text{/s L/min)/MPa}$$

Cross-Port Leakage

A plot of the flow factor versus pressure is shown in Figure 19. The data looks scattered, but in fact, there are three traces plotted together, the bottom trace being the most distinct. Separately, these curves appear to rise sharply near zero pressure and then become constant for higher pressures. Attempts to describe the cross-port flow as orifice flow or as a function of temperature were equally unsuccessful in explaining the data.

The mean of the flow factor data was used in the simulation as a constant flow term, independent of pressure.

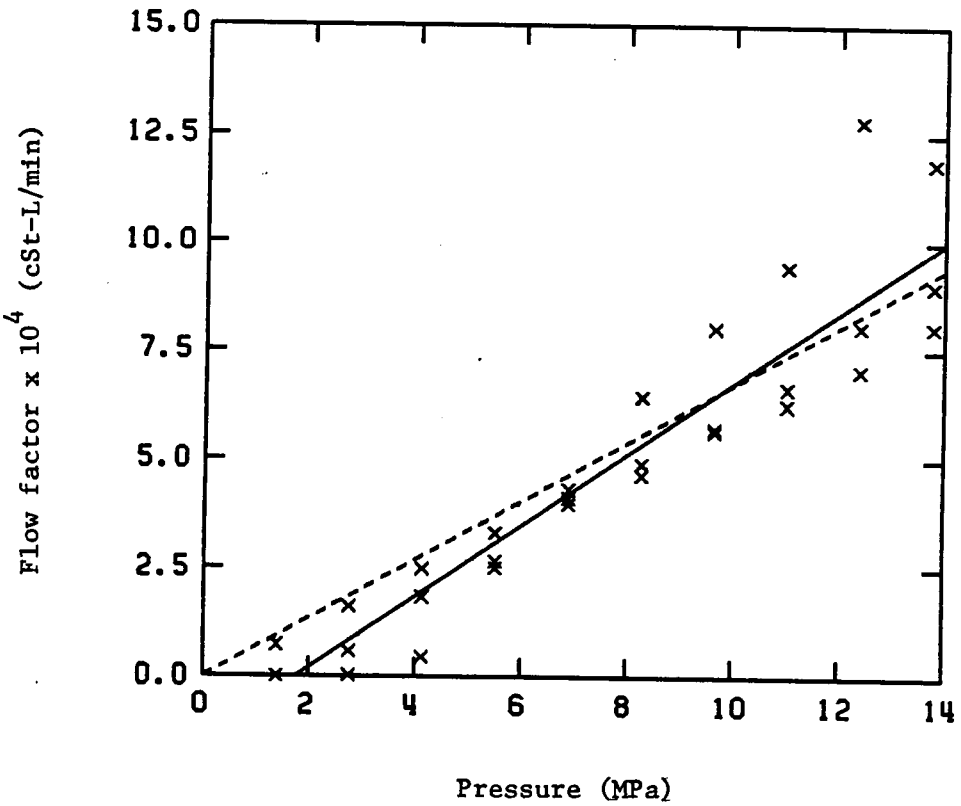

Figure 18: Hydraulic motor drain leakage flow factor versus inlet pressure with output shaft fixed

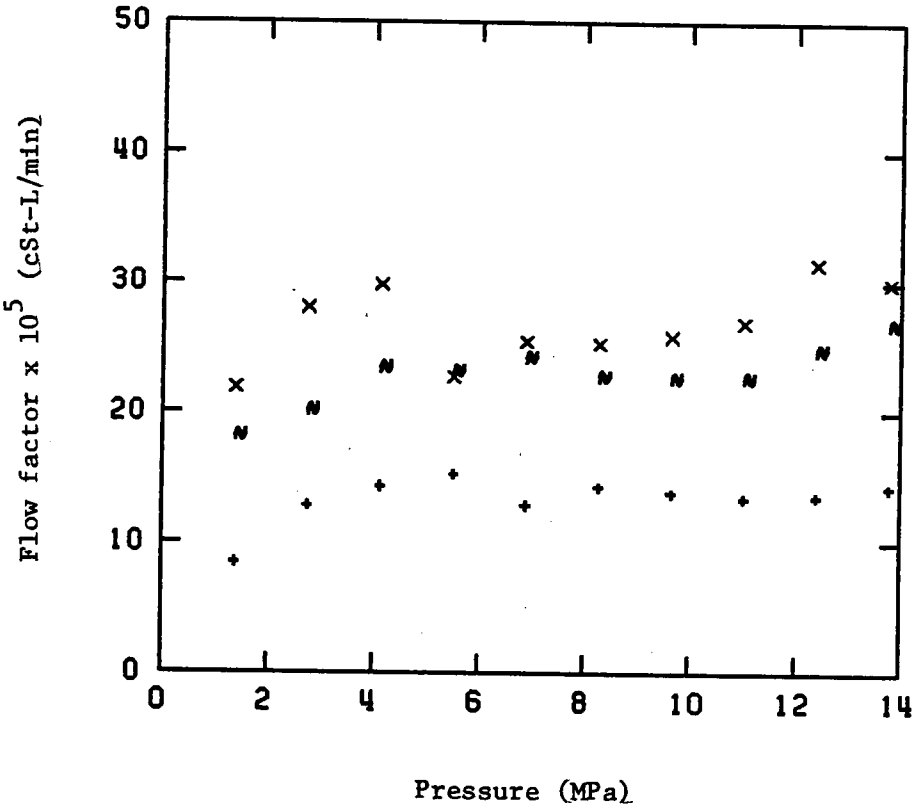

Figure 19: Hydraulic motor cross-port leakage flow factor versus inlet pressure with output shaft fixed

This caused gross errors in the predicted values. Therefore, the original laminar flow assumption was used, with the means of the flow factor and the maximum pressure used as one end point and zero as the other. From this, the calculated conductance was:

$$G_{12x} = q\,\mu\,/\,\Delta P = 0.0002076\,/\,13.8 \qquad (119)$$
$$= 1.50 \times 10^{-5}\ (m^2/s\ L/min)/MPa$$

This assumption seems to be a poor way to describe the cross-port leakage flows, but the alternatives also fail to explain the data and cause the simulation to fail.

Hydraulic Power Transmission Parameters

Flow Measurement

External flows were measured with two turbine-type flow sensors (Flow Technology model FT-6-8A in the case drain circuit, and Flow Technology model FT-10 in the main circuit). A flow indicator was developed by the author to output the signal from the flow meters in gallons per minute. The functional description of the indicator and the development of the flow algorithms are included as Appendices C and D, respectively.

The flow sensors, whose ranges were 0.5 to 5.0 and 1.0 to 10.0 gallons per minute respectively, were placed in the

appropriate lines and their output connected to the flow indicator. The indicator digitally computed the flow based on the value of the viscosity input by the user, and displayed the flow in gpm.

Line Losses

The formulae for computing the pressure drop in hydraulic lines are well established. Flows with Reynolds numbers under 1000 are considered laminar, those over 2300 turbulent, and those between transitive, (White, 1979). The computation scheme used by Levek and Young (1977) in SSFAN, however, set the upper limit of the laminar flow range at a Reynolds number of 100. The purpose of setting this upper limit was to ensure that the maximum laminar pressure drop was always exceeded by the minimum turbulent pressure drop. Otherwise, a pressure in the transitive region would have three flows associated with it.

Laminar Flow

Fox and McDonald (1978) give the laminar flow relationship as:

$$h_l = (32/R_e)\ (L/D)\ (V^2/2g) \qquad (120)$$

where h_l - head loss (m)

L - length (m)

D - diameter (m)

R_e - Reynolds number

V - average velocity (m/s)

g - gravitational constant = 9.81 m/s^2

but $$\Delta P = h_l \rho g \quad (121)$$

and $$R_e = \rho d V / \mu \quad (122)$$

Substituting eqs. (121) and (122) into eq. (120) and solving for ΔP gives:

$$\Delta P = 32 \mu L V / d^2 \quad (123)$$

but $$V = 4 q / \pi d^2 \quad (124)$$

Substituting eq. (124) into eq. (123) and simplifying:

$$\Delta P = (128 / \pi)(\mu L / d^4) q \quad (125)$$

where ΔP - presure (Pa)

q - flow (m^3/s)

μ - viscosity ($N\text{-}s/m^2$)

Converting pressure to MPa, flow to L/min, and solving for flow as a function of pressure:

$$q_{lam} = (1.473 \times 10^{-9} d^4 / \mu L) \Delta P \quad (126)$$

For a given physical configuration and fluid viscosity, the flow is proportional to the pressure difference. The

constant of proportionality was calculated in the simulation.

Turbulent Flow

For low Reynolds number turbulent flow, White (1979) gives an equation for head loss as:

$$h_l = 0.316\ (\nu / V\ d)^{1/4}\ (L/d)\ (V^2 / 2\ g) \qquad (127)$$

but $$h_l = \Delta P / \rho\ g \qquad (128)$$

Equating eqs. (128) and (127) and solving for ΔP:

$$\Delta P = 0.158\ L\ \mu^{1/4}\ V^{7/4}\ \rho^{3/4} / d^{5/4} \qquad (129)$$

Now, $$V = (4/\pi)\ (q/d^2) \qquad (130)$$

and substituting eq. (130) into (129) and simplifying:

$$\Delta P = (1.048 \times 10^{-9})\ L\ \mu^{1/4}\ \rho^{3/4}\ q^{7/4} / d^{5/4} \qquad (131)$$

Solving for q in L/min as a function of ΔP in MPa, gives:

$$q = [(9.54 \times 10^{14})\ d^{19/4}\ \Delta P / \mu^{1/4}\ \rho^{3/4}\ L]^{4/7} \qquad (132)$$

Transitive Flow

The flow required to achieve Reynolds numbers of 100 and 2300 were computed from the equation:

$$q = R_e\ \pi\ \mu\ d\ 15000 / \rho \qquad (133)$$

which results from substituting the relationship for average velocity as a function of flow into the Reynolds number equation and solving for q. The maximum laminar pressure drop was computed by:

$$\Delta P_{max\ lam} = R_{lam}\, q|_{R_e=100} \tag{134}$$

The minimum turbulent pressure drop was computed from eq. (131), by substituting the flow at Reynolds number of 2300. With these values calculated, the transitive flow computation was a simple linear interpolation.

$$q_{tran} = q_{100} + \frac{(q_{2300} - q_{100})(\Delta P - \Delta P_{max\ lam})}{(\Delta P_{min\ trb} - \Delta P_{max\ lam})} \tag{135}$$

The flows at Reynolds numbers of 100 and 2300 were calculated as 1.08 L/min and 30.6 L/min respectively. At the 252.2 rad/s speed set by the system, the maximum theoretical flow rate was 36.0 L/min, with the feasible limit approximately half of that. Therefore, the flows in the system were either laminar or transitive, eliminating the need to compute turbulent flows, save for that at Reynolds number of 2300.

Figure 20 shows the flows in the lines against a "turbulent pressure factor". This turbulent pressure factor is

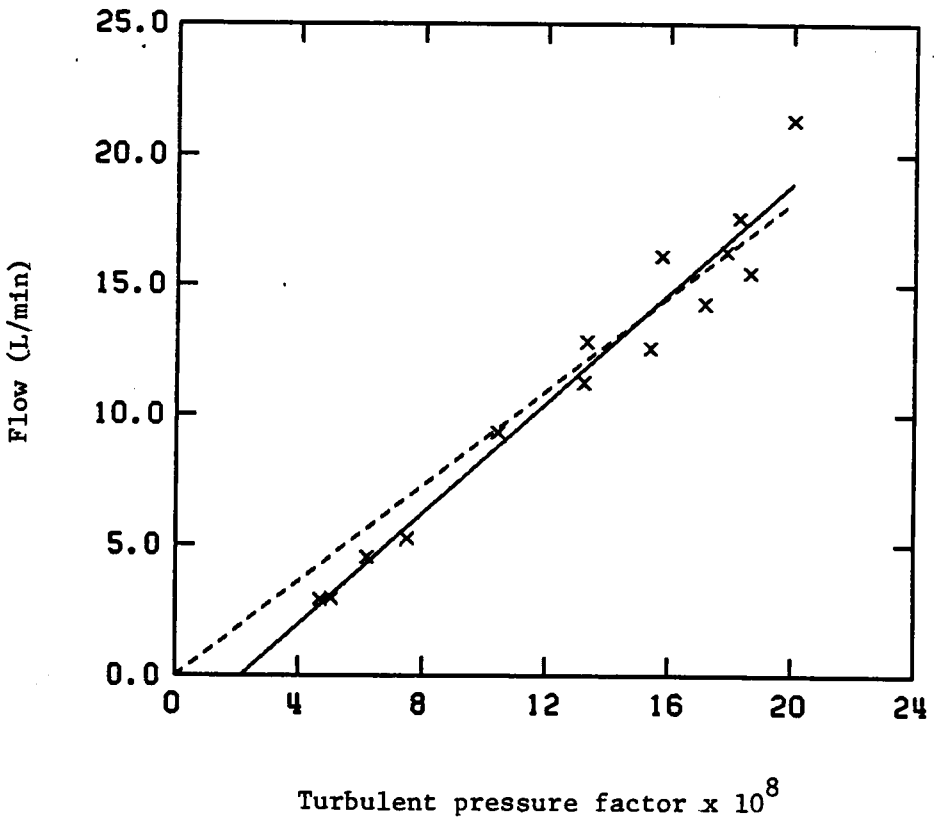

Figure 20: Hydraulic line flow factor versus turbulent pressure factor from the Blassius turbulent flow equation

defined as the part of eq. (132) to the right of the equal sign given by the expression:

$$(d^{19/4}\ \Delta P\ /\ \mu^{1/4}\ \rho^{3/4}\ L)^{4/7}$$

A linear regression was done, forcing the line through zero, to estimate the experimental value of the coefficient term in eq. (132). The resulting coefficient was 8.461×10^{13}, which was an order of magnitude smaller than the theoretical value, 9.54×10^{14}. The difference may be accounted for by the pressure drop across the flow meter, which was unavoidable. It was also recognized that the measured flows were not in the turbulent region. The simulation predictions using the theoretical coefficient were an order of magnitude too low, thus justifying the use of the experimental coefficient in the simulation.

Steady-State Testing Procedure

The test stand had to be operated for a period of time before any measurements were taken to allow the fluid to warm up. There was no temperature control for the fluid, so tests had to be done with the fluid as near to equilibrium as could be maintained manually.

Once the fluid was warm, a swashplate angle was set by turning a hand-wheel to move the swashplate control arm until the pointer on the protractor reached the desired

position. The system was then allowed to operate for a brief time at this condition before the measurements were made; the first and last measurements were always the thermistor probe resistance. This allowed the visocisty to be calculated at the start and finish of, and to be averaged over, the sampling interval.

Dynamic Testing Procedure

To perform a dynamic test on the test stand, the handwheel positioner for the pump swashplate was replaced with a variable speed electric motor. This motor drove the swashplate through a four-bar crank and rocker linkage, where both the crank and the link arm were adjustable. The linkage was adjusted to obtain a 6.5 degree maximum displacement and a zero degree minimum. The system was run with a constant swashplate angle, obtained by positioning the crank with the drive motor off, until the fluid temperature was approximately 45 °C. The swashplate drive motor was then turned on and the pump pressure difference and pump jackshaft torque recorded on the strip chart recorder.

RESULTS AND DISCUSSION

Steady State Response

Once the model parameters had been refined with the test data, the simulation was run to predict the steady-state performance of the system at a given temperature and varying swashplate angles. These predictions were then compared to the steady-state conditions of the test stand.

Clutch Drag and Bearing Friction Torques

In order to test the simulation prediction of clutch drag and bearing friction torques, the hydraulic motor was disconnected from its drive shaft, see Figure 1. This left the hydraulic motor driveshaft free to turn under the power of the clutch drag.

The motor jackshaft speed was maintained at 93.3 rad/s and the steady-state motor driveshaft speed was measured at 71.3 rad/s. A predicted speed was computed by equating the clutch drag to the bearing friction, and solving for the speed.

$$1.52\ (1 - \omega_m / 93.3) = 2\ (0.00318)\ \omega_m \qquad (136)$$

This gave:

$$\omega_m = 67.1 \text{ rad/s}$$

with the error between predicted and observed speeds of 5.9%.

Pump Pressure Difference

A comparison of experimental data with predicted values of the pump pressure difference, pump jackshaft torque and speed, pump supply flow-rate, and hydraulic motor speed at six swashplate angles is given in Table 2. It is seen that the pump pressure difference, measured between the pump supply and return ports, shows a small sensitivity to swashplate angle below 5.5 degrees, and a large sensitivity above 5.5 degrees. The system and the simulation agree that the clutch engages between 5.5 and 6.0 degrees, but the simulation exaggerates the sensitivity to increased swashplate angle.

The errors in the predicted values at swashplate angles below 6.0 degrees may be due to errors in coefficients that would tend to overestimate the pressure needed to turn the hydraulic motor at no load. The over-estimating the constant friction or the viscous drag torques in the hydraulic motor would cause an over-estimate of the pressure required to drive the motor.

Several reasons may account for the large simulation error above swashplate angles of 5.5 degrees. Firstly, the cross-port and drain leakage flows, given in their general

Table 2: Comparison of steady-state experimental and predicted values

Swashplate angle (degrees)	Pump pressure drop (P_p-P_s) (MPa)		Pump jackshaft torque (T_s) (N-m)		Pump jackshaft speed (ω_{js}) (rad/s)		Pump supply flow (Φ^{-1}_{L11}) (L/min)		Hydraulic motor speed (ω_m) (rad/s)	
	meas.	pred.	meas.	pred.	meas.	pred.	meas.	pred.	meas.	pred.
4.5	0.352	0.616	24.75	27.67	60.0	59.8	11.01	10.77	90.3	75.3
5.0	0.441	0.740	25.42	28.92	60.0	59.8	11.77	11.99	90.6	83.7
5.5	0.510	0.863	25.99	28.99	60.0	59.8	13.02	13.17	90.8	92.1
6.0	5.516	83.19	49.72	362.4	59.7	59.4	13.74	13.49	93.8	93.8
6.5	11.31	175.2	71.87	792.8	59.6	58.2	14.01	14.36	94.0	93.2
7.0	17.58	236.7	103.1	1137.	59.1	49.6	14.31	12.68	94.3	80.7

form in eq. (119), may underestimate the actual leakage flows, resulting in an overestimate of the pressure derivative in eqs. (47), (48), (54), and (55). The leakage equations were based on data taken from a test where the hydraulic motor was locked mechanically and various pressures were applied to the inlet port. The motor was fixed arbitrarily in a position that may not have allowed a representative amount of leakage to occur, implying that leakage might be a function of angular displacement. Another possible reason is that contaminants may have accumulated in the leakage paths during the test and thus increased the resistance to flow.

Secondly, the predicted efficiency with which the pump converts torque to pressure may to too high. This implies, among other things, that the coefficient of dry friction, (0.004177), may be too small. The results of the attempt to quantify this coefficient were not decisive, and may have underestimated it.

Lastly, the simulation assumed that the line relief valve was absent from the system. However, the relief valve, even though it was set at approximately 20.7 MPa, may have leaked enough to effectively decrease the system pressure. Operating the system without the variable relief valve in order to test this hypothesis would have been

unsafe and inadvisable, and determining its operating characteristics using this test stand was impractical.

Pump Jackshaft Speed and Torque

The agreement between the experimental and simulated results for the pump jackshaft torque (T_s) were similar to that for the pump pressure difference. The major cause of discrepancy was the overestimated pressure difference. If the pressure was brought more in line, the predicted torque would have be much closer to the measured torque.

The accuracy of the pump jackshaft speed can be attributed to good estimates of the sheave ratios and a reasonable estimate of the electric motor torque-speed curve (Figure 9). The predicted speed dropped off at seven degrees of swashplate angle because the greatly increased dry friction losses in the pump and hydraulic motor at the exaggerated pressures caused the predicted electric motor speed to lug down. More accurate predictions of the system pressures would reduce the calculated dry friction torques, which in turn would increase the estimated operating speeds.

Hydraulic Motor Speed

The hydraulic motor speed cycled at swashplate angles less than 4.5 degrees, ranging from zero rad/s to 50 rad/s, preventing the measurement of any steady-state parameters.

This cycling was due to an unexplained time-varying drag in the clutch, as exhibited in figure 12. Between 4.5 degrees and the point at which the clutch engaged, the system became more stable, maintaining fairly constant pressures and speeds. In this range of swashplate angles, the simulation underestimated the experimental speed. An over-estimate of the constant friction or viscous drag torques (T_c and T_v, respectively) in the hydraulic motor, or and underestimate of the clutch drag (T_{drag}) could be the cause. The marked reduction in the predicted hydraulic motor speed at seven degrees wsa a result of the reduced pump speed.

Pump Supply Flow

The predicted pump supply flow (Φ_{L11}^{-1}) corresponded well with the measured flows, except at the highest swash-plate angle where the predicted leakage was greatly increased. Some of the error can be accounted for by the varying viscosity during data collection. The fluid would typically start with temperature of about 25 °C and a viscosity of 100 cSt, and operate in a temperature range of 45 °C to 60 °C with the viscosity ranging from 35 cSt to 15 cSt. The fluid temperature was measured in the return line of the pump and the viscosity calculated and averaged for the sampling interval. The simulation, however, assumed a constant temperature and viscosity.

Dynamic Response

Pump Jackshaft Start-up Torque

Because of the apparent dynamics in the pump jackshaft, Figure 13, the model was altered to reflect the spring nature of this shaft. Figure 21 shows the corresponding simulation start-up torque curve plotted over the experimental trace. It is seen from comparing the traces that the simulation plot has a similar shape and frequency of oscillation as that of the experimental trace. The torque in the jackshaft oscillates as the masses at its ends are accelerated, then drops sharply as the break-over torque of the electric motor is surpassed. The torque oscillations damp out, and a steady-state torque is attained after about 3 seconds. The simulation plot indicates that the model underestimates the damping in the mechanical power transmission system. The test stand trace shows the steady state torque being attained after only one and one-half oscillations, while the simulation oscillates for nearly a half-second, beyond the break-over point. Another difference was that the actual start-up time was 1.2 seconds while the predicted was 3.8 seconds. This indicated that either the electric motor start-up curve was too low, the estimated inertias were too high, or a combination of these, these, with an emphasis on the first. If the electric motor

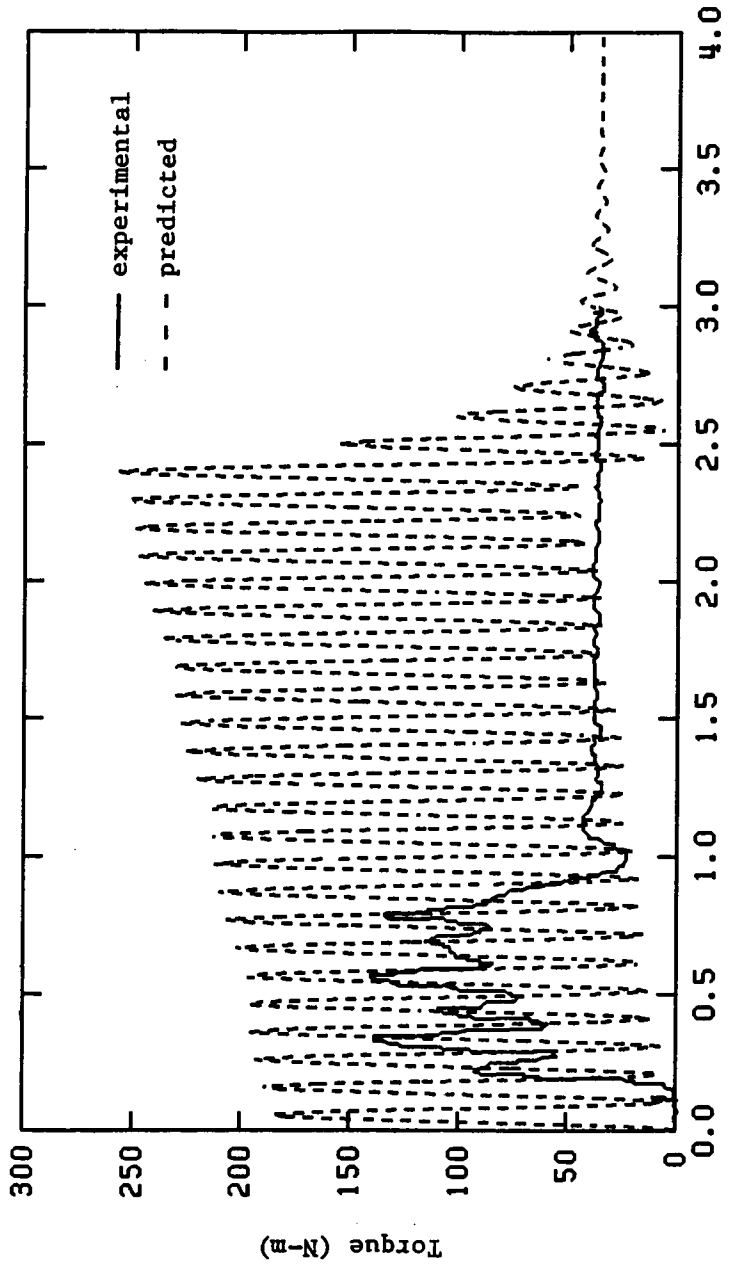

Figure 21: Experimental and predicted start-up torque in pump jackshaft with zero swashplate angle and fluid temperature of 25° C

start-up curve was too low, the predicted torque supplied by the motor would be low, which would require a greater length of time to accelerate the system to its operating speed. If the inertias were overestimated due to the fact that the electric motor inertia was guessed at with no supporting data, the model would predict that the system would take longer reach its operating speed.

The maximum measured torque was 147 N-m as compared to a maximum predicted value of 250 N-m. The smoothness of the electric motor torque-speed curve will affect the magnitude of the oscillations because of the "jerk" created at break-points in the simulation curve. The real motor will cause less "jerk" in the system because its torque-speed relationship has a continuous slope.

Driven Swashplate Results

Pump Jackshaft Torque

The pump jackshaft torque was recorded on the strip chart while the pump swashplate was being cycled. The digitized trace is shown in Figure 22 as the solid line with the corresponding simulation trace shown as the dashed line. The maximum swashplate displacement in the simulation was reduced from 6.5 degrees to 5.7 degrees to try to obtain a

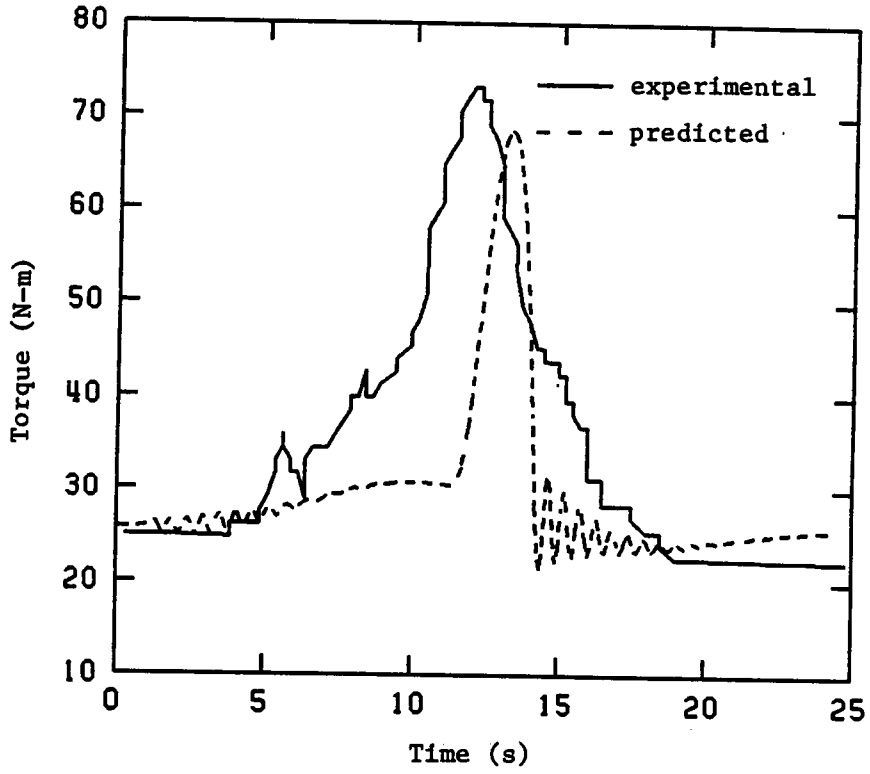

Figure 22: Experimental and predicted pump jackshaft torques for driven swashplate and fluid temperature of 45° C

torque peak similar to the experimental. The static friction in the hydraulic motor was estimated to be 12.0 N-m, though no data to support this was taken. This value did, however, provide for an initial pressure spike in the simulation data similar to that of the real system.

Both the plots exhibit a large torque peak in the middle of the cycle, lasting about 3 seconds, corresponding to the period that the clutch was engaged. Also, they both show disturbances near the beginning of the cycle at the point when the hydraulic motor began to rotate and accelerate. The misalignment in the timing of events was accounted for by the small amount of play in the joints of the swashplate drive linkage, and the difference between the actual four-bar linkage displacement and the simulated sinusoidal displacement.

The experimental torque trace rises to its peak and falls off less rapidly than does the simulation torque. This could be caused by the underestimated damping. It also implies that a resistance proportional to the swashplate angle was underestimated, including the pump and motor dry friction and viscous drag torques, or the hydraulic line losses. The viscous drag was measured at zero swashplate angle only and was assumed to be independent of the angle because of the inability to determine otherwise. This

assumption is not consistent with Wilson's equations which have a (1 - tan α) denominator in the visous drag term of both the pump and motor torque equations. The coefficient of dry friction was not experimentally determined independent of other values, and is subject to question.

Pump Pressure Difference

The solid line of Figure 23 shows the experimental pressure trace as the swashplate was cycled from zero to a maximum of 6.5 degrees. Comparing the experimental trace to the simulation trace, plotted as the dashed line, shows a general agreement. The initial pressure spike corresponds to that required to overcome static friction in the hydraulic motor and to start it accelerating. The second, larger spike resulted from the engagement of the clutch and the loading of the hydraulic motor.

At the point immediately after the initial pressure spike, the simulation plot shows a much greater pressure oscillation than was observed. After the initial pressure spike and rebound, the measured pressure dropped briefly, then rose steadily as the hydraulic motor speed increased. The simulation curve during this same time shows decaying oscillations for about four seconds and then remains constant until the clutch engaged. Again, it can be inferred from this that a factor proportional to either swashplate

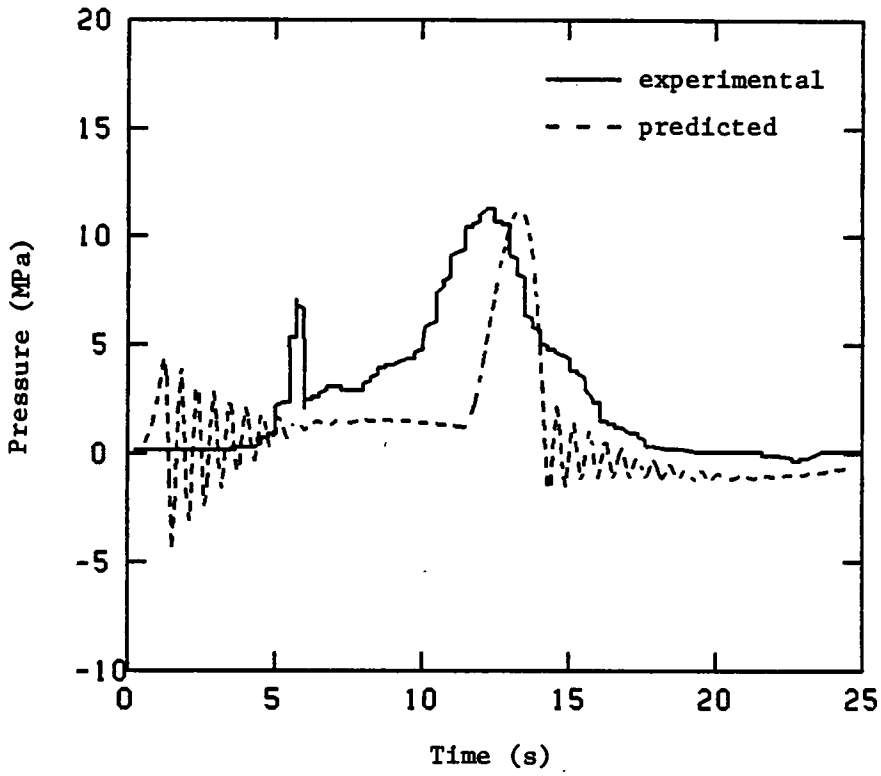

Figure 23: Experimental and predicted pump pressure differences with driven swashplate and fluid temperature of 45° C

angle in the pump or hydraulic motor speed, because it is hard to distinguish between the effects, was neglected.

The underdamping apparent in the simulation may be due in part to an underestimate of the charge pump capacitance. The volume used to calculate this value was assumed to be the displacement of the charge pump when it also includes the volume between the charge pump outlet, the check valves, and the charge pump relief valve. Other factors neglected were the dynamics of the check valves, which cannot open or close instantaneously as the model predicts, and the inertia of the fluid, both of which would affect the oscillation of the system pressure.

SUMMARY AND CONCLUSIONS

A test stand was built to demonstrate the characteristics of hydrostatic transmissions. Incorporated in its design were a variable displacement pump and a fixed displacement motor. The output shaft of the hydraulic motor was connected through an over-running clutch to the electric motor shaft. A load was developed in the hydraulic motor whenever the pump flow-rate was sufficient to cause the hydraulic motor speed to exceed the motor jackshaft speed, and thus transmit power back to the electric motor through the over-running clutch.

A mathematical model of the system was developed based on the equations derived by Wilson and Lemme (1970) for the steady-state performance of hydrostatic transmissions, and their subsequent improvement by Elder and Otis (1973), and the equations for the dynamic response of pump-controlled motors derived by Merritt (1967). The method of bond graphs, presented by Karnopp and Rosenberg (1975), was used to facilitate the equation development for the entire system as well as the understanding of the system. Bond graphs helped to define the independent and dependent effects within this closed-loop system, and thus clarified the causal relationships of the system.

The computer simulation of the mathematical model was implemented using the Advanced Continuous Simulation Language (ACSL). The evaluation of the state variables was done using a Gear's Stiff integration scheme which employed a variable step size. This allowed the system to be simulated more efficiently than if a fixed step size integration method had been used.

Various components on the test stand were tested to try to quantify and refine the model parameters. In the mechanical power transmission part of the system these parameters included bearing friction, sheave ratios, and over-running clutch drag and slip torques. The parameters in the hydrostatic transmission included viscous drag torques, constant friction torques, dry friction torques, filter losses, leakage coefficients, and hydraulic line losses. The tests that involved fluid flow had to be carried out with the fluid temperature near equilibrium because there was no temperature control mechanism in the system.

The steady-state and dynamic performance of the system was recorded experimentally, and was predicted with the simulation. The dynamic loading of the system was accomplished by cycling the swashplate angle with a variable speed motor and a four-bar crank-and-rocker linkage. For the sake of simulation, the resulting function of swashplate angle with

time was assumed to be sinusoidal cycling between zero and 6.5 degrees. The predicted and experimental data were plotted and compared.

The test stand was capable of demonstrating some of the characteristics of a variable displacement pump-fixed displacement motor hydrostatic transmission. For example, the hydraulic motor speed was dependent upon the pump swashplate angle, and volumetric efficiency decreased as operating pressure increased due to increased leakage. However, some of the characteristics of a hydrostatic transmission could not be demonstrated with this device due to the method of loading the hydraulic motor. The nature of the system prevented the selection of a particular motor load independent of the swashplate angle of the pump because the load was developed by creating a power loop where the hydraulic motor helped to drive the hydraulic pump.

It was shown that the test stand could be used to develop a time-varying load in the pump jackshaft, (Figure 22). The small spike at the beginning of each cycle could be eliminated by cycling the swashplate so that the hydraulic motor was not allowed to stop. The peak torque could be limited by limiting the maximum swashplate angle, the duration of the load by adjusting the speed at which the hydraulic motor caused the clutch to engage.

The analytic model was found to be in general qualitative agreement with the physical device. The simulation predicted the point at which the system pressure would rise sharply. It also adequately predicted the steady-state operating speeds. The predicted system pressure was, however, too sensitive to swashplate angle beyond the point where the clutch engaged. This was due to the underestimated dry friction torque and leakage loss coefficients.

The experimental data obtained by testing the major components of the test stand did help refine the model parameters. The use of the author developed flow indicator facilitated the measurement of the steady-state varying-viscosity flow-rates. However, certain important parameters, including viscous drag, dry friction torque, and line relief valve leakage, could not be adequately determined from the available test procedures and data. It is felt that more experimental work needs to be done to try to evaluate these parameters to improve the accuracy of the model. The ability to measure the output torque of the hydraulic motor is essential to continuing this effort. The measurement of fluid flows would also be enhanced by altering the flow indicator so that it would be capable of sensing the fluid temperature directly by means of a thermistor probe and automatically computing the viscosity for the fluid, rather

than requiring the operator to periodically alter the viscosity as the fluid temperature varied. Pressure measurement would be more easily calibrated with strain gage transducers than with a diaphragm transducer.

LIST OF REFERENCES

Binder, R. C., Fluid Mechanics, Prentice-Hall, Inc., Englewood Cliffs, NJ, 1962

Blackburn, J. F., G. Reethoff, and J. L. Shearer, Fluid Power Control, John Wiley and Sons, New York, NY, 1960

Elder, F. T. and D. R. Otis, "Simulation of a Hydraulic Hybrid Vehicle Power Train", ASME paper number 73-ICT-50, 1973

Fox, R. and A. McDonald, Introduction to Fluid Mechanics, John Wiley and Sons, New York, NY, 1978

Karnopp, D. and R. Rosenberg, System Dynamics: A Unified Approach, John Wiley and Sons, New York, NY, 1975

Levek, R. and R. Young, Aircraft Hydraulic Systems, Dynamic Analysis, (SSFAN) Computer Program Technical Description, McDonnell Douglas Co., 1977

Merritt, H. E., Hydraulic Control Systems, John Wiley and Sons, New York, NY, 1967

Mitchell and Gauthier, "Advanced Continuous Simulation Language (ACSL) User Guide/Reference Manual", Mitchell and Gauthier, Assoc., Inc., Concord, MA, 1981

Pacey, D. A., "The development of a Coefficient Model for a Hydrostatic Transmission", Kansas State University, Unpublished M.S. thesis, 1979

Popov, E. P., Mechanics of Materials, Prentice-Hall, Inc., Englewood Cliffs, NJ, 1976

Shigley, J. E., Kinematic Analysis of Mechanisms, McGraw-Hill Book Company, New York, NY, 1969

Shortley, G. and D. Williams, Elements of Physics, Prentice-Hall, Englewood Cliffs, NJ, 1971

Smith, R. J., Circuits Devices and Systems, John Wiley and Sons, New York, NY, 1976

Reid, K. N. and R. L. Woods, "Fluidic Control of a Hydrostatic Transmission in a Vehicle Power Train", ASME paper number 72-WA/Flcs-5, 1972

"User's Guide Interactive Simulation Language (ISL)", Queen Mary College of London University, August 31, 1982

White, F. M., Fluid Mechanics, McGraw Hill, New York, NY, 1979

Wilson, W. E. and C. D. Lemme, "Hydrostatic Transmissions", Parts 1 through 7, Hydraulics and Pneumatics, Vol. 23, 1970

Uncited References

Blundell, Alan, Bond Graphs for Modelling Engineering Systems, John Wiley and Sons, New York, NY, 1982

Graham, N., Microprocessor Programming for Computer Hobbyists, Tab Books, Blue Ridge Summit, PA, 1977

Ibrahim, B. B., "Closed Loop Control of Hydrostatic Drive Farm Tractors", Kansas State University, Unpublished Ph.D. dissertation, 1975

ICE-51 In-Circuit Emulator Operating Instructions for ISIS-II Users, Intel Corporation, Santa Clara, CA, 1981

Intel MCS-51 Family User's Manual, Intel Corporation, 1982

Karnopp, Dean and Ronald Rosenberg, Analysis and Simulation of Multiport Systems, The Bond Graph Approach to Physical System Dynamics, The MIT Press, Cambridge, MA, 1968

Martin, K. and J. Hart and G. Klassen, "A Microcomputer Based Flowrate Analyzer", Virginia Polytechnic Institute and State University, Unpublished report, 1983

Microcontroller User's Manual, Intel Corporation, 1982

Rosenberg, R. C. and D. C. Karnopp, "A Definition of the Bond Graph Language", Transactions of the ASME, Vol. 94, Series G, No. 3, September, 1972

Rubinovitz, J. and R. League, "Digital Flowmeter", Virginia Polytechnic Institute and State University, Unpublished report, 1984

APPENDIX A

LIST OF VARIABLES

Variable Name	Description	ACSL Name	Value	Units
α	Decimal ratio: swashplate displacement/maximum displacement of 15°	ALPHA	-	-
β_{den}	Fluid thermal expansion coefficient	-	0.001	1/°C
β_e	Effective bulk modulus of fluid	-	690	MPa
C_c	Capacitance of pressure side of charge pump	CC	7.84E-9	m^3/MPa
C_{Dm}	coefficient of viscous drag for a motor, as defined by Wilson	-	-	-
C_{Dp}	coefficient of viscous drag for a pump, as defined by Wilson	-	-	-
C_{dm}	Capacitance of case drain of hydraulic motor	CDM	1.085E-8	m^3/MPa
C_{dp}	Capacitance of case drain of main pump	CDP	1.085E-8	m^3/MPa

Variable Name	Description	ACSL Name	Value	Units
C_{fm}	coefficient of dry friction for a motor, as defined by Wilson	-	-	-
C_{fp}	coefficient of dry friction for a pump, as defined by Wilson	-	-	-
C_{L1}	Capacitance of pressure line from main pump to hydraulic motor	CL1	3.75E-7	m^3/MPa
C_{L2}	Capacitance of return line from hydraulic motor to main pump	CL2	3.75E-7	m^3/MPa
C_{sm}	coefficient of slip for a motor, as defined by Wilson	-	-	-
C_{sp}	coefficient of slip for a pump, as defined by Wilson	-	-	-
C_{lm}	Capacitance of pressure side of hydraulic motor	C1M	1.085E-8	m^3/MPa

Variable Name	Description	ACSL Name	Value	Units
C_{2m}	Capacitance of return side of hydraulic motor	C2M	1.085E-8	m^3/MPa
C_{1p}	Capacitance of pressure side of main pump	C1P	1.085E-8	m^3/MPa
C_{2p}	Capacitance of return side of main pump	C2P	1.085E-8	m^3/MPa
d	Diameter of hoses	D	0.0127	m
d_c	Displacement of charge pump	DC	8.61E-7	m^3/rad
d_m	Displacement of motor	DM	2.38E-6	m^3/rad
d_{pmax}	Maximum displacement of main pump	DPMAX	2.38E-6	m^3/rad
ΔP_{maxlam}	Maximum pressure drop in hose maintaining laminar flow	DPMXLM	-	MPa
ΔP_{mintrb}	Minimum pressure drop in hose maintaining turbulent flow	DPMXLM	-	MPa
ΔP_{tran}	Difference in pressures from maximum laminar to minimum turbulent flows	DPTRAN	-	MPa

Variable Name	Description	ACSL Name	Value	Units
F_{trb1}	Viscosity dependent term in turbulent flow calculation for hose 1	FTRB1	-	MPa/(Lpm)$^{7/4}$
F_{trb2}	Viscosity dependent term in turbulent flow calculation for hose 2	FTRB2	-	MPa/(Lpm)$^{7/4}$
G	Shearing modulus of steel	-	80.0E9	N/m^2
G_{1-dm}	Conductance from inlet side of motor to case drain	G1DM	1.50E-5	L/min /MPa
G_{2-dm}	Conductance from outlet side of motor to case drain	G2DM	1.50E-5	L/min /MPa
G_{1-dp}	Conductance from pressure side of main pump to case drain	G1DP	1.50E-5	L/min /MPa
G_{2-dp}	Conductance from suction side of main pump to case drain	G2DP	1.50E-5	L/min /MPa
G_{1-2c}	Conductance from inlet side to outlet side of charge pump	G12C	1.50E-5	L/min /MPa

Variable Name	Description	ACSL Name	Value	Units
G_{1-2m}	Conductance from inlet side to outlet side of motor	G12M	1.50E-5	L/min /MPa
G_{1-2p}	Conductance from pressure side to suction side of main pump	G12P	1.50E-5	L/min /MPa
G_{pf}	Conductance of pressure filter	GPF	62.5	L/min /MPa
J	Polar moment of inertia of pump jackshaft	-	1.29E-8	m^4
J_{emf}	Rotational inertia of electric motor	JEMF	0.4	$kg\text{-}m^2$
J_{lump}	Lumped rotational inertia of the electric motor and its connected shafts and sheaves	JLUMP	-	$kg\text{-}m^2$
J_{mjs}	Rotational inertia of motor jack-shaft	JMJS	0.1145	$kg\text{-}m^2$
J_{motor}	Rotational inertia of hydraulic motor	JMOTOR	0.2	$kg\text{-}m^2$

Variable Name	Description	ACSL Name	Value	Units
J_{pjs}	Rotational inertia of pump jack-shaft	JPJS	1.16	kg-m^2
J_{pjout}	Rotational inertia of output end of pump jack-shaft	JPJS	1.16	kg-m^2
J_{pjsin}	Rotational inertia of input end of pump jack-shaft	JPJS	1.16	kg-m^2
J_{pump}	Rotational inertia of both hydraulic pumps	JPUMP	0.2	kg-m^2
k	Spring rate of pump jackshaft	K	845.9	N-m/rad
L_{cm}	constant leakage coefficient, for a motor, as defined by Wilson	-	-	L/min/ /m^2/s
L_{cp}	constant leakage coefficient, for a pump, as defined by Wilson	-	-	L/min /m^2/s
L	Length of pump jackshaft	-	1.22	m

Variable Name	Description	ACSL Name	Value	Units
L1	Length of hose 1	LEN1	0.8125	m
L2	Length of hose 2	LEN2	0.8125	m
m1	Ratio: speed of pump jack-shaft/speed of electric motor	M1	0.3197	-
m2	Ratio: speed of pump/speed of pump jack-shaft	M2	4.203	-
m6	Ratio: speed of motor/speed of motor jackshaft	M6	1.00	-
m7	Ratio: speed of motor jackshaft/speed of electric motor	M7	0.498	-
μ	Dynamic viscosity	MU	-	N-s/m^2
ν	Kinematic viscosity	NU	-	cSt
P_{amb}	Ambient pressure	PAMB	0.0	MPa
P_c	Outlet pressure of charge pump	PC	-	MPa
P_{dm}	Motor case drain pressure	PDM	-	MPa

Variable Name	Description	ACSL Name	Value	Units
-	Initial pressure of hydraulic motor case drain	PDMIC	0.0	MPa
P_{dp}	Pump case drain pressure	PDP	-	MPa
-	Initial pressure of main pump case drain	PDPIC	0.0	MPa
-	Initial pressure of charge pump pressure side	PCIC	0.0	MPa
ϕ_{cl}	Non-linear torque through over-running clutch	PHICL	-	N-m
ϕ_{emf}	Non-linear torque from electric motor	PHIEMF	-	N-m
π	Constant	PI	3.141592	-
P_{L1}	Pressure at mid-point in pressure line from main pump to hydraulic motor	PL1	-	MPa
-	Initial pressure at mid-point in pressure line from main pump to hydraulic motor	PL1IC	0.0	MPa

Variable Name	Description	ACSL Name	Value	Units
P_{L2}	Pressure at mid-point in return line from hydraulic motor to main pump	PL2	-	MPa
-	Initial pressure at mid-point in return line from hydraulic motor to main pump	PL2IC	0.0	MPa
P_{me}	Effective pressure differencea across hydraulic motor	-	-	MPa
P_{mi}	Pressure of hydraulic motor inlet	PMI	-	MPa
-	Initial pressure hydraulic motor inlet	PMIIC	0.0	MPa
P_{mo}	Pressure of hydraulic motor outlet	PMO	-	MPa
-	Initial pressure hydraulic motor outlet	PMOIC	0.0	MPa
P_p	Pressure of main pump outlet	PP	-	MPa
-	Initial pressure of main pump outlet	PPIC	0.0	MPa

Variable Name	Description	ACSL Name	Value	Units
P_s	Suction pressure of main pump	PS	-	MPa
P_{sc}	Suction pressure of charge pump inlet	PSC	-	MPa
-	Initial pressure of main pump inlet	PSIC	0.0	MPa
Φ_{dl}^{-1}	Conductance of case drain line from pump to motor	XIDL	-	L/min
Φ_{crv}^{-1}	Non-linear flow in charge pump relief valve	XICRV	-	L/min
Φ_{cv1}^{-1}	Non-linear flow in check valve from charge pump to pressure line	XICV1	-	L/min
Φ_{cv2}^{-1}	Non-linear flow in check valve from charge pump to return line	XICV2	-	L/min
Φ_{L11}^{-1}	Non-linear flow in pressure line from pump to line relief valve	XIL11	-	L/min

Variable Name	Description	ACSL Name	Value	Units
Φ_{L21}^{-1}	Non-linear flow in pressure line from line relief valve to hydraulic motor	XIL12	-	L/min
Φ_{L21}^{-1}	Non-linear flow in return line from hydraulic motor to line relief valve	XIL21	-	L/min
Φ_{L22}^{-1}	Non-linear flow in return line from line relief valve main pump	XIL22	-	L/min
Φ_{lrv}^{-1}	Non-linear flow in line relief valve between pressure and return lines	XILRV	-	L/min
q_{clp}	Flow into main pump supply side capacitance	-	-	L/min
q_r	Flow in suction filter	-	-	L/min
q_{l-dm}	Leakage flow-rate from inlet side of hydraulic motor to case drain	Q1DM	-	L/min

Variable Name	Description	ACSL Name	Value	Units
$q_{2\text{-}dm}$	Leakage flow-rate from outlet side of hydraulic motor to case drain	Q2DM	-	L/min
$q_{1\text{-}dp}$	Leakage flow-rate from pressure side of main pump to case drain	Q1DP	-	L/min
$q_{2\text{-}dp}$	Leakage flow-rate from suction side of main pump to case drain	Q2DP	-	L/min
q_{100}	Flow-rate corresponding to Reynolds number = 100	Q100	-	L/min
q_{2300}	Flow-rate corresponding to Reynolds number = 2300	Q2300	-	L/min
q_c	Theoretical flow-rate from charge pump	QC	-	L/min
q_{dp}	Flow-rate from pump case drain	QDP	-	L/min
q_{dt}	Flow-rate from motor case drain, sum of pump and motor case drain flows	QDT	-	L/min

Variable Name	Description	ACSL Name	Value	Units
q_{12c}	Leakage flow-rate from pressure side to suction side of charge pump	Q12C	-	L/min
q_{12m}	Leakage flow-rate from pressure side to suction side of hydraulic motor	Q12M	-	L/min
q_{12p}	Leakage flow-rate from pressure side to suction side of main pump	Q12P	-	L/min
q_m	Effective flow-rate through hydraulic motor	QM	-	L/min
q_{mi}	Flow-rate into hydraulic motor inlet	QMI	-	L/min
q_{mo}	Flow-rate from hydraulic motor outlet	QMO	-	L/min
q_p	Theoretical flow-rate from main pump	QP	-	L/min
q_{pp}	Actural flow-rate from main pump supply pressure port	QPP	-	L/min

Variable Name	Description	ACSL Name	Value	Units
q_{s1}	Flow-rate through check valve from charge pump to supply line	QS1	-	L/min
q_{s2}	Flow-rate through check valve from charge pump to return line	QS2	-	L/min
q_{sp}	Flow-rate into main pump suction port	QSP	-	L/min
R	Electrical resistance of thermistor probe	R	-	kohm
R_c	Constant resistance torque in hydraulic motor or pump	RC	-	N-m
R_f	Resistance of bearings	RF	0.003188	N-m /rad/s
ρ	Density of hydraulic oil	RHO	900	kg/m^3
ρ_{ref}	Reference density of fluid at 15.6°C	-	869	kg/m^3
R_{sf}	Resistance of suction filter	RSF	-	MPa /L/min

Variable Name	Description	ACSL Name	Value	Units
θ	Swashplate angle	THETA	-	deg
T	Fluid temperature	TEMP	-	°C
T_c	Constant friction torque in pump or hydraulic motor	-	-	N-m
T_{cm}	constant friction torque for a motor, as defined by Wilson	-	-	N-m
T_{cp}	constant friction torque for a pump, as defined by Wilson	-	-	N-m
T_{CP}	torque required by charge pump	-	-	N-m
T_{drag}	Drag torque in over-running clutch	DRAG	-	N-m
T_{mj}	Sum of torques at hydraulic motor	TMJ	-	N-m
T_m	Torque output from hydraulic motor, including dry friction torque loss	-	-	N-m

Variable Name	Description	ACSL Name	Value	Units
T_{pt}	Torque required by both charge and main pumps	TPT	-	N-m
T_{ref}	Reference temperature of fluid	-	15.6	°C
T_s	Torque in pump jackshaft	TS	-	N-m
T_{slip}	Torque through over-running clutch	-	-	N-m
T_v	Viscous drag torque in pump hydraulic motor	-	-	N-m
T1	Torque on electric motor shaft inertia	-	-	N-m
T2	Torque output to pump jackshaft from electic motor	-	-	N-m
T3	Friction torque in electric motor	-	-	N-m
T4	Torque input to electric motor from motor jackshaft	-	-	N-m

Variable Name	Description	ACSL Name	Value	Units
T5	Torque input to pump jackshaft from electric motor	-	-	N-m
T6	Torque input to motor jackshaft inertia	-	-	N-m
T7	Friction torque in pump jackshaft	-	-	N-m
T8	Torque output to pump driveshaft from pump jackshaft	-	-	N-m
T9	Torque input to pump driveshaft from pump jackshaft	-	-	N-m
T10	Torque input to pump inertia	-	-	N-m
T11	Friction torque in pump driveshaft	-	-	N-m

Variable Name	Description	ACSL Name	Value	Units
T12	Torque output to over-running clutch from motor driveshaft	-	-	N-m
T13	Torque transmitted through over-running clutch	-	-	N-m
T14	Friction torque in motor jackshaft	-	-	N-m
T15	Torque input to motor jackshaft inertia	-	-	N-m
T16	Torque output from motor jackshaft to electric motor	-	-	N-m
T17	Friction torque in hydraulic motor jackshaft	-	-	N-m
ω_{in}	Speed of input end of pump jackshaft	-	-	rad/s
ω_{js}	Speed of output end of pump jackshaft	WJS	-	rad/s
ω_{slip}	Speed difference across over-running clutch	SLIP	-	rad/s

Variable Name	Description	ACSL Name	Value	Units
$\omega_{maxslip}$	Maximum speed difference across over-running clutch	MAXSLIP	-	rad/s
ω_1	Rotational speed of electric motor	W1	-	rad/s
$\dot{\omega}_1$	Derivative of electric motor speed	-	-	rad/s^2
-	Initial rotational speed of electric motor	W1IC	0.0	rad/s
ω_m	Rotational speed of hydraulic motor	WM	-	rad/s
$\dot{\omega}_m$	Derivative of hydraulic motor speed	-	-	rad/s^2
-	Initial rotational speed of hydraulic motor	WMIC	0.0	rad/s

APPENDIX B

ACSL Simulation Program for Hydrostatic Drive Test Stand

```
PROGRAM DEVICE MODEL
'BOND GRAPH VERSION DATE 3/12/85'
'13TH ORDER MODEL'
'PHI DESIGNATES NONLINEAR ELEMENTS WITH F = H(G)'
'XI DESIGNATES NONLINEAR ELEMENTS WITH E = H(F)'
INITIAL
'------------ START OF INITIAL SEGMENT --------------------
ALGORITHM IALG=2
NSTEPS    NSTP=1
MAXTERVAL MAXT=1.0E-2
CONSTANT  TMAX=.1,  MODE=0.0
'------------ FLUID PROPERTIES ----------------------------
'        TEMP = FLUID TEMPERATURE (C), ASSUMED CONSTANT'
'          NU = VISCOSITY (CENTISTOKES), FROM CONIC CURVE'
'          MU = DYNAMIC VISCOSITY (N*SEC/M**2)'
'         RHO = FLUID DENSITY (KG/M**3)'
CONSTANT TEMP=60.
NU=-0.441829E2*TEMP-0.342896E3+SQRT(0.3978E6+0.26496E5*...
   TEMP+0.19692E4*TEMP**2)
RHO=869.*(1-0.001*(TEMP-15.6))
MU=NU*1.E-6*RHO
'------------ RESISTANCES ---------------------------------
'WHERE  E = F * RX'
'       RF = FRICTION PER BEARING (N*M/(RAD/SEC)/BEARING)'
'      RCP = CONSTANT FRICTION OF PUMP (N*M)'
'      RCM = CONSTANT FRICTION OF MOTOR (N*M)'
'      CFP = COEFFICIENT OF DRY FRICTION, DIMENSIONLESS'
'      RSF = RESISTANCE OF SUCTION FILTER (MPA/LPM)'
'       RV = VISCOUS DRAG OF PUMP OR MOTOR
(NM/CST/RAD/SEC)'
CONSTANT  RF=0.00318,  RCP=0.742,  CFP=0.4177E-2
CONSTANT  RCM=0.250
RV=0.271*NU/M2/252.2
'------------ CAPACITANCES --------------------------------
'      CXY = VOLUME/BETA (M**3/MPA);  BETA = 690 MPA'
'  1=PRESSURE SIDE; 2=RETURN SIDE; D=DRAIN; M=MOTOR; P=PUMP'
'  L=LINE; C=CHARGE PUMP'
CONSTANT  CL1=3.75E-7,   CL2=3.75E-7,    CC=1.048E-8
CONSTANT  C1P=1.084E-8,  C2P=1.084E-8,  C1M=1.084E-8
CONSTANT  C2M=1.084E-8,  CDP=1.084E-8,  CDM=1.084E-8
'------------ AMBIENT PRESSURE (MPA) ----------------------
CONSTANT  PAMB=0.0
'------------ ROTATIONAL INERTIAS (KG*M**2) ---------------
'      JPJSIN = ELECTRIC MOTOR SIDE OF PUMP JACK-SHAFT'
```

```
'       JPUMP = PUMP'
'      JMOTOR = HYDRAULIC MOTOR'
'        JMJS = MOTOR JACK-SHAFT'
'        JEMF = ELECTRIC MOTOR'
'      JPJOUT = PUMP SIDE OF PUMP JACK-SHAFT'
CONSTANT  JPJSIN=0.36,    JPUMP=0.2,      JMOTOR=0.22
CONSTANT  JMJS=0.115,     JEMF=0.4,       JPJOUT=0.80
'---- SWASHPLATE RAMP, RELIEF VALVE ON/OFF -----------------
CONSTANT  SLOPE=1.0,      F=0.,           WDRIVE=0.25
CONSTANT  MAG=0.04950
'------------ INITIAL CONDITIONS --------------------------
CONSTANT  W1IC=0.0,  WMIC=0.0,  PPIC=0.0,  PSIC=0.0
CONSTANT  PCIC=0.0,  PDPIC=0.0, PMIIC=0.0, PMOIC=0.0
CONSTANT  PDMIC=0.0, PL1IC=0.0, PL2IC=0.0, TSIC=0.0
CONSTANT  WJSIC=0.0
'------------ MISC. CONSTANTS -----------------------------
'        D = DIAMETER OF HOSES (M)'
'   STATIC = COEFFICIENT OF STATIC FRICTION, DIMENSIONLESS'
'     LENX = LENGTH OF HOSES (M)'
CONSTANT  D=0.0127,  LEN1=1.02,  LEN2=1.02,
STATIC=12.
PI=4.*ATAN(1.0)
'------------ CONDUCTANCES --------------------------------
'    WHERE  F(LPM) = E(MPA) * GXYZ(LPM/MPA)'
' XYZ: 1=PRESSURE SIDE; 2=RETURN SIDE; D=DRAIN;'
'       M=MOTOR; P=PUMP'
'       PF = PRESSURE FILTER'
G1DM=6.6842E-5/MU
G2DM=6.6842E-5/MU
G1DP=6.6842E-5/MU
G2DP=6.6842E-5/MU
G12C=1.50E-5/MU
G12M=1.50E-5/MU
G12P=1.50E-5/MU
GPF=24.83/MU
'------------ DISPLACEMENTS -------------------------------
'    DPMAX = MAXIMUM MAIN PUMP DISPLACEMENT (M**3/RAD)'
'       DM = MOTOR DISPLACEMENT (M**3/RAD)'
'       DC = CHARGE PUMP DISPLACEMENT (M**3/RAD)'
DPMAX=1.496E-5/2./PI
DM=1.496E-5/2./PI
DC=5.048E-6/2./PI
'------------- SHEAVE RATIOS ------------------------------
'  M1 = ELECTRIC MOTOR TO PUMP JACK-SHAFT;  NOM.= 4.2/13.6'
'  M2 = PUMP JACK-SHAFT TO PUMP;            NOM.= 18.4/5.0'
'  M6 = MOTOR JACK-SHAFT TO HYDRAULIC MOTOR;NOM.= 7.0/7.0'
'  M7 = ELECTRIC MOTOR TO MOTOR JACK-SHAFT; NOM.= 4.2/8.6'
CONSTANT M1=0.31967,  M2=4.2026,  M6=1.0,  M7=0.49782
MODM=(1.-CFP*1.366)*DM
'------------- MISCELLANEOUS CONSTANTS --------------------
```

```
' JLUMP = LUMPED INERTIA OF ELECTRIC MOTOR (KG*M**2)'
'     K = SPRING CONSTANT OF PUMP JACK-SHAFT (N*M/RAD)'
'   PSC = INITIAL CHARGE PUMP SUCTION PRESSURE (MPA)'
'MXSLIP = MAXIMUM SPEED DIFFERENCE IN CLUTCH (RAD/SEC)'
'    ZZ = M**3/SECOND TO LITERS/MINUTE'
JLUMP=JEMF+M1**2*JPJSIN+M7**2*JMJS
K=1.29E-8*80.0E9/1.22
PSC=PAMB
MXSLIP=187.4*M7
ZZ=60000.
'------------- FLOW CALCULATION CONSTANTS -----------------
'    GLAM = LAMINAR PRESSURE DROP (LPM/MPA)'
'    Q100 = FLOW AT REYNOLDS NUMBER OF 100 (LPM)'
'   Q2300 = FLOW AT REYNOLDS NUMBER OF 2300 (LPM)'
'  DPMXLM = MAXIMUM PRESSURE DROP FOR LAMINAR FLOW (MPA)'
'  DPMNTB = MINIMUM PRESSURE DROP FOR TURBULENT FLOW (MPA)'
'       FTBX = CONSTANT PART OF TURBULENT FLOW EQUATION (?)'
GLAM=PI*6.0E9*D**4/(128.*MU*LEN1)
Q100=100.*PI*MU*D*15000./RHO
Q2300=2300.*PI*MU*D*15000./RHO
DPMXLM=Q100/GLAM
DPMNTB=1.048E-15*LEN1*MU**0.25*RHO**0.75*Q2300**1.75/D**4.75
FTB1=(8.461E13*D**4.75/MU**0.25/RHO**0.75/LEN1)**(4./7.)
FTB2=(8.461E13*D**4.75/MU**0.25/RHO**0.75/LEN2)**(4./7.)
'------------ WRITE PRESSURE HEADINGS ---------------------
WRITE(30,30)
30..FORMAT(6X,'T',8X,'THETA',7X,'PP',9X,'PS',9X,'PC',9X,...
'PDP',8X,'DELL1',6X,'DELL2',6X,'PMI',8X,'PMO',8X,'PDM',...
8X,'PSC')
'------------ WRITE FLOW HEADINGS -------------------------
WRITE(40,40)
40..FORMAT(/,6X,'T',8X,'THETA',7X,'XIL11',6X,'XIL12',6X,...
'XIL21',6X,'XIL22',6X,'XIDL',7X,'XILRV',7X,'XICRV',6X,...
'XICV1',6X,'XICV2',6X,'QDT')
'------------ WRITE TORQUE AND SPEED HEADINGS -------------
WRITE(50,50)
50..FORMAT(/,6X,'T',8X,'THETA',7X,'TS',7X,'PHICL',6X,...
'PHIEMF',7X,'W1',9X,'WM',9X,'WJS')
'------------ WRITE LEAKAGE FLOW HEADINGS -----------------
WRITE(60,60)
60..FORMAT(/,6X,'T',8X,'THETA',7X,'Q12P',7X,'Q1DP',7X,...
'Q2DP',7X,'Q12M',7X,'Q1DM',7X,'Q2DM',9X,'QP',9X,'QM',9X,...
'QC')
'------------ WRITE FLUID PROPERTIES ----------------------
WRITE(70,70) TEMP,NU,MU,RHO
  70..FORMAT(132('*'),/,...
       ' FLUID TEMPERATURE (C)              = ',F11.5,/,...
       ' KINEMATIC VISCOSITY (CENTISTOKES) = ',F11.5,/,...
       ' DYNAMIC VISCOSITY (N*SEC/M**2)    = ',F11.5,/,...
       ' FLUID DENSITY (KG/M**3)           = ',F11.5,/,...
```

```
,132('*'))
'------------ WRITE DYNAMIC OUTPUT HEADINGS ---------------
WRITE(80,80) MAG,TEMP
  80..FORMAT(' MAG = ',F11.5,'    TEMP = ',F11.5,/
6X,'T',8X,'THETA',7X,'PP-PS',8X,'TS',9X,'WM')
END $'-------- END OF INITAL -------------------------------
DYNAMIC
DERIVATIVE
'------------- INTEGRALS ----------------------------------
W1=INTEG((PHIEMF+M7*PHICL-M1*TS-(M1**2+M7**2+1.)*2*RF*W1)...
         /JLUMP,W1IC)
    PHICL=RSW(SLIP.LT.0.0375,1.522*SLIP/MXSLIP,...
              163.3*SLIP-6.1)
        SLIP=M6*WM-M7*W1
    PHIEMF=RSW(T.LE.0.01,RAMP(0.0)*6000.,...
           RSW(W1.LT.176.8,60.+0.1697*W1,1450.-7.6923*W1))
WM=INTEG(TMJ/JMOTOR,WMIC)
    TMJ=RSW((TMARG.LE.STATIC).AND.(WM.EQ.0.),0.0,...
             TMARG-(RCM+RV*WM)*SIGN(1.,WM))
        TMARG=(PMI-PMO)*MODM*1.0E6-RF*3.*WM-PHICL
WJS=INTEG((TS-RF*WJS*(3.+3*M2**2)-M2*(RCP+RV*M2*WJS+TPT))...
          /(JPJOUT+M2**2.*JPUMP),WJSIC)
    TPT=(MODP*(PP-PS)+DC*(PC-PSC))*1.E6
        MODP=(ALPHA+CFP/(1.-TAN(RTHETA)))*DPMAX
        PSC=PAMB-(0.01752+0.07292*MU*QC)
TS=INTEG(K*(M1*W1-WJS),TSIC)
PP=INTEG((QP-Q12P+XICV1-Q1DP-XIL11)/ZZ/C1P,PPIC)
    QP=ALPHA*DPMAX*M2*WJS*ZZ
    Q12P=(PP-PS)*G12P
    XICV1=RSW((PC-PP).GE.0.,(PC-PP)/0.01,(PC-PP)/1.0E20)
    Q1DP=(PP-PDP)*G1DP
    XIL11=FLOW(DELP11,DPMXLM,DPMNTB,GLAM,Q100,Q2300,FTB1)
        DELP11=PP-PL1
PS=INTEG((-QP+Q12P+XICV2-Q2DP+XIL22)/ZZ/C2P,PSIC)
    XIL22=FLOW(DELP22,DPMXLM,DPMNTB,GLAM,Q100,Q2300,FTB2)
        DELP22=PL2-PS
    Q2DP=(PS-PDP)*G2DP
    XICV2=RSW((PC-PS).GE.0.,(PC-PS)/0.01,(PC-PS)/1.0E20)
PMI=INTEG((XIL12-Q12M-Q1DM-QM)/ZZ/C1M,PMIIC)
    XIL12=FLOW(DELP12,DPMXLM,DPMNTB,GLAM,Q100,Q2300,FTB1)
        DELP12=PL1-PMI
    Q12M=(PMI-PMO)*G12M
    Q1DM=(PMI-PDM)*G1DM
    QM=DM*WM*ZZ
PMO=INTEG((-XIL21+Q12M-Q2DM+QM)/ZZ/C2M,PMOIC)
    XIL21=FLOW(DELP21,DPMXLM,DPMNTB,GLAM,Q100,Q2300,FTB2)
        DELP21=PMO-PL2
    Q2DM=(PMO-PDM)*G2DM
PC=INTEG((QC-XICV1-XICV2-XICRV)/ZZ/CC,PCIC)
    QC=DC*M2*WJS*ZZ
```

```
PL1=INTEG((XIL11-XILRV-XIL12)/ZZ/CL1,PL1IC)
    XILRV=(PL1-PL2)*G1DP
PL2=INTEG((XIL21+XILRV-XIL22)/ZZ/CL2,PL2IC)
PDP=INTEG((Q1DP+Q2DP+XICRV-XIDL)/ZZ/CDP,PDPIC)
    XICRV=RSW((PC-PDP).LT.0.689,(PC-PDP)/1.E20,(PC-PDP)/...
          0.02875-24.0)
    XIDL=FLOW(DELDL,DPMXLM,DPMNTB,GLAM,Q100,Q2300,FTB1)
        DELDL=PDP-PDM
PDM=INTEG((Q1DM+Q2DM-QDT+XIDL)/ZZ/CDP,PDMIC)
    QDT=PDM*GPF
'------------ SWASHPLATE ANGLE (DEG) ----------------------
THETA=RSW(MODE.NE.0.0,DTHET,STHET)
ALPHA=THETA/15.0
RTHETA=THETA*PI/180.
'============ SWASHPLATE RAMP SERIES ======================
STHET=SLOPE*(RAMP(5.)-RAMP(5.5)+RAMP(15.)-RAMP(15.5)...
      +RAMP(25.)-RAMP(25.5)+RAMP(35.)-RAMP(35.5)...
      +RAMP(45.)-RAMP(45.5)+RAMP(55.)-RAMP(55.5)...
      +RAMP(65.)-RAMP(65.5)+RAMP(75.)-RAMP(75.5)...
      +RAMP(85.)-RAMP(85.5)+RAMP(95.)-RAMP(95.5)...
      +RAMP(105.)-RAMP(105.5)+RAMP(115.)-RAMP(115.5)...
      +RAMP(125.)-RAMP(125.5)+RAMP(135.)-RAMP(135.5)...
      +RAMP(145.)-RAMP(145.5)+RAMP(155.)-RAMP(155.5))
'============ SWASHPLATE SINE APPROXIMATION ===============
DTHET=(MAG*(SIN(GAMMA-PI/2.)+1.))*180./PI
    PROCEDURAL (GAMMA=WDRIVE,PI,T)
        GAMMA=RSW(T.LE.5.0,0.0,WDRIVE*(T-5.0))
        IF(GAMMA.GE.(2.*PI)) GAMMA=GAMMA-2.*PI
    END $'-------- END OF PROCEDURAL ----------------------
END $'-------- END OF DERIVATIVE ---------------------------
'------------ WRITE PRESSURES -----------------------------
DELL1=PP-PMI $ DELL2=PMO-PS
WRITE(30,300)T,THETA,PP,PS,PC,PDP,DELL1,DELL2,PMI,PMO,PDM...
             ,PSC
300..FORMAT(12F11.5)
'------------ WRITE FLOWS ---------------------------------
WRITE(40,400)T,THETA,XIL11,XIL12,XIL21,XIL22,XIDL,XILRV...
            ,XICRV,XICV1,XICV2,QDT
400..FORMAT(12F11.5)
'------------ WRITE TORQUES AND SPEEDS --------------------
WRITE(50,500) T,THETA,TS,PHICL,PHIEMF,W1,WM,WJS
500..FORMAT(8F11.5)
'------------ WRITE LEAKAGE FLOWS -------------------------
WRITE(60,600)T,THETA,Q12P,Q1DP,Q2DP,Q12M,Q1DM,Q2DM,QP,QM,PC
 600..FORMAT(12F11.5)
'------------ WRITE DYNAMIC OUTPUTS -----------------------
DPUMP=PP-PS
WRITE(80,800) T,THETA,DPUMP,TS,WM
 800..FORMAT(5F11.5)
'-------------------------------------------------------------
```

```
TERMT(T.GE.TMAX)
END $'-------- END OF DYNAMIC ------------------------------
END $'-------- END OF PROGRAM ------------------------------
      FUNCTION FLOW(DELP,DPMXLM,DPMNTB,GLAM,Q100,Q2300,FTB)
      ADELP=ABS(DELP)
      IF(ADELP.LE.DPMXLM) FLOW=DELP*GLAM
      IF((ADELP.GT.DPMXLM).AND.(ADELP.LE.DPMNTB))
      FLOW=(Q100+(Q2300-Q100)*(ADELP-DPMXLM)/
     .(DPMNTB-DPMXLM)*SIGN(1.,DELP)
     IF(ADELP.GT.DPMNTB) FLOW=FTB*(ADELP)**(4./7.)
     .*SIGN(1.,D
      RETURN
      END
```

APPENDIX C

FLOW INDICATOR USER MANUAL

A flow indicator was designed to compute the flow rate from two turbine-type flow meters based on linear regression equations formulated from the calibration data. The square wave output pulses from each meter were to be counted for a period determined by the user and multiplied by the appropriate factor to obtain the input frequency. The available periods are given in the Table C1. Both frequencies may be displayed simultaneously, with a range from 0 to 9999 hz and a resolution depending upon the period.

Operation at Power-Up or Reset

Four switches were used to determine the mode of operation of the indicator (Figure C1). There are two SPST flow-rate/frequency switches (HZ/GPM), one for each flow-meter, a SPDT increment/set switch (INC/SET), and a reset button.

The indicator displayed the flow or frequency output on the four four-character on-board displays. It was also able to output serially to a terminal through its RS-232 port at a number of common baud rates ranging from 300 to 9600 baud. On power-up or after reset, the indicator prompted the user to set the baud rate. If the indicator was to be used in

Table C1: Indicator commands and their functions

Command	Function
"B<n>"	changes baud rate to:
n = 1	300
2	1200
3	2400
4	4800
5	9600
"C<n>"	changes sampling interval (seconds) to:
n = 1	0.100
2	0.125
3	0.200
4	0.500
5	1.000
"H"	outputs a listing of available commands
"L"	starts or stops line-feeds after each period
"R"	resets the indicator, same as reset button
"T"	starts or stops the test function which by-passes the input and assumes that 125 pulses were input during the period
"V"	outputs the current viscosity in floating-point format to the terminal terminal
"x"	when entered after "TYPE 'X' TO XMIT" prompt, enables output to RS-232 serial port

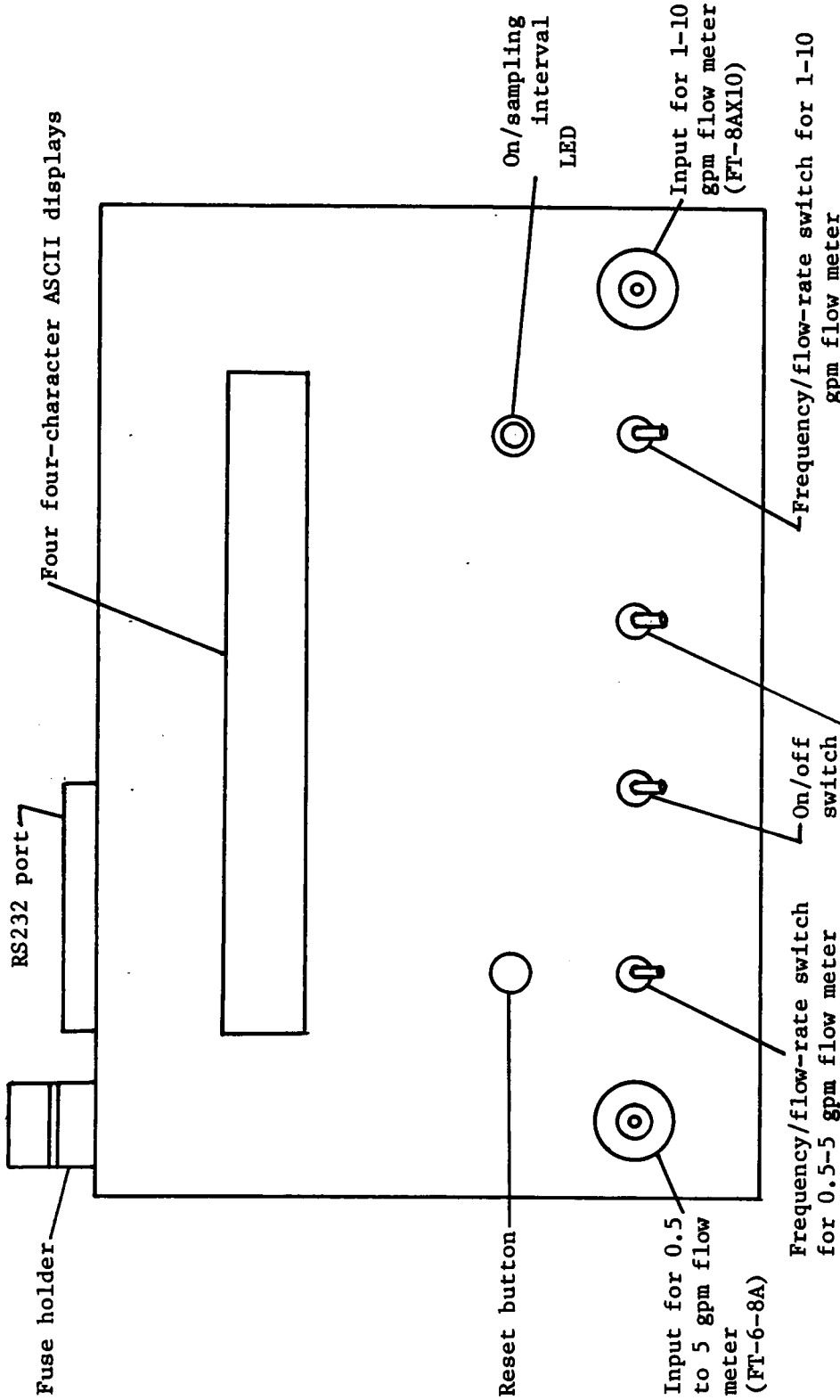

Figure C1: Face of flow indicator (actual size)

the stand-alone mode, the user had only to wait five seconds for the indicator to assume the no-transmission default mode. If the user desired to have the data sent to the serial port, he would select the appropriate baud rate. Placing the INC/SET switch in the "set" position selected the baud rate being displayed; setting the switch to the "increment" switch caused the indicator to display indefinitely the possible baud rates at the rate of one each half second. Setting the INC/SET switch to the neutral position caused the incrementing to halt at the current display and wait for further action by the user. With the baud rate set, the indicator prompted the user to input an "x" to enable transmission. Without an "x" input, data will not be output to the RS-232 port, and operation reverted to the stand-alone mode. After the "x" was input, the indicator accepted its commands from the terminal and output data to both the displays and the terminal.

Operation as Stand Alone Device

If the user failed to either take some action within 5 seconds to set the baud rate or failed to properly input an "x" through the serial port, the indicator assumed the stand-alone mode. In this mode, data was not sent to or received from the serial port.

The indicator then prompted the user for the desired sampling interval. If no action was taken within 5 seconds, the default period of 0.2 seconds was assumed. The INC/SET switch was used to select the sampling interval in a manner similar to that described above for the selection of the baud rate: the "set" position selected the sampling interval currently displayed, neutral held the current display and waited, and "increment" caused the available sampling intervals to be displayed sequentially at half second intervals.

The viscosity of the fluid, in centi-Stokes, had to be enterred to compute the flow-rates correctly. A four-digit number with two decimal places was required. The INC/SET switch was placed in the "set" position causing the tens-digit to increment until the desired digit appeared. One-half second occurred between increments to allow the operator time to react. When the desired digit was reached, the INC/SET switch was set to neutral and incrementing stopped. The switch was then put in the "set" position to indicate that the user was ready to select the ones digit, and so on until four digits are enterred. In the stand-alone mode, the current viscosity was saved and used as the initial four digits displayed in the viscosity selection procedure after a reset.

Immediately after the last viscosity digit was enterred, the indicator began to sample the input from the flow meters and display the computed flow-rate or the input frequency to the displays. In either the stand-alone or terminal mode, the choice of whether frequency or flow-rate was displayed, or output, was made by setting the HZ/GPM switches.

Operation with a Terminal

After typing an "x" in response to the prompt following the selection of the baud rate, the viscosity was enterred from a terminal keyboard in either decimal or exponential format. The indicator then immediately began to display the flow in gallons per minute to two decimal places on the terminal and also on the four four-character displays. The terminal output had the form "Hxxxx" or "Fxxxxx" depending on how the GPM/HZ switches were set. Capital "F" or "H" indicated the mode of meter 1, and lower case "f" or "h" the mode of meter 2.

The indicator operated continuously until the reset button was pushed. It then required that the viscosity be enterred again and operation continued as described above in the Operation at Start-Up or Reset section.

The user changed the baud rate or the sampling interval from the terminal by typing a "B" or "C" respectively. The

indicator then halted sampling and waited for the input of a number corresponding to the new rate, as given in Table C1. When the baud rate was changed, the indicator waited after the input of the number for a carriage return character at the new baud rate to also be input. If one was not forthcoming, the baud rate change was aborted and the current baud rate used.

An "L" input toggled the linefeed setting. This caused the terminal display to start or stop scrolling with each output. With the linefeed off, the output rate was still indicated by an flashing asterisk at the end of the display.

A "T" input caused the indicator to assume an input sample of 125 pulses from the flow meters regardless of the actual count. The current viscosity was also displayed to the terminal typing a "V". However, after displaying the current viscosity, the indicator required the user to enter a new viscosity.

A list of the indicator commands was obtained by entering an "H". The indicator displayed to the terminal brief descriptions of the format of each command, two lines at a time. The user was asked after each pair of lines whether he wanted to continue, by hitting return, or to quit, by typing "Q". After a complete list was output, the indicator prompted the user for a new viscosity, and the program continued from that point.

If the meter frequency went above 2000 hz or below 100 hz while in the GPM mode, error messages were generated. An over-speed caused a "HIGH" to be displayed and an underspeed a "LOW ".

The indicator had limited on board data storage capability. However, a host device could have been used to store the output from the indicator.

APPENDIX D

Flow Meter Algorithm Constants

Flow calibration data for FT-6-8AX5-LJC, serial no. 8603677, and FT-8AX10-LB, serial no. 803236, was supplied by Flow Technology, Inc. Thirteen values of flow rate in gallons per minute with their corresponding meter output frequencies were given for each of three different viscosities for each meter.

Plotting frequency versus flow rate for each viscosity showed that frequency was linear with flow rate. Simple linear regression (least squares) was used to fit the best line through the data, for each viscosity.

Using these regression equations to estimate flow rates at several fixed frequencies, it was found that viscosity had a parabolic relationship with flow rate. The combined function was then assumed to have the form:

$$GPM = (c0 + c1\ V + c2\ V^2) + (c3 + c4\ V + c5\ V^2)\ Hz$$

or

$$\{GPM\} = [DATA]\ \{c\}$$

in matrix form. [GPM] was a 39 element column matrix, [DATA] a 39 by 6 matrix from the calibration data, and {c} a six element vector of coefficients.

The procedure for finding {c} was:

$$[DATA]\ \{c\} = \{GPM\}$$

$$[DATA]^T\ [DATA]\ \{c\} = [DATA]^T\ \{GPM\}$$

$$\{c\} = ([DATA]^T\ [DATA]^{-1})\ [DATA]^T\ \{GPM\}$$

The coefficients were found to be:

Coefficient	FT-6 (.5-5 gpm)	FT-8 (1-10 gpm)
1	-0.02133	-0.04162
2	7.7136×10^{-3}	5.6135×10^{-3}
3	2.7089×10^{-3}	4.4723×10^{-3}
4	-1.8628×10^{-5}	-9.1298×10^{-6}
5	1.9738×10^{-5}	-3.0175×10^{-5}
6	4.3424×10^{-7}	2.4598×10^{-7}

These coefficients were used in the equation above to estimate flow rates based on the data from the calibration. These estimates were checked against the known values. The percent error of the estimated values for both flow meters are given in Tables E1 and E2, respectively. The largest errors occur at flow rates below the rated minimum for each meter.

Table D1: Comparison calibrated to regression-predicted flow-rates for flow-meter FT-6-8A (0.5 to 5.0 gpm range)

Calibrated Flow (gpm)	Predicted Flow (gpm)	Percent Error
5.2040	5.195	-0.1689
4.4735	4.4708	-0.06002
3.9371	3.9403	0.0809
3.3896	3.3968	0.2132
2.8301	2.8389	0.3094
2.2035	2.2095	0.2704
1.6079	1.6141	0.3829
1.0943	1.0943	0.0025
0.6881	0.6824	-0.8341
0.4923	0.4849	-1.4984
5.1686	5.1609	-0.1496
2.8222	2.8305	0.2950
0.4957	0.4884	-1.4747
5.0394	5.0226	-0.3343
4.3041	4.3031	-0.0237
3.8384	3.8395	0.0286
3.2685	3.2806	0.3710
2.7481	2.7633	0.5522
2.2012	2.2165	0.6947
1.7116	1.7205	0.5193
1.1054	1.1045	-0.0796
0.7112	0.7196	-1.2992
0.4870	0.4740	-2.6766
5.0387	5.0250	-0.2724
2.7660	2.7814	0.5567
0.4913	0.4781	-2.6922
5.1109	5.1141	0.0620
4.3525	4.3673	0.3390
3.7596	3.7606	0.0272
3.1067	3.1004	-0.2035
2.6211	2.6084	-0.4863
2.1055	2.0905	-0.7132
1.4810	1.4774	-0.2430
1.0009	0.9899	-1.0960
0.7518	0.7503	-0.1973
0.4791	0.4981	3.9571
5.0099	5.0154	0.1101
2.6326	2.6216	-0.4196
0.4828	0.5006	3.6789

Table D2: Comparison calibrated to regression-predicted flow-rates for flow-meter FT-8AX10 (1.0 to 10.0 gpm range)

Calibrated Flow (gpm)	Predicted Flow (gpm)	Percent Error
10.4043	10.3742	-0.2889
9.2108	9.2240	0.1431
7.9940	8.0015	0.0942
7.1504	7.1701	0.2752
6.0128	6.0340	0.3529
4.8498	4.8660	0.3346
3.5598	3.5659	0.1725
2.5376	2.5340	-0.1402
1.3909	1.3805	-0.7461
0.9823	0.9676	-1.4996
0.9799	0.9651	-1.5142
6.0747	6.0933	0.3057
10.4210	10.3920	-0.2781
10.3702	10.3478	-0.2157
9.0415	9.0399	-0.0182
8.0857	8.0971	0.1410
7.1234	7.1450	0.3030
6.0388	6.0607	0.3621
4.8999	4.9096	0.1976
3.5769	3.5837	0.1897
2.4275	2.4270	-0.02135
1.3839	1.3727	-0.8058
0.9759	0.9611	-1.5205
0.9681	0.9532	-1.5392
6.0472	6.0716	0.4028
10.1929	10.1627	-0.2968
10.0745	10.0572	-0.1720
8.9864	9.9809	-0.06127
7.7887	7.7937	0.0637
6.8824	6.8938	0.1662
5.5814	5.5985	0.3060
4.5054	4.5261	0.4591
3.3511	3.3682	0.5110
2.3609	2.3624	0.0615
1.3373	1.3262	-0.8316
0.9988	0.9800	-1.8845
0.9958	0.9772	-1.8728
5.5415	5.5593	0.3204
10.0569	10.0378	-0.1896

The vita has been removed from the scanned document